Regulation of intracellular traffic by TBK1 and its relevance to ALS

David Villarroel Campos

University College London

PhD Supervisor: Giampietro Schiavo

A thesis submitted for the degree of

Doctor of Philosophy

University College London

March 2020

Declaration

I, David Villarroel Campos, confirm that the work presented in this thesis is my own. Where information has been derived from other sources, I confirm that this has been indicated in the thesis.

In addition, I purposely wrote this document in first person plural, to acknowledge the fact that science is a collaborative and collective effort. These might be my experiments, but they are our results.

Abstract

Neurons are highly polarised cells, typically comprising a somatodendritic compartment and an axon that can extend for a meter or more. Their extreme morphology challenges neurons to establish an efficient communication system between the axonal terminal and the soma, a mechanism known as axonal transport. Axonal transport is required for the maintenance of neuronal homeostasis, and is impaired in many neurodegenerative diseases, such as Amyotrophic Lateral Sclerosis (ALS). Mutations in TANK-binding kinase-1 (TBK1) have been described as causative for familial ALS. TBK1 phosphorylates Rab7, a small GTPase regulating the endolysosomal pathway. We have previously shown that the retrograde transport of signalling endosomes carrying neurotrophic receptors relies on Rab7, and that deficits in retrograde axonal transport can be detected at early symptomatic stages during ALS pathogenesis.

In this work, we address whether TBK1 loss-of-function or Rab7-S72 phosphorylation alters the retrograde transport of signalling endosomes. We transfected Rab7 WT, S72A (phospho-deficient) and S72E (phospho-mimetic) in primary motor neurons and assessed the trafficking of signalling endosomes. Our results show that the directionality of transport is affected upon transfection of Rab7-S72E, whilst neuronal polarity remains unaltered. Axonal microtubule polarity also remains unchanged. We then characterised a set of shRNAs against TBK1 and showed that reduced TBK1 expression phenocopies the S72E condition. This alteration in transport is specific for signalling endosomes, as lysosomes and mitochondria were not affected. Altogether, these results suggest an involvement of TBK1 in the regulation of axonal transport of signalling endosomes and suggest that deficits in TBK1 activity determines retrograde transport dysfunction, which may be causative in ALS pathogenesis.

Impact statement

Amyotrophic lateral sclerosis (ALS) is a progressive neurodegenerative disease, characterised by motor neurons loss which leads to muscle paralysis and death. About 90% of cases are sporadic, whilst the remaining 10% correspond to familial cases. Recent advances in next generation sequencing have expanded the range of genes mutated in familial ALS. One of these genes is TANK-binding kinase 1 (TBK1), a serine/threonine kinase part of the NF-κB pathway, with roles on innate immune response and autophagy. In this work, we have shown that TBK1 is also relevant for the axonal transport of signalling endosomes carrying neurotrophic signalling. This is, to the best of our knowledge, the first evidence linking TBK1 function to axonal transport. Therefore, we have extended the phenotypes associated to TBK1 loss-of-function to disruption in signalling endosome retrograde trafficking, and at the same time, reinforced the contribution of axonal transport defects to ALS pathology.

TBK1 inhibitors have been used in research as tools to modify the inflammatory response against viruses and pathogenic bacteria. Nevertheless, their use in neuronal cells is not widely extended. Surprisingly, we found conflicting results regarding TBK1 activation and catalytic inhibition in motor neurons, highlighting the necessity of generating more specific inhibitors which can be applied safely across different cell types. This will be a crucial requirement for the design of new TBK1 inhibitors aimed to be employed in animal models of ALS, as well as in translational medical approaches.

From the mechanistic perspective, our group and others have previously reported TBK1 phosphorylates Rab7 at Ser72. This phosphorylation impacts Rab7 functions during mitophagy, as well as EGFR destination to degradative compartments. Here we have shown that a Rab7 mutant mimicking TBK1 phosphorylation (Rab7-S72E) also impairs the retrograde transport of signalling endosomes. Despite its cytosolic intracellular

distribution, Rab7-S72E mutant retains the ability to interact with some effectors, hence it may uncouple the tightly associated relationship between Rab GTPase activity and Rab GTPase subcellular localisation. This result challenges the conventional Rab cycle and is likely to drive further research projects aimed to characterise the interplay between Rab7 phosphorylation and function.

In conclusion, we have described a new function for TBK1, regulating retrograde transport of signalling endosomes in motor neurons, whose alteration may impact in neurodegeneration during ALS.

Acknowledgements

If I managed to finish this thesis, it is certainly due to the support of many people who directly or indirectly pushed me away from biscuits, into the experiments. I would like to thank my supervisor Gipi Schiavo, a group leader who displays the exact equilibrium between giving the student complete freedom, and not losing him out of sight. I believe doubts were kept at bay because Gipi directed the project like a doge administrating *La Serenissima*. I also want to thank all the past and present members of the Schiavo, Greensmith and Fratta labs, for showing me that sometimes, the key to overcome problems lies in Perseverance. I am particularly grateful to Dr Alex Fellows for showing me the road, the Fellows road, to Dr Ione Frederica Greensmith Meyer for sharing a genuine interest in the many ways to deliver dulce de leche in cakes, and to Dr Marta Budzinska, I wouldn't be here if you wouldn't have chosen me as your faithful minion.

To my parents, thank you for always being present, even if you stand more than 13,000 kilometres away, and to Dafne, after ten years finally no more theses for both of us. I have had the privilege of sharing your path and I wouldn't have wanted it any other way. Thank you for everything.

This work was supported by the Motor Neurone Disease Association (MNDA) and by a CONICYT/ANID PhD scholarship 2016/72170645.

Table of Contents

Table of Figures

Abbreviations

(+)TIPs	microtubule plus-end tracking protein
A.U.	arbitrary units
Ac-Tub	acetylated tubulin
ALS	amyotrophic lateral sclerosis
AMP	adenosine monophosphate
APPL1	Adaptor protein, phosphotyrosine interacting with PH domain and leucine zipper 1
ARF	ADP-ribosylation factor
aTAT1	α-tubulin N-acetyltransferase 1
ATG	autophagy-related proteins
ATP	Adenosine triphosphate
BDNF	brain-derived neurotrophic factor
BICD	Bicaudal D
BICDR1	BICD family-like cargo adapter 1
BICDR2	BICD family-like cargo adapter 2
bv-FTD	behavioural-variant frontotemporal dementia
CCD1	coiled-coil domain 1
CCD2	coiled-coil domain 2
Cdc25A	cell division cycle 25A
cGAS	cyclic GMP-AMP synthase
CHMP2B	charged multivesicular body protein 2b
CLIP170	CAP-Gly domain-containing linker protein 1
CMT	Charcot-Marie-Tooth
CNS	central nervous system
CNTF	Ciliary neurotrophic factor
DAPI	4′,6-diamidino-2-phenylindole

DENN	differentially expressed in normal and neoplastic cells
DFCP1	Double FYVE-Containing Protein 1
DHC	dynein heavy chain
DIC	dynein intermediate chain
DIV	days *in vitro*
DLC	dynein light chain
DLIC	dynein light intermediate chain
DMEM	Dulbecco's Modified Eagle Medium
DMSO	dimethyl sulfoxide
DNA	deoxyribonucleic acid
DRG	Dorsal root ganglion
dsRNA	double-stranded RNA
EAAT2	excitatory amino acid transporter 2
EB3	end-binding protein
EEA1	early endosome antigen 1
EGFR	epidermal growth factor receptor
ER	endoplasmic reticulum
ERAD	ER-associated degradation
ERK	extracellular signal-regulated kinase
ESCRT	endosomal complex required for transport
fALS	familial amyotrophic lateral sclerosis
FG-NUPS	Phenylalanine-glycine rich nucleoporins
FBS	Fetal bovine serum
FIP200	FAK Family Kinase-Interacting Protein Of 200 KDa
FLCN	folliculin
FNIP1	folliculin-interacting protein 1
FTD	frontotemporal dementia

FUS	fused in sarcoma
FYCO1	FYVE and coiled-coil domain-containing protein 1
GABARAP	gamma-aminobutyric acid receptor-associated protein
GAP	GTPase activating proteins
GDF	GDP dissociation inhibitor-displacement factor
GDI	GDP dissociation inhibitor
GDNF	Glial cell-derived neurotrophic factor
GDP	guanosine diphosphate
GEF	guanine nucleotide exchange factor
GFP	green fluorescent protein
GLT-1	glutamate transporter 1
GTP	Guanosine triphosphate
H_CT	C-terminal region of the heavy chain of the tetanus toxin
HDAC6	histone deacetylase 6
HEK	Human embryonic kidney
HMGB1	high-mobility group box 1
HOPS	homotypic fusion and sorting complex
HSP	hereditary spastic paraplegia
IBMPFD	inclusion body myopathy with Paget disease of bone and frontotemporal dementia
IF	immunofluorescence
IFN	interferon
IFNβ	interferon beta
IGF-1	insulin-like growth factor-1
IKKe	Inhibitor of Nuclear Factor Kappa B Kinase Subunit Epsilon
iNeurons	induced neurons
iPSC	induce pluripotent stem cells

IRF3	interferon regulatory factor 3
JIP	c-Jun N-terminal kinase (JNK)-interacting protein
JNK	c-Jun N-terminal kinase
KD	kinase domain
KIFs	Kinesins Gene Family
KLC	kinesin light chain
LAMP1	lysosomal-associated membrane protein 1
LAMP2	lysosomal-associated membrane protein 2
LAMP2A	lysosome-associated membrane glycoprotein 2A
LC3	microtubule-associated protein light chain 3
LIR	LC3 interacting region
LIS1	lissencephaly 1
LMW	low molecular weight
LPS	lipopolysaccharide
LRRK1	Leucine-rich repeat kinase 1
LRRK2	Leucine-rich repeat kinase 2
MAP2	microtubule-associated protein 2
MAPK	mitogen-activated protein kinases
MAPs	microtubule-associated proteins
MAVS	mitochondrial antiviral-signalling protein
MCT1	monocarboxylate transporter 1
MDA5	melanoma differentiation-induced protein 5
MEFs	mouse embryonic fibroblasts
MEM	Minimum Essential Medium
MIRO	mitochondrial Rho
MN	motor neuron
MND	motor neuron disease

mRNPs	messenger ribonucleoproteins
mTORC1	mammalian target of rapamycin complex 1
MVB	multivesicular bodies
NADPH	nicotinamide adenine dinucleotide phosphate oxidase
NAK	NF-κB-activating kinase
NAP1	NF-kB activating kinase associated protein 1
NDP52	nuclear dot protein 52 kDa
NF-κB	nuclear factor kappa-light-chain-enhancer of activated B cells
NGF	nerve growth factor
NIN	Ninein
NINL	Ninein-like protein
NMJ	neuromuscular junction
NT-3	neurotrophin 3
NT-4/5	neurotrophin 4/5
Nude	nuclear distribution E
Nudel	Nuclear distribution protein nudE-like 1
NUPS	Nucleoporins
OA	oligomycin A/antimycin A
ORD	oxysterol binding protein-related domain
ORP1L	oxysterol-binding protein-related protein 1L
$p75^{NTR}$	p75 neurotrophin receptor
PH	pleckstrin homology
PINK1	PTEN-induced kinase 1
PKA	protein kinase A
PLS	primary lateral sclerosis
PMA	progressive muscular atrophy
poly I:C	polyinosinic:polycytidylic acid

PRRs	pattern-recognition receptors
PtdIns(3)P	phosphatidylinositol 3 phosphate
PTEN	PtdIns(3,4,5)trisphosphate 3-phosphatase and dual-specificity protein phosphatase
R-DPRs	arginine-containing dipeptide repeats proteins
Rab11-FIP3	Rab11 family-interacting protein 3
Rabex-5	Rabaptin-5-associated exchange factor for Rab5
RabGGT	Rab geranylgeranyl transferase
RAN	repeat-associated non-AUG
REP	Rab escort protein
RIG-1	retinoic acid-inducible gene I
RILP	Rab-interacting lysosomal protein
RNA	ribonucleic acid
rRNA	ribosomal RNA
sALS	sporadic amyotrophic lateral sclerosis
SEM	standard error of the mean
shRNA	short hairpin RNA
SINTBAD	TANK-binding kinase 1-binding protein 1
SKIP	SifA and kinesin-interacting protein
SMCR8	Smith-Magenis syndrome chromosomal region candidate gene 8
SMN	survival of motor neuron
SOD1	superoxide dismutase 1
STING	stimulator of interferon genes
TANK	TRAF Family Member Associated NF-κB Activator
TBC	Tre-2/Bub2/Cdc16
TBK1	TANK-binding kinase 1
TCEP	tris(2-carboxyethyl)phosphine

TDP-43	TAR DNA-binding protein 43
TFEB	transcription factor EB
TGN	trans-Golgi network
TLR3	Toll-like receptor 3
TLR4	Toll-like receptor 4
TMRE	tetramethylrhodamine ethyl ester
TRAK1	trafficking kinesin-binding protein 1
TRAK2	trafficking kinesin-binding protein 2
TRK	tropomyosin-related kinase receptors
Tyr-Tub	tyrosinated tubulin
UBA	ubiquitin-associated domain
ULD	ubiquitin-like domain
ULK1	Unc-51-like kinase 1
UPS	ubiquitin-proteasome system
USP32	ubiquitin-specific protease 32
VAP	vesicle-associated membrane protein
VPS34	vacuolar sorting protein 34
WB	western blotting
WIPIs	WD repeat domain phosphoinositide-interacting proteins
WT	wild type

Chapter 1

Introduction

1.1 ALS: an overview

Amyotrophic lateral sclerosis (ALS), also known as motor neuron disease (MND), is a progressive neurodegenerative disease characterized by both upper and lower motor neuron loss, leading to muscle weakness and wasting, paralysis and death (Hardiman et al., 2017). It has a median survival of 2-4 years, although current efforts are being made in order to predict prognosis at a personalised level (del Aguila et al., 2003; Westeneng et al., 2018). ALS annual incidence in the European population is 2-3 cases per 100,000 individuals (Logroscino et al., 2010), however, global studies suggest a non-uniform distribution. For instance, the incidence in South East Asia is lower (~0.8/100,000), whilst regions with relatively homogeneous populations, such as Scandinavia, Scotland and Ireland have a high incidence (~ 2.6/100,000) (Al-Chalabi and Hardiman, 2013; Chiò et al., 2013; Joensen, 2012). ALS incidence is expected to increase by almost 70% in the next 20 years, as a consequence of population aging, especially in developing countries (Arthur et al., 2016).

About 90% of ALS cases are of unknown aetiology, therefore they are classified as sporadic (sALS). The remaining ~10% belong to the familial ALS (fALS) group, since they are related to inherited mutations in genes with a wide spectrum of functions (Renton et al., 2014). In this regard, the characterisation of ALS genetics, as well as modern advances in neuropathology and imaging have demonstrated an involvement outside the motor system of the central nervous system (CNS) during ALS pathogenesis. In fact, up to 50% of patients exhibit cognitive symptoms and 5%-15% also develop frontotemporal dementia (FTD), to a point where both conditions are currently considered as the extremes of a disease spectrum (van Es et al., 2017).

In this introduction, we will briefly describe ALS clinical characteristics, present its genetic features, and the molecular mechanisms involved in the disease.

1.2 ALS: clinical manifestations

The clinical hallmark of “classical” ALS is the involvement of both upper motor neurons (UMN, located in the primary motor cortex) and lower motor neurons (LMN, located in the bulbar region and spinal cord). Patients present a progressive motor deficit that develops within weeks or months, and death most often result from respiratory failure. There is great variability regarding the region of onset, pattern of spreading, population of motor neurons affected and genetic factors involved, making this disease highly heterogenous (Swinnen and Robberecht, 2014).

In the classical manifestation, ALS starts in the fifth or sixth decade of life. Affected individuals can present predominantly UMN signs (pseudobulbar affect, hyperreflexia, hypertonia (resistance to passive movement) or spasticity (resistance to passive movement that is velocity dependent, higher resistance is exerted against faster passive movements)) or LMN signs (weakness, atrophy, fasciculation or hyporeflexia/areflexia). The disease onset is focal; however, it spreads locally or to neuroanatomically linked regions. Nevertheless, the oculomotor nuclei and Onuf’s nucleus remain unaffected, hence eye movement and sphincter control are preserved (van Es et al., 2017; Ravits and La Spada, 2009).

From the site of onset perspective, ALS can be classified as follows:

- **Bulbar onset**: About 1/3 of patients present bulbar onset, which starts with dysarthria (difficulties on articulation of speech), and that may be followed by dysphagia, tongue fasciculations and in some cases emotional lability. Bulbar-onset ALS used to be considered a different disease, termed “progressive bulbar palsy”, but since that denomination refers to a phenotypic description already present in ALS, rather than a diagnostic, the term bulbar onset became widely accepted (Al-Chalabi et al., 2016). Bulbar onset ALS associates with shorter survival (2-3 years), and patients are prone to earlier respiratory disfunctions (Turner et al., 2010).

- **Spinal onset**: It affects around 60% of patients. UMN and LMN signs are usually present asymmetrically in the upper or lower limbs. This focal onset might seem patchy, however the disorder inevitably spreads in a fashion that hypothetically mirrors the progression at cellular level (Ravits and La Spada, 2009). Spinal onset ALS is a predictor of longer survival, compared to bulbar onset (Talbot, 2009).

- **Respiratory onset**: A small proportion of patients (3-5%) present with respiratory problems such as dyspnoea (shortness of breath) and weakness of diaphragm and neck flexors. The prognosis is poor, with a mean survival of 1.4 years (Shoesmith et al., 2007).

ALS diagnosis requires involvement of both UMN and LMN, however, there are restricted phenotypes affecting ~ 10% of patients, where just one population of motor neurons seems to be implicated. In this regard, from the motor neuron involvement perspective ALS can be considered as a spectrum disorder, with primary lateral sclerosis (PLS, pure UMN) on one end and progressive muscular atrophy (PMA, pure LMN) on the other (Kiernan et al., 2011). Below, some PLS and PMA features are presented:

- **Primary lateral sclerosis**: Patients present with slowly progressive spasticity, usually beginning in the lower limbs, which ascends and eventually reaches the arms and bulbar region. The boundary between PLS and ALS is diffuse, since it is not clear at disease onset whether the patient will develop LMN symptoms or not, but in general it is considered PLS if LMN signs are absent for more than 4 years (Gordon et al., 2006, 2009). PLS prognosis is significantly better than classical ALS, with patients having survival ranges of more than 10 years, and reduced mortality rates (Tartaglia et al., 2007).

- **Progressive muscular atrophy**: On the other end of the spectrum, PMA patients develop LMN signs (mainly weakness, atrophy, fasciculations and hyporeflexia) asymmetrically in distal limb muscles, which spread within months or years. Similar to the PLS-ALS distinction, the differentiation between pure LMN presentations and ALS is not straightforward, however, UMN features usually appear in the first 2 years during ALS progression. PMA patients have a slightly better prognosis than classical ALS cases (Liewluck and Saperstein, 2015).

Since the original description of ALS during the XIX century, the disease was considered a neurodegenerative disorder with pure motor neuron involvement. Nevertheless, over the last 20 years there has been increasing evidence regarding cognitive impairment, as well as clinical signs of frontotemporal dementia in ALS patients, consequently, ALS and FTD are currently considered part of the same pathological spectrum (Grad et al., 2017). Here, we briefly introduce some of the features from the ALS-FTD continuum:

- **ALS-FTD**: Around 50% of ALS patients have some degree of cognitive or behavioural symptoms, whilst the diagnostic criteria for FTD are met in ~ 15% of cases. On the other hand, up to 40% of FTD patients have a mild motor involvement and 12.5% develop ALS (Burrell et al., 2011; Lomen-Hoerth et al., 2002; Phukan et al., 2012).

In FTD, frontal and temporal areas of the brain show reduced volume and spongiform degeneration (vacuolation and gliosis) due to neuronal loss (Cairns et al., 2007). In addition, ALS-FTD patients also present degeneration in the substantia nigra, amygdala and subcortical gliosis (Strong et al., 2009). From the clinical perspective, FTD is divided in three categories: a behavioural (behavioural-variant frontotemporal dementia, or bv-FTD) and two language variants. ALS-FTD patients mostly present the behavioural variant, with marked changes in personality and behaviour, such as executive

dysfunction, apathy and disinhibition (Lillo and Hodges, 2009; Rabinovici and Miller, 2010).

Interestingly, neuropathological evidence about the ALS-FTD relationship has also been found, supporting the clinical manifestation of the spectrum. For instance, more than 95% of ALS cases and 50% of FTD cases present aggregates of TAR DNA-binding protein 43 (TDP-43) (Arai et al., 2006; Neumann et al., 2006). Additionally, the most common genetic cause of ALS and FTD, an expansion in the gene *C9ORF72*, can result in either disease separately, or the combination of both (DeJesus-Hernandez et al., 2011; Renton et al., 2011). This highlights the importance of characterising the genetic factors linked to ALS pathology, not only to expand the disease description, but also to understand the molecular mechanisms and propose further effective therapeutics targets. As a summary, the regions of the nervous system involved in ALS are depicted in Figure 1.1.

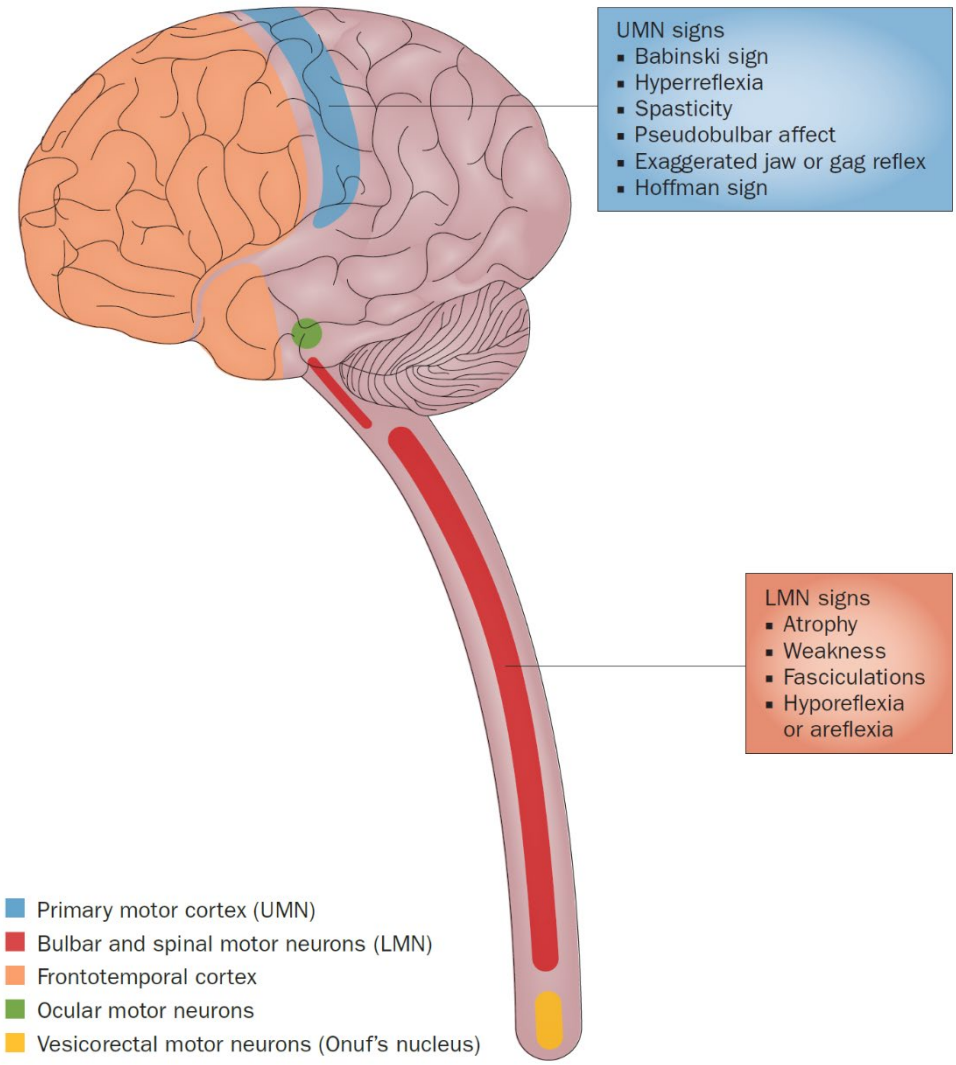

Figure 1.1. Preferential regions of the CNS involved in ALS. The main location of neuronal degeneration in the brain and spinal cord are depicted, as well as unaffected regions (oculomotor nuclei and Onuf's nucleus). Main signs derived from UMN and LMN dysfunction are also given. Image from: (Swinnen and Robberecht, 2014).

1.3 ALS: genetics

Our ability to understand the clinical features of ALS and to develop treatments crucially depends on our knowledge of the genetic causes and the molecular mechanisms they affect. The first ALS-associated mutation reported was found on *SOD1* in 1993 (Rosen et al., 1993), however the identification of new gene variants was rather slow, until next generation sequencing techniques were widely available. There are currently >30 ALS-linked genes, and their analysis shows the disease is a complex genetic disorder

associated with rare variants, some of them with incomplete penetrance, which might mask them as sporadic cases (Murphy et al., 2017). Additionally, there is evidence for oligogenic inheritance (phenotypic traits determined by more than one gene), and for gene variations in untranslated regions, making them undetectable in whole exome sequencing (Mejzini et al., 2019; Morgan et al., 2017). Despite these difficulties, we currently know the genetic cause of ~70% of fALS, but only ~10% of the sporadic cases. Interestingly, pathogenic variants in four genes (*SOD1*, *TARDBP*, FUS and *C90RF72*) account for the majority of fALS-linked causing mutations (Renton et al., 2014; Zou et al., 2017). Here, we will present the main ALS-associated genes, before discussing the molecular pathway affected by their genetic products.

- ***SOD1***: This was the first ALS-linked gene described, opening the way to a molecular characterisation of the disease (Rosen et al., 1993). *SOD1* encodes superoxide dismutase 1, a homo-dimeric metalloenzyme that catalyses the conversion of the radical superoxide to hydrogen peroxide and molecular oxygen, therefore it is relevant for the oxidative stress response (McCord and Fridovich, 1969). Up to date, there are more than 180 different *SOD1* mutations distributed throughout its sequence, accounting for ~15% of fALS in European populations (~30% in Asian populations) and ~2% of sALS (Zou et al., 2017). There is great variability on the disease severity linked to each mutation, for instance, the most common North American *SOD1* variant, A4V, is associated to aggressive limb-onset ALS, with death within 12-18 months, whilst the D90A variant, the most common worldwide, can be inherited as a dominant or recessive trait, although it is mostly recessive, in which case it associates to slow progression and extended survival (Juneja et al., 1997; Pansarasa et al., 2018).

Shortly after the *SOD1* mutation was reported, a *Sod1* knockout mouse model was generated. Strikingly, it did not display any ALS-related phenotype, suggesting SOD1 pathology is a toxic gain of function, rather than a loss of function (Reaume et al., 1996).

Additional mice models have been designed, with *Sod1* G93A being one of the most studied. Albeit carrying an uncommon mutation, the G93A model was the first one exhibiting a motor neuron phenotype (Gurney et al., 1994), hence the wide interest.

One of the hallmarks of *SOD1* ALS is the formation of insoluble SOD1 aggregates in motor neurons. Nevertheless, other protein aggregates commonly found in familial and sporadic ALS cases, such as TDP-43 and FUS (Fused in sarcoma), are absent. In addition, SOD1 inclusions are not detected in sALS. Based on this, *SOD1* ALS is now considered a particular form of the disease, distinct from all other ALS types (Da Cruz et al., 2017; Mackenzie et al., 2007).

- ***TARDBP***: This gene encodes the DNA/RNA binding protein TDP-43. Dominant mutations appear in ~5% of fALS and ~1% of sALS (Ingre et al., 2015; Sreedharan et al., 2008). Crucially, ubiquitinated TDP-43 inclusions are found in >95% of ALS cases and in ~50% of FTD cases without ALS involvement. Other post-translational modification also associate with pathogenic TDP-43 (Buratti, 2018). These aggregates appear even when *TARDBP* is not mutated, and constitute a hallmark of ALS (Arai et al., 2006; Neumann et al., 2006). TDP-43 shuttles between the nucleus and the cytoplasm, and participates on the regulation of gene expression at many levels, such as gene transcription, RNA splicing, synthesis of non-coding RNAs, and RNA stability, transport and translation (Ederle and Dormann, 2017). *TARDBP* mutations cluster in the C-terminal region, which is involved in ribonucleoprotein binding and splicing. Since TDP-43 intracellular localisation is mostly nuclear, it is still debatable whether its pathogenic effect arises from a nuclear loss of function or a cytoplasmic toxic gain or function (or a combination of both). In this regard, the characterisation of *TDP-43* mice models showed that overexpressing human wild-type (WT) TDP-43 is sufficient to trigger motor neuron degeneration (Mitchell et al., 2015). On the other hand, TDP-43 loss of function effect has been addressed using heterozygous models, since its complete ablation, either

constitutive or inducible, is lethal. The evidence from TDP-43 heterozygous mice showed these animals display motor deficits, but without motor neuron loss or reduction in TDP-43 expression (Kraemer et al., 2010). This highlights the fine-tuned regulation of TDP-43 expression levels, as the protein expression is self-regulated (Avendaño-Vázquez et al., 2012).

- ***FUS***: Pathogenic variants of *FUS*, which encodes fused in sarcoma (FUS), account for ~6% of fALS cases and ~1% of sALS cases (Kwiatkowski et al., 2009; Vance et al., 2009). FUS is an RNA binding protein which shares several functions with TDP-43 (although targeting different RNAs), highlighting the relevance of RNA metabolism in ALS. *FUS* mutations cluster near its RNA-binding domain and nuclear localisation signal (Vance et al., 2013), and some mutations associate with early onset/juvenile ALS (Gromicho et al., 2017). *FUS* ALS is characterised by pathological FUS aggregates, without TDP-43 inclusions, although FUS mislocalisation in the cytoplasm seems to be a widespread phenomenon during ALS (Tyzack et al., 2019).

FUS regulates gene transcription, pre-mRNA splicing, mRNA transport and translation, therefore, just like TDP-43, it is not clear if the disease mechanism involves a loss or gain of function (Birsa et al., 2019). Whilst *FUS* knock out mouse does not display an ALS phenotype, knocking down the Drosophila homologue (*Cabeza*) induce neuronal degeneration and motor defects (Kino et al., 2015; Sasayama et al., 2012). On the other hand, overexpressing WT FUS in mice is sufficient to generate motor neurodegeneration. Besides, aggregation prone FUS induce neuronal toxicity even when it is unable to bind RNA, further supporting a toxic gain of function (Mitchell et al., 2013; Shelkovnikova et al., 2013).

- ***C9ORF72***: The most common genetic cause of ALS, an intronic hexanucleotide repeat (GGGGCC) in *C9ORF72* was discovered almost ten years ago (DeJesus-Hernandez et

al., 2011; Renton et al., 2011). In most people the number of repeats range between 5-10, whilst ALS patients have from hundreds to thousands. Recent evidence shows carrying >24 repeats is enough to exert pathogenicity (Iacoangeli et al., 2019). The expanded repeats, located between exons 1a and 1b, are the cause of ~40% of fALS cases and ~7-9% of sALS cases in European populations (Goldstein et al., 2018). As mentioned before, *C9ORF72* intronic expansion links ALS to FTD at the molecular level. In fact, ~25% of familial FTD patients carry this mutation (Majounie et al., 2012).

At least three hypotheses have emerged to explain the consequences of *C9ORF72* intronic expansion. Since the protein carries a DENN (differentially expressed in normal and neoplastic cells) domain, which is commonly present in guanine nucleotide exchange factors (GEFs) for Rab GTPases (Marat et al., 2011), it was proposed that C9ORF72 loss of function could impact on intracellular trafficking. However, C9ORF72 knock out mice do not develop a motor phenotype, although there is an abnormal immune response (Koppers et al., 2015). Alternatively, it has been proposed that *C9ORF72* mRNA containing the expanded repeats accumulates in the nucleus forming RNA foci, and it is possible that these foci sequester additional essential RNAs and RNA-associated proteins, inducing a more general defect (Todd and Petrucelli, 2016). Lastly, the hexanucleotide expansion has been shown to undergo repeat-associated non-AUG (RAN) translation, in which the sequence is translated in all reading frames and from both the sense and antisense strands. *C9ORF72* RAN translation generate five different dipeptide repeats: GA, GR, PR, PA and GP (Gendron et al., 2013; Mori et al., 2013). In particular, dipeptide repeats containing arginine induce neuronal toxicity (Mizielinska et al., 2014). One of the possible downstream effects from arginine-containing dipeptide repeats is a deleterious effect on components of the nuclear pore complex, suggesting a negative impact on nucleocytoplasmic transport (Freibaum et al., 2015; Jovičić et al., 2015).

There is a growing list of ALS-related genes that appear with a lower frequency than the four genes previously mentioned. However, they are crucial to understand the disease mechanisms, and to highlight the molecular pathways involved. Some of the ALS causative genes involved in RNA metabolism are:

- *ANG*: it encodes Angiogenin, a ribonuclease which stimulates cell growth through the promotion of ribosomal RNA (rRNA) transcription. Angiogenin is sequestered in the cytoplasm during stress conditions, and its activity is downregulated in ALS pathology (Greenway et al., 2006; McLaughlin et al., 2010).

- ***MATR3***: it encodes Matrin 3, a DNA and RNA binding protein with functions related to transcription, RNA processing, mRNA transport and stability. Matrin 3 interacts with TDP-43, FUS, and forms cytoplasmic inclusions in the spinal cord of some ALS patients (Johnson et al., 2014; Yamaguchi and Takanashi, 2016).

- ***HNRNPA1***: it encodes heterogeneous nuclear ribonucleoprotein A1 (hnRNPA1), an RNA-binding protein with roles in transcription, mRNA stabilisation, transport and translation. Mutations in the low complexity domain of hnRNPA1, as well as in the closely related hnRNPA2/B1, increase their incorporation into membraneless organelles, such as stress granules (Fifita et al., 2017; Kim et al., 2013).

- ***SETX***: It encodes Senataxin, a DNA/RNA helicase associated with juvenile-onset, slow progressing ALS, which overlaps with certain types of ataxia and hereditary motor neuropathy (Chen et al., 2004; Hirano et al., 2011). Despite lacking a low complexity domain, *SETX* ALS mice models show mislocalised cytoplasmic TDP-43 and increased number of stress granules (Bennett et al., 2018).

- ***TAF15***: it encodes TATA-box binding protein associated factor 15, an RNA-binding protein which shares common RNA targets with FUS (Kapeli et al., 2016). Normally located in the nucleus, it mislocalises to granular cytoplasmic aggregates in *TAF15* ALS and sALS (Ticozzi et al., 2011).

- ***EWSR1***: it encodes Ewing sarcoma breakpoint region 1, and similar to *TAF15*, it is an RNA-binding protein whose ALS mutant variants accumulate in cytoplasmic inclusions (Couthouis et al., 2012).

Some of the ALS causative genes involved in cytoskeletal dynamics and intracellular transport are:

- ***DCTN1***: it encodes the p150^{Glued} subunit of dynactin, a component of the retrograde motor complex dynein-dynactin. *DCTN1* mutations have been reported in ALS and FTD cases (Münch et al., 2005; Puls et al., 2003). The expression of the ALS variant G59S, which reduced p150^{Glued} affinity for microtubules, inhibited vesicular transport in neurons and induced distal axonal degeneration (Laird et al., 2008).

- ***KIF5A***: It encodes the anterograde motor kinesin family member 5A (KIF5A). *KIF5A* mutations had been reported previously in hereditary spastic paraplegia (HSP) and Charcot-Marie-Tooth (CMT) disease. However, in these pathologies the mutations affect the motor domain, whilst ALS-linked variants cluster in the C-terminal region, which is involved in cargo binding (Brenner et al., 2018; Nicolas et al., 2018).

- ***TUBA4A***: this gene encodes Tubulin α4a, a structural component of microtubules. Functional experiments suggest the mutations destabilise the microtubule network (Smith et al., 2014).

- ***PFN1***: it encodes the actin-binding protein Profilin-1. *PFN1* mutations identified in ALS patients highlight the involvement of the actin cytoskeleton in the disease (Wu et al., 2012). The mechanism remains largely unknown.

- ***SPG11***: mutations in this gene, encoding Spatacsin, are linked to juvenile-onset ALS, as well as HSP and CMT (Montecchiani et al., 2016; Orlacchio et al., 2010). *SPG11* mutations reduce anterograde vesicular trafficking, and interestingly, also disrupt cholesterol trafficking and ganglioside clearance from lysosomes (Boutry et al., 2018, 2019; Pérez-Brangulí et al., 2014).

- ***ANXA11***: this gene encodes the calcium-dependent phospholipid-binding protein Annexin A11. Mutations in this gene cluster in its N-terminal region, which is an hydrophobic and disordered low complexity domain that binds several partners (Smith et al., 2017)

- ***ALS2***: it encodes alsin, a GEF for Rab5. Mutations in *ALS2* are associated with juvenile-onset ALS (Hadano et al., 2001; Yang et al., 2001), and disrupt endosomal motility and AMPA receptor trafficking. Alsin mutations phenocopy the overactivation of the small GTPase Rab5, which regulates early endosome formation and trafficking (Lai et al., 2006, 2009).

- ***CHMP2B***: it encodes charged multivesicular body protein 2b (CHMP2B), a member of the endosomal complex required for transport-III (ESCRT-III). This complex exerts membrane deformation functions in many intracellular trafficking processes, such as multivesicular bodies (MVB) formation and autophagy (Odorizzi, 2015). *CHMP2B* mutations found in ALS and FTD disrupt the endolysosomal pathway and induce the accumulation of autophagosomes containing ubiquitinated proteins (Krasniak and Ahmad, 2016; Parkinson et al., 2006).

- **PRPH**: this gene encodes the type III intermediate filament peripherin. Peripherin is found with other neurofilament proteins forming inclusion in motor neurons of ALS patients (Corbo and Hays, 1992). Peripherin expression is upregulated during ALS, and mice overexpressing peripherin display motor neuron death (Beaulieu et al., 1999), whilst peripherin knockdown inhibits TDP-43 and FUS accumulation at distal neurites (Muresan and Ladescu Muresan, 2016). Interestingly, Rab7 is a peripherin binding partner which regulates its soluble/insoluble ratio (Cogli et al., 2013).

Some of the ALS causative genes involved in protein homeostasis are:

- ***VCP***: it encodes valosin-containing protein (VCP/p97), an AAA-type ATPase involved in a multi-systemic proteinopathy known as inclusion body myopathy with Paget disease

of bone and frontotemporal dementia (IBMPFD), as well as ALS (Johnson et al., 2010). VCP facilitates the proteasomal degradation of large ubiquitinated complexes, and is required for intracellular clearance by autophagy (van den Boom and Meyer, 2018; Ju et al., 2009).

- **OPTN**: this gene encodes the autophagy receptor Optineurin, involved in the clearance of protein aggregates, nuclear factor kappa B (NF-κB) signalling, and mitophagy among other functions (Ryan and Tumbarello, 2018; Wong and Holzbaur, 2014). ALS mutations in *OPTN* negatively affect these processes, as well as the crosstalk between them (Markovinovic et al., 2017; Maruyama et al., 2010).

- ***SQSTM1***: it encodes the autophagy receptor p62/SQSTM1 (Sequestosome-1). p62 mutations have been described in ALS and FTD (Fecto et al., 2011; Rubino et al., 2012), where they impair p62 association to autophagosomes (Goode et al., 2016).

- ***UBQLN2***: it encodes Ubiquilin-2, a member of the ubiquitin-proteasome system which delivers ubiquitinated proteins to the proteasome for degradation (Zhang et al., 2014). In *UBQLN2* ALS cases, Ubiquilin-2 inclusions that are also positive for TDP-43, FUS, optineurin and p62 are detected (Deng et al., 2011; Williams et al., 2012).

- ***DNAJC7***: The most recent ALS-related gene discovered (at the time of writing), it encodes the heat-shock protein DNAJC7, which is involved in protein quality control and protein clearance. Fibroblast from ALS patients show reduced DNAJC7 expression, suggesting a loss of function (Farhan et al., 2019).

- ***TBK1***: it encodes TANK-binding kinase 1 (TBK1), also known as NAK or T2K. This kinase phosphorylates p62, Optineurin, and participates in the NF-κB pathway (Ahmad et al., 2016). *TBK1* pathogenic variants have been reported in both ALS and FTD (Cirulli et al., 2015; Freischmidt et al., 2015; Pottier et al., 2015). Given its relevance for the project, we will discuss TBK1 in more detail later.

Here we have presented most ALS-related genes up to date. For a complete list of ALS genes and risk factors, we refer the reader to recent reviews (Hardiman et al., 2017; Mejzini et al., 2019).

1.4 ALS: molecular mechanisms

The wide range of clinical manifestations and the variety of genes involved exemplify the heterogenicity of ALS. There is, however, a degree of convergence on the cellular mechanisms underlying ALS pathogenesis, which culminate in neuronal death. As suggested by the list of genes presented in section 1.3, the main ALS molecular mechanisms proposed can be classified as dysregulation of RNA metabolism, alterations in proteostasis, and defects in axonal transport, as well as the contribution of glial cells in a non-cell autonomous manner. A scheme of these mechanisms is depicted in Figure 1.2.

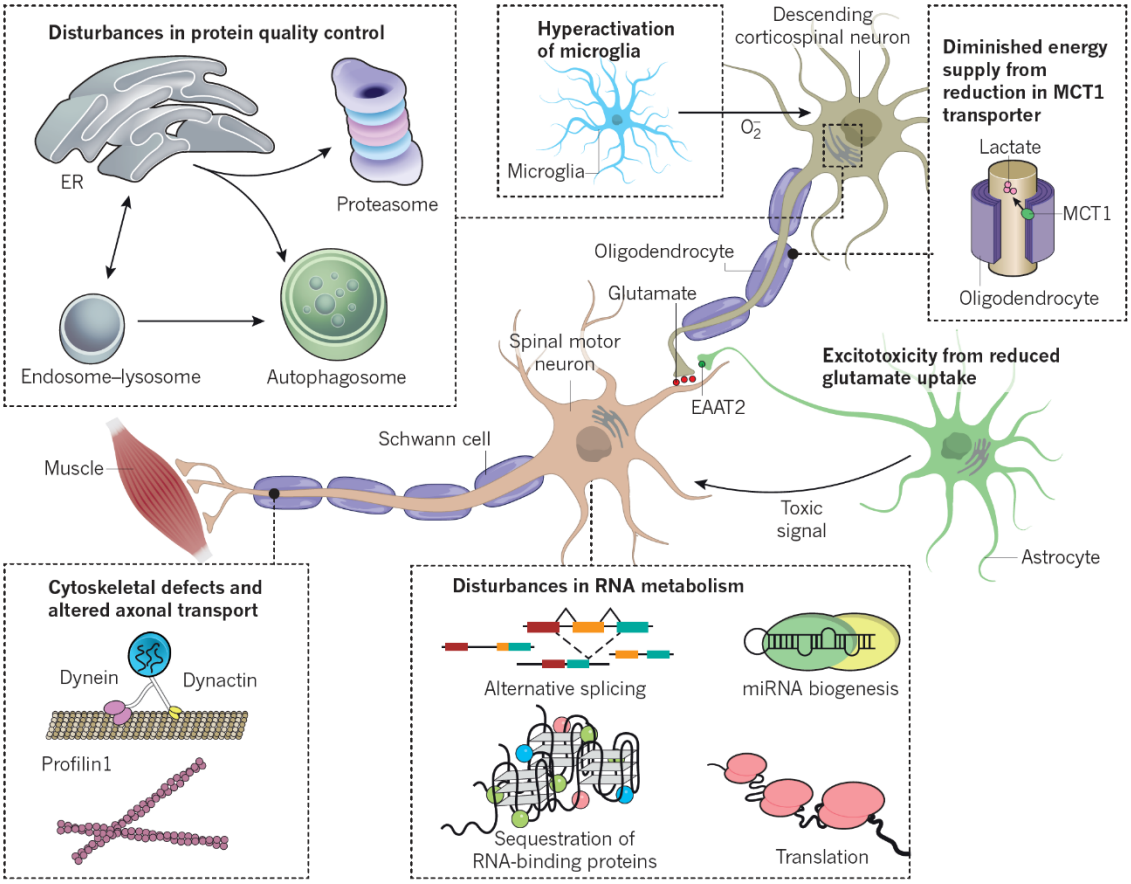

Figure 1.2. Molecular mechanisms of ALS. The main cellular processes affected during ALS are shown. This includes disturbances in proteostasis, alteration in RNA metabolism, cytoskeletal/axonal transport dysfunctions, as well as the contribution of non-neuronal cells. Image from: (Taylor et al., 2016)

The contribution of glial cells to ALS pathogenesis is relevant to fully understand the disease, however their involvement has been studied to a lesser extent than the other mechanisms. Therefore, we will discuss non-cell autonomous mechanisms first, and then we will approach disruption in RNA metabolism, disruption in proteostasis and defects in axonal transport.

Non-cell autonomous mechanisms

Despite being a pathology characterised by motor neuron death, the role of glial cells during ALS is now widely recognised. Evidence from a chimeric mouse in which all motor neurons express high levels of mutant $SOD1^{G37R}$, but only a proportion of non-neuronal cells does, showed that the presence of non-neuronal WT cells delays disease onset

and progression (Yamanaka et al., 2008a). In addition, reducing the expression of $SOD1^{G37R}$ either in microglia or astrocytes slows late disease progression (Boillée et al., 2006; Yamanaka et al., 2008b). These observations have been complemented by graft experiments, for instance, the transplantation of WT human induced pluripotent stem cells (iPSC)-derived glial-rich neural progenitors in the spinal cord of $SOD1^{G93A}$ mice improves motor function and survival (Kondo et al., 2014). Conversely, transplanting $SOD1^{G93A}$ glial-restricted precursor cells (which differentiate to astrocytes) into the spinal cord of WT rats induce ubiquitin-positive aggregates and motor neuron death (Papadeas et al., 2011). Graft experiments on mice using iPSC from sALS patients show they not only differentiate to astrocytes, but also replace the endogenous astrocytes, induce ubiquitin-positive aggregates and motor dysfunction (Qian et al., 2017). This is intriguing, since it suggests the fibroblast from sporadic patients used to generate the iPSCs already had pathological features, which were retained during the differentiation process. Microglial role during ALS are closely linked to neuroinflammation. Microglia expressing mutant SOD1 exhibit a neuroprotective (M2/alternatively-activated) phenotypic state at disease onset, whilst end-stage microglia show a toxic (M1/classically-activated) profile, releasing more neurotoxins and less insulin-like growth factor-1 (IGF-1) (Liao et al., 2012; Xiao et al., 2007). In fact, mutant SOD1 binds Rac1, a GTPase member of the nicotinamide adenine dinucleotide phosphate oxidase (NADPH oxidase) complex, leading to enhanced production of superoxide radical and glial toxicity (Harraz et al., 2008).

Oligodendrocytes myelinate axons in the CNS and provide neurons with energy support through the transport of lactate. In this regard, $SOD1^{G93A}$ mice and sALS patients show reduced expression of the lactate transporter monocarboxylate transporter 1 (MCT1), which induces motor neuron toxicity and axonopathy in this mouse model (Lee et al., 2012). Oligodendrocyte precursor cells are also affected during ALS, as they fail to

complete their differentiation process, resulting in progressive demyelination (Kang et al., 2013).

Astrocytes support motor neurons in a wide range of homeostatic functions, such as neurotrophic factor secretion, ion buffering, and neurotransmitter recycling, among many others (Yamanaka and Komine, 2018). Astrocytic expression of excitatory amino acid transporter 2 (EAAT2, also known as glutamate transporter 1 (GLT-1)) is reduced in SOD1 murine models and sALS patients, therefore, surplus glutamate accumulates in the synapse and triggers excitotoxicity (Bruijn et al., 1997; Howland et al., 2002; Rothstein et al., 1995). Additionally, astrocytes expressing $SOD1^{G93A}$ lose the ability to promote AMPA receptor subunit GluR2 expression in motor neurons, consequently, those receptors become permeable to Ca^{2+}, enhancing the excitotoxic effect (Van Damme et al., 2007). Lastly, astrocytes derived from ALS mouse models or sALS patients exert a toxic effect on motor neurons in co-cultures *in vitro*, however the toxic factor remains elusive (Di Giorgio et al., 2007; Haidet-Phillips et al., 2011; Marchetto et al., 2008; Nagai et al., 2007).

Disruption in RNA metabolism

Many ALS-related genes encode proteins involved in RNA metabolism, including three of the most frequently mutated genes (*C9ORF72*, *FUS* and *TARDBP*). Whilst dysfunctions in this process are recognised as an important ALS mechanism, the dichotomy “gain vs loss of function” remains, due to the plethora of effects carried out by these proteins.

One crucial mechanism regulating RNA metabolism is the formation of membraneless organelles containing RNA and associated proteins, such as processing bodies (P-bodies) and stress granules (Spector, 2006). Stress granules are constituted by pools of messenger ribonucleoproteins (mRNPs) stalled in translation initiation, establishing a reversible way to preserve energy during stress conditions by limiting translation

(Anderson and Kedersha, 2008). Stress granules contain an internal stable substructure referred as “core”, and a surrounding, more dynamic shell (Souquere et al., 2009). They assemble through conventional protein-protein interactions between mRNA binding proteins, and through dynamic interactions between protein low complexity domains. These promiscuous low complexity domain interactions form a network which concentrate the granule in a separate phase, a phenomenon termed liquid-liquid phase separation (Protter and Parker, 2016). In this regard, ALS-mutations in the low complexity domain of TDP-43, FUS, hnRNPA1 and hnRNPA2/B1 promote their localisation into stress granules, altering their assembly/disassembly dynamic (Bosco et al., 2010; Liu-Yesucevitz et al., 2010; Molliex et al., 2015). For example, mutant TDP-43 reduces stress granules disassembly, whilst mutant FUS increases their number and size (Birsa et al., 2019). At least three models have emerged to explain the impact of persisting stress granules (Li et al., 2013): 1) increased TDP-43 and FUS concentration on granules promote their aggregation into toxic beta-amyloid fibrils. 2) many mRNAs and translation initiation factors are sequestered on stress granules, reducing their availability at specific locations which rely on local translation, for instance, TDP-43 regulates translation of Futsch, the Drosophila homologue of microtubule associated protein 1B, at the neuromuscular junction (NMJ), hence, Futsch neuroprotective effect on NMJs is lost after mutant TDP-43 expression in motor neurons (Coyne et al., 2014). 3) persistent assembly of stress granules might act as a cytoplasmic sink, mobilising nuclear RNA binding proteins to the cytosol. This nuclear depletion, together with ALS-linked mutation on TDP-43 and FUS nuclear localisation signal, point towards a nuclear loss of function. Since many ribonucleoproteins sequestered in stress granules participate on transcription, alternative splicing and synthesis of regulatory microRNAs, the motor neuron transcriptome becomes significantly altered. For example, up to one-third of the transcriptome is altered in an ALS mouse model carrying TDP-43^{Q331K} (Arnold et al., 2013). Thus, many factors required for neuronal survival are expected to be

affected. One example of this is the premature polyadenylation of *STATHMIN-2* mRNA, which emerges from a cryptic site deregulated in TDP-43 knockdown conditions. Stathmin-2 regulates microtubule dynamics and promotes axonal regeneration in vitro, hence, reduced TDP-43 nuclear function result in a truncated, non-functional Stathmin-2 variant which exacerbates neuronal vulnerability to degeneration (Melamed et al., 2019).

C9ORF72 roles in RNA metabolism were presented in section 1.3. They follow a similar pathological pattern, i.e. RNA sequestration into aggregates (in nuclear RNA foci) and disruption of nucleocytoplasmic transport, in this case by alterations in components of the nuclear pore (Kim and Taylor, 2017). The nuclear pore complex is a ~ 110 MDa structure composed of 30 different proteins termed nucleoporins (Nups), which are present in multiple copies. According to their position within the pore, Nups are classified in seven categories: 1) cytoplasmic filament Nups, 2) nucleocytoplasmic and cytoplasmic ring Nups, 3) inner ring complex Nups, 4) transmembrane Nups, 5) central/channel phenylalanine-glycine rich (FG) Nups, 6) nuclear basket Nups and 7) adaptor Nups. Nucleocytoplasmic and cytoplasmic ring Nups, together with inner ring Nups form a scaffold that supports the central channel pore (Hoelz et al., 2016). FG-Nups forming the central pore contain low complexity domains projected towards the channel inner surface. Recent evidence shows FG-Nups undergo liquid-liquid phase separation, forming liquid droplets which retain the pore filtering properties (Celetti et al., 2020). Nucleocytoplasmic transport is regulated by nuclear transport receptors from the karyopherin β family, known as importins and exportins, and by RanGTPases interacting with these receptors. C9ORF72 arginine-containing dipeptide repeats proteins (R-DPRs) bind importin β, inhibit its cargo loading, and impair the nucleocytoplasmic transport of importin α/β in HeLa cells (Hayes et al., 2020). In addition, R-DPRs bind FG-Nups and accumulate in the central channel of the nuclear pore, blocking nuclear import and export (Shi et al., 2017).

Disruption of proteostasis

Given the propension of many ALS-associated proteins to form insoluble aggregates, alterations in protein quality control are not completely unexpected. In fact, endoplasmic reticulum (ER) stress is recognised as a transversal mechanism implicated in ALS (Rozas et al., 2017). Pioneering studies showed $SOD1^{G93A}$ expression inhibits ER-associated degradation (ERAD), and reported ER stress as one of the earliest pathological ALS signatures (Nishitoh et al., 2008; Saxena et al., 2009). In agreement with this, the two main protein clearance pathways, autophagy and the ubiquitin-proteasome system (UPS), are also disrupted in ALS.

Ubiquitination is used in both clearance pathways as a degradation signal, although in different ways. In the UPS system, ubiquitinated proteins are recognised and degraded by the proteasome, a multi-catalytical protease complex formed by a core 20S particle and a regulatory 19S particle (Dikic, 2017). ALS-mutated SOD1 expression reduces proteasome activity in motor neurons, as well as the levels of 20S subunit in mouse lumbar spinal cord (Kabashi et al., 2004; Urushitani et al., 2002). Besides, proteins facilitating the delivery of ubiquitinated proteins to the proteasome, such as VCP and Ubiquilin 2, are also affected in ALS. VCP is a ubiquitin-dependent segregase which extract proteins from membranes and large complexes to target them for proteasomal degradation. The ALS-associated VCP mutation in Asp^{592} impairs its interaction with the 20S subunit of the proteasome, reducing degradation of substrates (Barthelme et al., 2015). Similarly, ALS-mutated Ubiquilin 2 retains the ability to bind polyubiquitinated proteins, but fails to associate with the proteasome, resulting in impaired degradation of its cargoes (Chang and Monteiro, 2015).

Whilst the UPS mostly degrades short-lived, misfolded and damaged proteins, autophagy deals with long-lived proteins and larger components, such as protein aggregates and organelles (Kocaturk and Gozuacik, 2018). The material targeted for degradation eventually reach the lysosome, where it is hydrolysed by resident enzymes.

The route towards lysosomal degradation is not unique, as cargoes might be either engulfed into a double membrane autophagosome that then fuses with the lysosome (macroautophagy), or enter the lysosome directly through invagination in its membrane (microautophagy), or even be targeted to degradation by a chaperone complex, translocating into the lysosome assisted by a Lysosome-associated membrane glycoprotein 2A (LAMP2A) complex, in a process termed chaperone-mediated autophagy (Mizushima and Komatsu, 2011). The most frequently studied mechanism, and the one that has been described as affected during ALS pathology is macroautophagy, which here we refer to as autophagy. With the exception of one report studying chaperone-mediated autophagy in blood cells from ALS patients, the involvement of this process, as well as microautophagy in ALS remain largely unexplored (Vicencio et al., 2020).

Autophagy can be classified as non-selective or selective. Non-selective autophagy is a cellular response to nutrient deprivation, where components of the cytoplasm are taken up by the nascent phagophore (the precursor of the autophagosome) in a non-specific way. In contrast, selective autophagy removes defined cellular material by physically linking the autophagosome membrane to cargoes through autophagy receptors (Gatica et al., 2018). Several selective autophagy pathways has been characterised and named up to date, such as protein aggregate degradation (aggrephagy), pathogen degradation (xenophagy) and mitochondrial degradation (mitophagy) among many others (Stolz et al., 2014).

From the molecular perspective, autophagy is a tightly controlled mechanism coordinated by a set of core autophagy-related proteins (ATGs), initially characterised in yeast (Mizushima et al., 2011). Briefly, autophagosome initiation starts when stress signals such as starvation, hypoxia or ER stress activate the ULK complex, which is formed by Unc-51-like kinase 1 (ULK1), FAK Family Kinase-Interacting Protein Of 200

KDa (FIP200), ATG13 and ATG101. Activated ULK1 triggers phagophore nucleation by phosphorylating components of the Beclin1-VPS34 complex. VPS34 (vacuolar sorting protein 34) is a class III phosphatidylinositol 3 kinase (PI3K), which promotes the production of phosphatidylinositol 3 phosphate (PtdIns(3)P) in a special structure on the ER membrane, called the omegasome. PtdIns(3)P recruit its effectors WD repeat domain phosphoinositide-interacting proteins (WIPIs) and zinc-finger FYVE domain-containing protein 1 (DFCP1), which in turn binds the ATG12-ATG5-ATG16L1 complex to the omegasome, initiating the phagophore expansion. The ATG12-ATG5-ATG16L1 complex act as an E3-Ubiquitin ligase-like in a pathway initiated by ATG7 (E1-like enzyme). This pathway, instead of ubiquitin, conjugates ATG8 family proteins to phosphatidylethanolamine resident in the phagophore membrane. There are 6 ATG8 family proteins in mammals, three from the microtubule-associated protein light chain 3 (LC3) family and three from the gamma-aminobutyric acid receptor-associated protein (GABARAP) family. The presence of LC3/GABARAP in the phagophore membrane is required for membrane elongation and closure. In addition, during selective autophagy, LC3/GABARAP bind autophagy receptors such as p62, optineurin and nuclear dot protein 52kDa (NDP52), which are associated to poly-ubiquitin chains in cargoes destined for degradation, hence sequestering the cargo into the elongating autophagosome (Alers et al., 2012; Dikic and Elazar, 2018; Lamb et al., 2013).

Monitoring starvation-induced autophagy through GFP-LC3B in different mouse tissues revealed to be organ-dependent, since autophagy was significantly upregulated in liver but not in brain (Mizushima et al., 2004). In agreement with this, recent evidence suggest that whilst starvation successfully induces autophagy in primary astrocytes *in vitro*, the effect in cultured hippocampal neurons is much milder, requiring starvation for longer periods, and reaching a less pronounced induction (Kulkarni et al., 2019). Despite starvation-induced autophagy seems to be ineffective in neurons, they do exhibit constitutive autophagy. Autophagosomes form in the distal axonal compartment of

dorsal root ganglion (DRG) neurons, in close proximity to DFCP1-positive subdomains of the ER. After their biogenesis, autophagosomes move retrogradely towards the cell body, concomitantly with their progressive acidification and maturation into autolysosomes (Maday and Holzbaur, 2014, 2016; Maday et al., 2012).

Several ALS-associated genes encode proteins involved in autophagy, and since one of the hallmarks of the disease is the presence of ubiquitinated protein aggregates in motor neurons, autophagy is considered to have a central role during ALS pathogenesis (Evans and Holzbaur, 2019). For instance, C9ORF72 binds the ULK1 complex and promotes its translocation to the nascent phagophore via Rab1, hence C9ORF72 depletion inhibits autophagy and induces p62 accumulation. This was supported by reduced basal levels of autophagy in induced neurons (iNeurons) from *C9ORF72* ALS patients (Webster et al., 2016). A second mechanism by which C9ORF72 impacts on autophagy initiation involves its interactor partner Smith-Magenis syndrome chromosomal region candidate gene 8 (SMCR8). The C9ORF72-SMCR8 complex acts as a guanine nucleotide exchange factor (GEF) for Rab8 and Rab39, which in turn interact with p62 and Optineurin, in what might be a mechanism for membrane delivery during phagophore elongation (Sellier et al., 2016; Yang et al., 2016). C9ORF72 roles on autophagy are not restricted to phagophore initiation, as it has been shown that symmetrically methylated FUS present in stress granules is recognised by a complex formed by survival of motor neuron (SMN), C9ORF72 and p62. This complex targets the stress granule for degradation by associating to LC3 in the autophagosome membrane (Chitiprolu et al., 2018). How this C9ORF72 loss of function impacts on *in vivo* ALS models remains to be explored, since *C9ORF72* knockout mouse lacks a motor phenotype (Koppers et al., 2015; O'Rourke et al., 2016).

ALS-associated mutations on autophagy receptors further support a role for this pathway in the disease. In this regard, p62 binds ALS-mutated SOD1 in an ubiquitin-independent

manner, targeting SOD1 for autophagy (Gal et al., 2009). Besides, ALS-linked p62^{L341V} is defective in LC3B recognition (Goode et al., 2016), whilst p62 genetic depletion worsens SOD1^{H46R} disease progression (Hadano et al., 2016). Similarly, the ALS-associated mutation optineurin^{E478G} abolish its recruitment to damaged mitochondria during selective mitophagy in HEK cells (Wong and Holzbaur, 2014). Several other optineurin mutations cluster on *OPTN* ubiquitin-associated domain (UBA), suggesting impaired binding to cargoes poly-ubiquitinated chains as a mechanism for inhibited delivery to autophagosomes (Nguyen et al., 2019). Interestingly, both p62 and optineurin are TBK1 substrates, with shared roles during induced mitophagy, which we will discuss later.

Altogether, this evidence points towards an involvement of autophagy during ALS pathology, however, its exact role is still unclear. This is better exemplified by the unexpected results obtained from autophagy inhibition through genetic ablation of ATG7 on SOD1^{G93A} mouse motor neurons. In this model, autophagy inhibition accelerates muscle denervation and the onset of tremor, but extends lifespan and reduces glial inflammation. In contrast, depletion of ATG7 in motor neurons of WT mice does not affect survival nor innervation, except for a small subset of vulnerable NMJs in the tibialis anterior muscle (Rudnick et al., 2017). This suggests a temporally regulated dual role for autophagy, i.e. protective at disease onset, but detrimental at later stages, with a clear non-cell autonomous component.

Defects in axonal transport

Their peculiar morphology challenges neurons to maintain an efficient communication system between the cell body and the axonal terminal. In this regard, axonal transport emerges as a mechanism for the delivery of intracellular component to the distal portion of the axon and vice versa. Axonal transport has been linked to many neurodegenerative diseases, and ALS is no exception (De Vos and Hafezparast, 2017; Sleigh et al., 2019).

We will describe the main components of axonal transport and then discuss evidence of their disfunction during ALS.

1.5 Axonal transport: the machinery

Supporting long distance intracellular transport underlies a network of microtubules, who provide the structure allowing movement of molecular motors and their associated cargoes.

Microtubules are long polymers formed by α- and β-tubulin heterodimers, which are incorporated into the microtubule growing end. Soluble heterodimers contain β-tubulin bound to guanosine triphosphate (GTP), and following binding to the microtubule end, GTP is hydrolysed, generating guanosine diphosphate (GDP) tubulin. This hydrolysis occurs with a delay, hence a cap of GTP-tubulin forms at the microtubule tip (Brouhard and Rice, 2018). This GTP cap has stabilising properties, and its loss leads to a rapid depolymerisation and shrinkage of microtubules, known as catastrophe. Nevertheless, this shrinking can be rescued, switching to microtubule growth. Therefore, microtubules exist in an equilibrium between catastrophe and growth, a property termed dynamic instability (Brouhard, 2015; Mitchison and Kirschner, 1984). Microtubules have a plus-end, where β-tubulin is exposed, and a minus-end, at which α-tubulin is exposed. The plus-end grows faster than the minus-end, whilst the minus-end undergoes catastrophe less frequently (Desai and Mitchison, 1997). The existence of these two ends is crucial for intracellular trafficking, since recognising the microtubule orientation allows for vectorial transport. This is especially relevant in neurons, where axonal and distal dendritic microtubules form an array with their plus-ends facing distally, whereas in proximal dendrites the polarity is mixed (Baas and Lin, 2011; Baas et al., 1988).

Microtubule organisation is regulated by a group of proteins called microtubule-associated proteins (MAPs). Based on their function, MAPs can be classified as molecular motors, severing/depolymerising MAPs, microtubule nucleator, end-binding

proteins and structural MAPs (Bodakuntla et al., 2019). Structural MAPs promote microtubule polymerisation and stabilisation (Sloboda et al., 1976), although the molecular mechanism is still unclear, since their disordered structure makes crystallisation difficult. Cryo-electron microscopy techniques have been used just recently, and only on the most studied structural MAP, the protein Tau (Kellogg et al., 2018). End-binding MAPs can be divided into microtubule minus-end targeting proteins and microtubule plus-end tracking protein (+TIPs), with the former being the group most frequently studied (Akhmanova and Hoogenraad, 2015; Akhmanova and Steinmetz, 2015). Some +TIPs recruit soluble tubulin dimers and increase microtubule polymerisation, whilst others remove tubulin from the microtubule end. One remarkable +TIP group is constituted by End-binding proteins (EBs), which are considered the main regulator of the +TIP network, as they recognise the GTP-cap autonomously and recruit additional factors to the microtubule tip (Nehlig et al., 2017). EB proteins are also an useful tool for determining microtubule orientation, as they form comet-like accumulations on plus-tips when studied in live cells (Mimori-Kiyosue et al., 2000).

Whilst microtubules provide the tracks for long-distance axonal transport, ultimately the movement of cargoes along the axons is carried out by molecular motors from the dynein and kinesin superfamilies. Actin-based myosins will not be discuss here, however, detailed information can be found elsewhere (Svitkina, 2018).

Kinesin superfamily comprises 45 genes in mammals (also known as KIFs), organised into 15 subfamilies, with kinesin-1, kinesin-2, kinesin-3 and kinesin-4 showing the highest involvement in axonal transport (Hirokawa et al., 2009; Lipka et al., 2016). Kinesins can be classified according to the position of their motor domain as N-terminal KIFs, middle-region KIFs and C-terminal KIFs. There are 3 M-KIFs and 3 C-KIFs in mammals, with all the rest corresponding to N-kinesins, which exert plus-end directed transport (Hirokawa and Tanaka, 2015). Hence, kinesins are the main anterograde molecular motor.

In general, the motor domain binds to microtubules and moves along their lattice by coupling ATP hydrolysis, whilst the C-terminal tail binds to cargoes, but since kinesins are such an heterogeneous family, there is space for diversification in terms of structure and cargo recognition (Hirokawa and Noda, 2008). For instance, kinesin-1 (encoded by *KIF5A*, *KIF5B*, and *KIF5C*) is formed by a dimer of kinesin heavy chains (KHC), and a dimer of kinesin light chains (KLC) that bridge KHC tail to cargoes, although there is evidence for efficient KIF5 KHC transport without KLC association (Sun et al., 2011). On the other hand, kinesin-2 can form homodimeric or heterotrimeric complexes, whilst kinesin-3 exists as a monomer that dimerises after binding its cargo (Sweeney and Holzbaur, 2018). Notably, kinesin-1 heterotetrameric complex (two KHC and two KLC) takes a folded, autoinhibited conformation that can be reverted by kinesin adaptors (Cross and Dodding, 2019).

In contrast to the extended kinesin superfamily, neurons rely on a single molecular motor, cytoplasmic dynein, to drive retrograde axonal transport. Cytoplasmic dynein is a large 1.4 MDa complex formed by six subunits, each one present in pairs. Dynein heavy chain (DHC) contains the motor domain, and its N-terminal end forms a tail by which both DHC homodimerize and recruit dynein intermediate chains (DIC), dynein light intermediate chains (DLIC) and three pairs of dynein light chains (DLC): Roadblock, LC8, and Tctex (Reck-Peterson et al., 2018). Most dynein functions in cells require an additional complex, the dynein activator dynactin (Schroer, 2004). Dynactin consist of a ~ 37 nm filament formed by 8 copies of the actin-related protein Arp1 and one copy of β-actin, flanked by accessory proteins and a “shoulder” which emerge from the filament barbed end. This shoulder is composed by two copies of $p150^{Glued}$ (150 K subunit, an orthologue of *Drosophila melanogaster Glued*), four copies of p50 dynamitin and two p24 subunits (Chowdhury et al., 2015). $p150^{Glued}$ interacts with DIC and also binds microtubules in a ATP-insensitive way (Waterman-Storer et al., 1995). The additional binding to

microtubules by p150^{Glued} increases processivity of the dynein-dynactin complex, and has a role on the initiation of transport at the distal axon (Ayloo et al., 2014; Moughamian and Holzbaur, 2012). Cytoplasmic dynein is regulated by an additional complex, constituted by lissencephaly 1 (LIS1) and nuclear distribution E (NudE) or its paralogue NudEL. The LIS1-NudE/NudEL complex acts as a clutch that uncouples ATP hydrolysis from the microtubule binding domain, promoting a strongly bound state that result in an increased ability to transport high loads (Vallee et al., 2012).

1.6 Axonal transport: regulators

Many different regulators have been described for different aspects of intracellular transport. We will present factors controlling microtubule dynamics and regulators involved in the recruitment of motors to their cargoes.

Tubulin post-translational modifications

Microtubules adapt to a variety of functions by regulating the combination of α- and β-tubulin isotypes forming the polymer and by tubulin post-translational modifications, asymmetrically distributed along the microtubule. The combination of both is referred as the “tubulin code” (Gadadhar et al., 2017; Park and Roll-Mecak, 2018). Acetylation of α-tubulin on Lys 40 is generally enriched in stable microtubules (Janke and Montagnac, 2017). This acetylation increases microtubule flexibility, and allows them to better resist mechanical stress (Xu et al., 2017). α-tubulin acetylation also impact on transport, since kinesin-1 shows a preference for acetylated microtubules (Reed et al., 2006). Strikingly, recent evidence showed that the enzyme responsible for this acetylation, α-tubulin N-acetyltransferase 1 (aTAT1), is transported on the cytosolic side of motile vesicles. This vesicular pool of aTAT1 promotes microtubule acetylation and thereby, fast axonal transport (Even et al., 2019).

Additional post-translational modifications include the reversible removal of α-tubulin C-terminal tyrosine (detyrosination and tyrosination), removal of the α-tubulin penultimate glutamate (Δ2) or the last two glutamates (Δ3) following detyrosination, and the addition of a glutamate chain (polyglutamylation) or a glycin chain (polyglycylation) to α- and β-tubulin C-terminal ends (Magiera et al., 2018a). Detyrosination protects microtubules from certain types of depolymerisation, hence increases their longevity (Peris et al., 2009). On the other hand, the +TIP CLIP170 and $p150^{Glued}$ specifically interact with tyrosinated tubulin (Bieling et al., 2008; Peris et al., 2006). The interplay between acetylated and tyrosinated microtubules fine tunes their spatial distribution and therefore, has an impact on axonal transport. For example, after studying microtubule mixed polarity in dendrites, it was reported that stable and acetylated microtubules are more often oriented with their minus-ends towards the distal end, whilst dynamic and tyrosinated microtubules are oriented on the opposite direction. Therefore, kinesin-1, which prefers acetylated microtubules, moves out of the dendrites, whilst kinesin-3 (KIF1A), which prefers tyrosinated microtubules, is able to access into dendrites (Tas et al., 2017).

Regarding the other modifications, excessive polyglutamylation reduces axonal transport of mitochondria, lysosomes, bicd (LAMP1) positive endosomes and brain-derived neurotrophic factor (BDNF)-containing vesicles, causing cell-autonomous neurodegeneration (Bodakuntla et al., 2020; Magiera et al., 2018b), suggesting regulation of polyglutamylation might be a central mechanism for the regulation of neuronal traffic.

Microtubule-associated proteins

The distribution of MAPs is an additional way to regulate microtubule dynamics and intracellular transport. In an analogous way to the tubulin code, it has been referred as the “MAP code” (Bodakuntla et al., 2019). Perhaps the most well documented case is

the effect of Tau on axonal transport. Tau competes with dynein and kinesin for binding to microtubules, exerting a stronger inhibition on kinesin. Therefore, neurons overexpressing tau accumulate cargoes in their somas (Wang and Mandelkow, 2016). However, the fact that in vivo axonal transport is not affected in mice overexpressing or lacking tau, suggest compensatory mechanisms operate (Yuan et al., 2008). Studies using *in vitro* reconstitution systems have shown MAP7 competes with Tau for microtubule binding and displaces it from the microtubule lattice. MAP7 then recruits kinesin-1 to microtubules, whilst inhibiting kinesin-3 (Monroy et al., 2018). Further *in vitro* experiments support the MAP code model. For instance, dendrite-enriched MAP doublecortin inhibits kinesin-1 but not kinesin-3. In addition, MAP9, which localises both to dendrites and axons, enhances kinesin-3 motility, but inhibits dynein-dynactin processivity by blocking $p150^{Glued}$ binding to microtubules (Monroy et al., 2020).

An interesting regulation of transport is carried out by MAP2 in sensory neurons. Since the axon initial segment in these neurons is absent, MAP2 localises there and regulates cargo filtering: it impairs “slow” KIF5 activity and promotes “fast” KIF1 entry into the axon, allowing axonal transport of dense core vesicles (Gumy et al., 2017).

Motor adaptors

The recruitment of just one type of retrograde motor to a plethora of different cargoes establishes another level of regulation on axonal transport, carried out by adaptor proteins. Given that processivity of isolated dynein *in vitro* is poor, since dynein adopts an autoinhibited conformation in this condition (Zhang et al., 2017), some of the adaptors function also as activators, enhancing dynein interaction with dynactin (Olenick and Holzbaur, 2019). There is no consensus sequence for identifying dynein adaptors/activators, instead, they contain a long ~ 30 nm coiled-coil domain which aligns along dynactin Arp1 filament, and bears a binding site for DLIC C-terminal end (Lee et al., 2018; Reck-Peterson et al., 2018). Regarding this DLIC C-terminus binding region,

Bicaudal D (BICD) family adaptors and Spindly use a “CC1 box” domain, Hook family proteins use a “hook” domain, and Rab11 family-interacting protein 3 (Rab11-FIP3) binds through a region containing EF hand motifs (Gama et al., 2017; Horgan et al., 2010; Schroeder and Vale, 2016).

Bicaudal D was initially identified in *Drosophila* through the characterisation of *BicD* mutations, which turns the anterior embryonic segments into posterior ones, generating a “two tails” (bicaudal) phenotype (Mohler and Wieschaus, 1986). There are two BICD orthologues in mammals (BICD1 and BICD2), as well as two BICD-related proteins: BICDR1 and BICDR2 (Hoogenraad and Akhmanova, 2016). BICD2 and BICDR1 are confirmed dynein activators, whilst BICD1 and BICDR2 are adaptors with proposed but unconfirmed activator status (Olenick and Holzbaur, 2019). Interestingly, whilst BICD2 is able to recruit one dynein-dynactin complex, BICDR1 can recruit two dynein dimers to one dynactin molecule, thus enhancing the force and speed generated by the motor complex (Grotjahn et al., 2018; Urnavicius et al., 2018).

BICD proteins and Drosophila BicD are recruited to Golgi-derived exocytic carriers (Grigoriev et al., 2007; Matanis et al., 2002; Schlager et al., 2010). In addition, BICD2 participates on nuclear migration and mitotic entry in brain progenitor cells (Hu et al., 2013), and Drosophila BicD associates to Egalitarian, an RNA binding protein not yet found in mammalian cells, that links mRNA to the dynein-dynactin complex (Dienstbier et al., 2009).

There are three members of the Hook family, with Hook1 and Hook3 acting as activating adaptors (Olenick et al., 2016). They activate dynein in a similar way to BICD2, and just like BICDR1, Hook3 is able to recruit two dynein dimers to one dynactin molecule (Grotjahn et al., 2018; Urnavicius et al., 2018). Regarding their subcellular roles, Hook1 and Hook3 have been implicated in endosomal trafficking and Golgi positioning (Guo et al., 2016; Walenta et al., 2001).

Other dynein activator adaptors include Spindly, which recruit dynein to kinetochores during mitosis (Griffis et al., 2007), Rab11-FIP3, which is involved on recycling endosome transport towards pericentrosomal regions (Horgan et al., 2010), and Ninein (NIN) and Ninein-like (NINL) proteins, two adaptors with EF hands motifs, similar to Rab11-FIP3 (Redwine et al., 2017).

Some adaptors recruit the dynein-dynactin complex by different mechanisms, and they are not considered dynein activators. This category includes Rab-interacting lysosomal protein (RILP) and c-Jun N-terminal kinase (JNK)-interacting proteins (JIP) 1, 3 and 4 (Olenick and Holzbaur, 2019). RILP was identified as one of the factors required for recruitment of the dynein-dynactin complex to late endosomes and lysosomes (Cantalupo et al., 2001; Jordens et al., 2001). RILP interacts with both $p150^{Glued}$ and DLIC, with the latter interaction being negatively regulated by a protein kinase A (PKA)-dependent phosphorylation on DLIC T213 (Johansson et al., 2007; Scherer et al., 2014). JIP family protein comprises four members (JIP1 to JIP4), and whilst all of them bind kinesin-1, they can also act as dynein adaptors (Montagnac et al., 2009; Verhey et al., 2001). For instance, during autophagosome transport in DRGs, LC3 recruits JIP1 to the autophagosome membrane in the distal axon, JIP1 in turn binds simultaneously to dynactin and kinesin-1 in a phosphorylation-dependent manner. Unphosphorylated, LC3-bound JIP1 is unable to activate kinesin-1, allowing for autophagosome retrograde transport (Fu et al., 2014). In addition, JIP3 interacts with both KLC and $p150^{Glued}$, but following mouse sciatic nerve injury, JIP3 and activated JNK are transported mainly retrogradely, suggesting a differential regulation of dynein and kinesin (Cavalli et al., 2005). JIP3 has also been linked to lysosomal transport, since JIP3 knockout mouse neurons accumulate lysosomes in their axons (Gowrishankar et al., 2017). Lastly, JIP4 is recruited to lysosomes as well. In response to nutrient starvation, mammalian target of rapamycin complex 1 (mTORC1) induces the expression of transmembrane protein

55B (TMEM55B), which in turn recruits JIP4 and promotes minus-end directed lysosomal transport (Willett et al., 2017).

Besides the current 8 dynein activator adaptors hitherto validated (BICD2, BICDR1, Spindly, Hook1, Hook3, Rab11-FIP3, NIN and NINL) and the non-activator adaptors, there are many candidates activators still unconfirmed (Reck-Peterson et al., 2018). Some of them are at the same time kinesin adaptors too, such as mitochondrial motor adaptors Trafficking kinesin-binding protein 1 and 2 (TRAK1 and TRAK2) and huntingtin-associated protein 1 (HAP1) (Engelender et al., 1997; van Spronsen et al., 2013). Given that the autoinhibited state of cytosolic kinesin-1 and kinesin-3 is overridden by their adaptors (Guedes-Dias and Holzbaur, 2019) and the fact that many cargoes recruit multiple motors simultaneously, these poses a fundamental question, not only for axonal transport but for intracellular trafficking in general: how multiple motors are coordinated on a single cargo? Although the picture is not complete yet, at least two models have emerged: one proposes a tug-of-war mechanism where dynein and kinesin exert opposing forces simultaneously. An alternative model suggests the coordinated switching between motors, so they undergo successive activation and the force generated against each other is minimised (Hancock, 2014; Soppina et al., 2009). A scheme depicting the two models of bidirectional cargo transport regulation is shown in figure 1.3. Strikingly, motors can regulate the axonal transport of opposing motors directly. For example, kinesin-1 binds the JIP3 orthologue UNC-16 in *C. elegans* neurons, and the complex recruit free dynein through a JIP3-DIC interaction, thereby mediating dynein anterograde transport, and dynein delivery to the axon terminal (Arimoto et al., 2011). This seems to be an evolutionary conserved mechanism, since in mouse hippocampal neurons KIF5 directly binds dynein and mediates its constitutive delivery to the axonal tip (Twelvetrees et al., 2016).

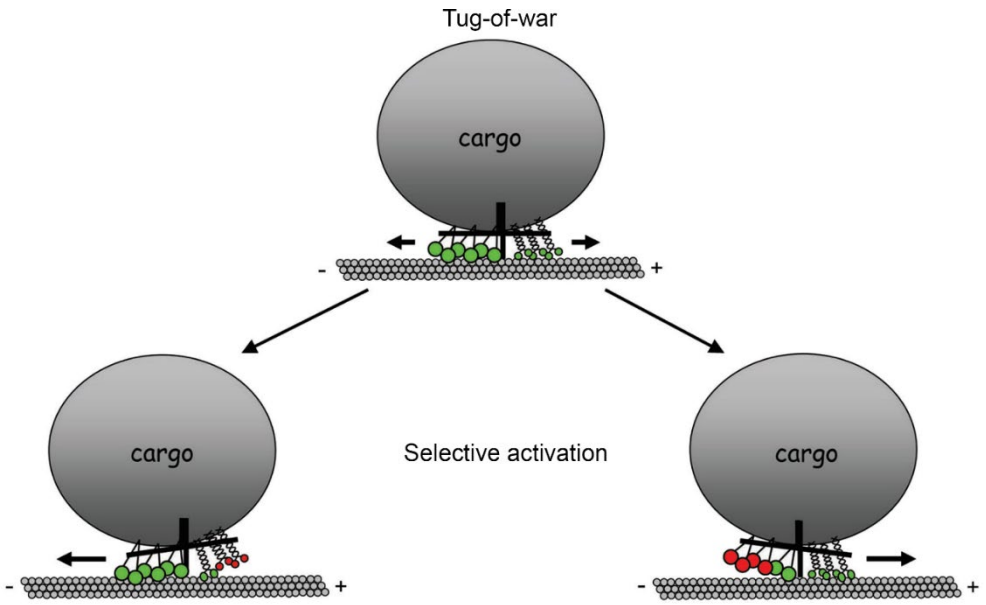

Figure 1.3. Bidirectional models of cargo transport. In the Tug-of-war model, opposing motors pull against each other. Under equally opposing forces the cargo is paused and might have an elongated shape. Stochastic instability on motor binding to microtubules result in advantages of one type of motor over the other type, and the cargo starts moving. In the Selective activation model, a coordination complex determines which group of motors are active, leading to directional movement for long distances. However, the motors opposing the cargo movement are not completely inhibited. Image modified from (Bryantseva and Zhapparova, 2012).

Rab GTPases

Ras-like proteins from rat brain (Rab) GTPases act as molecular switches regulating every step of membrane trafficking, including membrane fission, transport, tethering and fusion (Pfeffer, 2017; Zerial and McBride, 2001). Rab GTPases constitute an evolutionary conserved family, with 11 members in yeast, 31 in *Drosophila* and almost 70 in humans (Klöpper et al., 2012; Zhang et al., 2007b). They cycle between a GTP-bound active state and a GDP-bound inactive state, the GTP-bound state is promoted by guanine nucleotide exchange factors (GEFs) and the GDP-bound state by GTPase activating proteins (GAPs) both of which are specific for single Rab GTPases or Rab subfamilies (Barr and Lambright, 2010; Müller and Goody, 2018). Rab GTPases also cycle between the cytosol and the membrane of their respective target organelle, coupling their localisation and their nucleotide-bound state.

After the Rab protein is translated, it binds Rab escort protein (REP), which presents it to Rab geranylgeranyl transferase (RabGGT), the enzyme catalysing the addition of one, or in most cases two, lipophilic geranylgeranyl groups to cysteine residues on the Rab C-terminal region. The prenylated Rab is then delivered to its target membrane, in a process that may be assisted by GDP dissociation inhibitor-displacement factor (GDF). Once in the membrane a GEF acts on the Rab protein, converting it to the GTP-bound state. In this active state, Rabs bind to their effectors and regulate intracellular traffic. Eventually the Rab protein is converted to the GDP-bound state by a GAP, and extracted from the membrane by GDP dissociation inhibitor (GDI), providing a pool of cytosolic inactive Rab available for the next cycle (Hutagalung and Novick, 2011). A scheme of the Rab cycle is presented in figure 1.4.

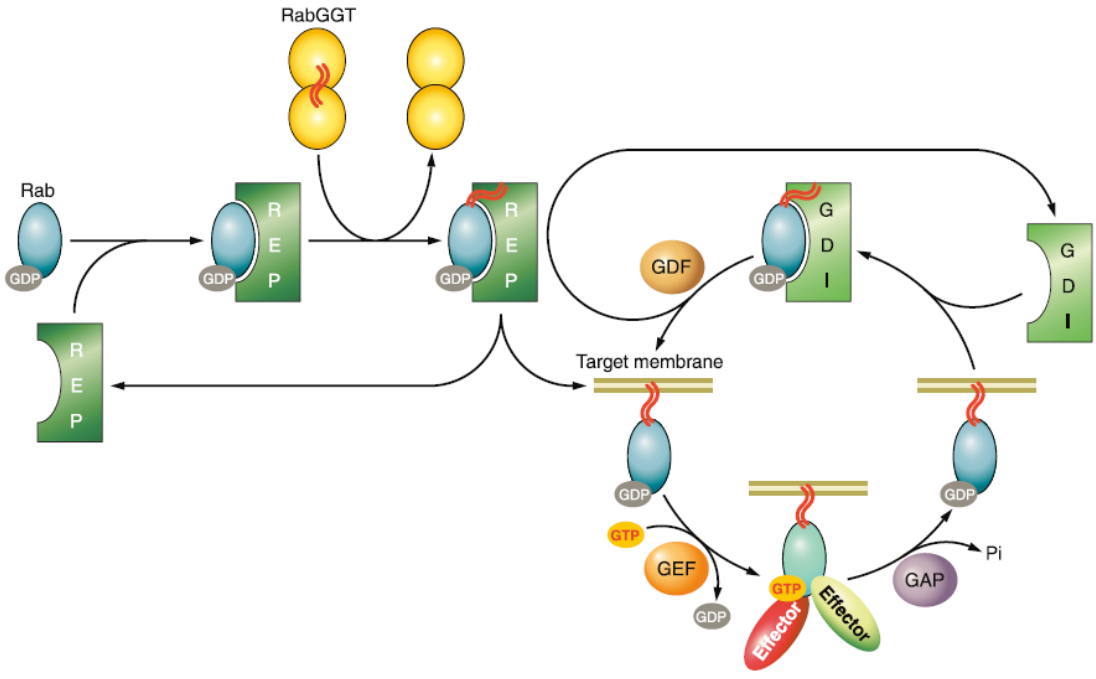

Figure 1.4. The Rab cycle. The image shows the steps a Rab GTPase goes through after its translation. These include the prenylation, targeting to the membrane, activation by GEFs, binding to effectors, inactivation by GAPs and extraction from the membrane by the GDI. Image modified from (Hutagalung and Novick, 2011).

From a structural perspective, Rabs exhibit a similar conformation, therefore their unique properties and function emerge from sequences that distinguish them from other members of the family. In this regard, five sequences have been identified (F1-F5) which are conserved among Rab GTPases but not on Rho or Ras GTPases, as well as four Rab subfamily motifs (RabSF1-4) which allowed for the classification of Rabs in subfamilies, and that are predicted to be relevant for effector binding (Pereira-Leal and Seabra, 2000). One crucial structural feature for Rab GTPase function are the regions that exhibit large conformational differences depending on what nucleotide is bound to the Rab, called switch I and switch II regions. These regions interact with effector when GTP is bound (Pfeffer, 2005). Rab effectors are diverse, but most of them have functions linked to membrane trafficking, such as tethering complexes, coiled-coil proteins and motor adaptors, among other roles (Gillingham et al., 2014; Zhen and Stenmark, 2015). Despite evidence showing that some protein bind Rabs in the GDP-bound state, such as protrudin to Rab11, or VPS34 to Rab7, these are not considered *bona fide* “effectors” (Shirane and Nakayama, 2006; Stein et al., 2003; Stenmark, 2009).

Many Rab effectors are GEFs, GAPs or effectors for other Rabs, or for members of the ADP-ribosylation factor (ARF) GTPase family, establishing Rab cascades (Mizuno-Yamasaki et al., 2012). One of the best described Rab cascade is the conversion from Rab5 to Rab7 taking place in the endolysosomal pathway (Rink et al., 2005). Briefly, endocytosed material transition from Rab5 positive early endosomes to Rab7 positive late endosomes (Chavrier et al., 1990). Rab5 GEF Rabaptin-5-associated exchange factor for Rab5 (Rabex-5) recruits and activates Rab5 on early endosomes. Rab5-GTP then recruits VPS34, which generates PtdIns(3)P, and Rabaptin, which bind Rabex-5 and enhances its GEF activity, generating a positive-feedback loop (Horiuchi et al., 1997; Lippé et al., 2001). Rabex-5 and high levels of PtdIns(3)P are required for the association of Mon1, a member of the Mon1-Ccz1 complex which acts as a GEF for Rab7 (Nordmann et al., 2010). Mon1-Ccz1 displaces Rabex-5 from the endosome, and together with the

Rab5 effector homotypic fusion and sorting complex (HOPS) recruit Rab7, ending in this way the Rab5 positive loop and promoting endosome maturation (Poteryaev et al., 2010).

Besides C-terminal prenylation, Rab GTPases can also be regulated by other post-translational modifications. Phosphorylation was one of the first modification detected (Bailly et al., 1991). For instance, Rab4 phosphorylation on the C-terminal region (Ser 196) promotes its cytosolic localisation during mitosis (van der Sluijs et al., 1992). Rab phosphorylation started dragging more attention recently, since Parkinson's related Leucine-rich repeat kinase 2 (LRRK2) was reported to phosphorylate a subset of Rab GTPases, including Rab8 and Rab10, on a residue in the switch II region (T72 for Rab8 and T73 for Rab10). This phosphorylation inhibits Rab8 binding to its GEF Rabin8 and to GDIs, increasing Rab8 accumulation in membranous fractions (Steger et al., 2016). Interestingly, two enzymes derived from the pathogen *Legionella pneumophila*, DrrA/SidD and AnkX/Lem3, can reversibly modify two residues located in the switch II. DrrA attaches adenosin monophosphate (AMP) to Rab1b Tyr77, whilst AnkX attaches a phosphocholine moiety to Rab1b Ser76 and Rab35 Thr76, inducing the dissociation of the GDI (Mukherjee et al., 2011; Müller et al., 2010; Oesterlin et al., 2012). Rab GTPases can also be ubiquitinated, like Parkin-dependent Rab7 ubiquitination (Song et al., 2016b), palmitoylated (Modica et al., 2017) and sumoylated (Striz and Tuma, 2016). It is likely that additional post-translational modification in other residues will be detected in the future.

Many of the regulatory transport mechanisms described in this section can be regulated by a member of the Rab GTPase family. For instance, BICD2 recruitment to Golgi-derived exocytic vesicles depends on Rab6 (Grigoriev et al., 2007), and RILP recruitment to late endosomes and lysosomes is controlled by Rab7 (Cantalupo et al., 2001; Jordens et al., 2001). Given that a comprehensive understanding of the multiple regulatory facets of axonal transport is better achieved appreciating the phenomenon as a whole, in the

next section we present three examples of cargo transport: lysosomes, mitochondria and signalling endosomes.

1.7 Axonal transport: putting the pieces together

Lysosomes

We have presented a glimpse of lysosomal transport regulation in previous sections, but this is far from a comprehensive picture. Lysosomes move bidirectionally, therefore they have mechanisms for the recruitment of both cytoplasmic dynein and kinesins. As mentioned before, Rab7-GTP present in lysosomes recruits its effector RILP. Interestingly, RILP homodimerises (Colucci et al., 2005), and the dimer interacts with two Rab7 molecules, forming a dyad Rab7-RILP-RILP-Rab7 (Wu et al., 2005). Rab7 also binds oxysterol-binding protein-related protein 1L (ORP1L) through a region different from the switches, hence, independently from the Rab7 GTP/GDP state (Ma et al., 2018). The Rab7-RILP-ORP1L complex interacts with $p150^{Glued}$ and recruits the dynein-dynactin complex, promoting retrograde transport (Johansson et al., 2007). This mechanism is regulates by cholesterol levels, since ORP1L C-terminal oxysterol binding protein-related domain (ORD) binds 25-hydroxycholesterol (Im et al., 2005). When cholesterol levels in the lysosome are high, ORP1L ORD domain associates to the lysosome membrane and dynein is recruited, but when cholesterol levels in the membrane decrease, ORP1L exposes a FFAT motif which binds vesicle-associated membrane protein (VAP) in the ER membrane, docking the lysosome to the ER and displacing dynein from RILP (Rocha et al., 2009). A similar cholesterol-dependent mechanism takes place during the regulation of autophagosome transport and fusion with lysosomes (Wijdeven et al., 2016).

Lysosomal transport can be also regulated by calcium after starvation. During maturation of late endosomes to lysosomes, PtdIns(3)P is converted to phosphatidylinositol 3,5 biphosphate ($PtdIns(3,5)P_2$), which activate the calcium channel TRPML1 (Dong et al.,

2010). TRPML1 induce Ca^{2+} efflux from the lysosome, recruiting the calcium sensor apoptosis-linked gene-2 (ALG-2) (Vergarajauregui et al., 2009). ALG-2 then recruits dynein and directs lysosomal retrograde transport (Li et al., 2016). An additional mechanism for lysosomal transport regulation during starvation or cholesterol depletion include mTORC1 activation, which acting through transcription factor EB (TFEB) upregulates TMEM55B expression. TMEM55B then binds JIP4 and dynein, promoting centripetal lysosomal transport (Willett et al., 2017).

Anterograde lysosomal transport involved the recruitment of the BLOC1-related complex (BORC), an octameric complex which associates to lysosomal membranes and recruits the small GTPase Arl8 (Pu et al., 2015). Arl8 binds SifA and kinesin-interacting protein (SKIP), which in turn interacts with kinesin-1 (KIF5B) KLC and directs anterograde transport (Rosa-Ferreira and Munro, 2011). The Arl8/SKIP complex also binds kinesin-3 (KIF1Bβ and KIF1A), and their differential regulation is achieved at the microtubule level, since kinesin-1 prefers acetylated microtubules and kinesin-3 tyrosinated (more peripheral) microtubules (Guardia et al., 2016). The BORC/Arl8/SKIP/kinesin-1 mechanism is important for the axonal transport of lysosomes, but not for their transport in dendrites, hinting at a contribution to neuronal polarity, since polarised transport to the somatodendritic and axonal compartments is required for the maintenance of neuronal polarity (Farías et al., 2017). The BORC complex has also been involved in the transport of other organelles, such as synaptic vesicle precursors (Niwa et al., 2017) and has roles unrelated to transport, such as the fusion of autophagosomes with lysosomes, through the recruitment of the HOPS complex (Jia et al., 2017).

Lysosomes can use an additional mechanism for anterograde movement, which relies on Rab7. FYVE and coiled-coil domain-containing protein 1 (FYCO1) is a Rab7 effector which binds Rab7-GTP and PtdIns(3)P on the lysosomal membrane (Pankiv et al., 2010). The ER membrane protein protrudin binds Rab7 and PtdIns(3)P, acting as a detector coincidence, transfers kinesin-1 from protrudin to FYCO1 (Raiborg et al., 2015).

The similarities of this mechanism with the docking of lysosomes on ER domains by ORP1L suggest it might be a way to induce lysosomal anterograde transport after the ER-lysosome contacts were formed.

Mitochondria

The axonal transport of mitochondria is bidirectional, however, it can be biased towards one direction or another depending on whether the axons is growing, retracting, or responding to stimuli (Saxton and Hollenbeck, 2012). Mitochondria dynamics alternate between moving and docking states in areas of high energetic demand. In cultured hippocampal neurons, about 20%-30% of mitochondria are motile, moving almost equally in both directions (Hollenbeck and Saxton, 2005). *In vivo*, about 10% of mitochondria are motile in mouse sciatic nerve, and 2/3 of them move anterogradely (Misgeld et al., 2007), confirming previous observations in *Drosophila* motor axons (Pilling et al., 2006). Mechanistically, mitochondrial anterograde transport is mediated by the Rho GTPase Miro (mitochondrial Rho) (Fransson et al., 2003; Guo et al., 2005). Miro has two EF hand motifs which bind Ca^{2+}, two GTPase domains, and associates with the kinesin-1 adaptors TRAK1 and TRAK2, the orthologues of *Drosophila* Milton (Fransson et al., 2006; Stowers et al., 2002). Increased levels of intracellular calcium, for example from sustained synaptic activity, inhibit mitochondrial transport. Although it is clear this depends on Miro, the mechanism is not fully understood. One model proposes that Ca^{2+} binding allows Miro to interact directly with kinesin-1 motor domain, preventing its association with microtubules (Wang and Schwarz, 2009). An alternative model suggests Ca^{2+} binding dissociates kinesin-1 from Miro (Macaskill et al., 2009). Miro acetylation state is also relevant for this function, since deacetylation on Lys105 by histone deacetylase 6 (HDAC6) decreases mitochondrial axonal transport (Kalinski et al., 2019). Additional evidence from cells double knock out for Miro 1 and Miro 2 showed that in this condition, the motor adaptors TRAK1 and TRAK2 still localise to the

mitochondria outer membrane, indicating that alternative recruitment mechanisms might compensate for Miro loss of function (López-Doménech et al., 2018). Other mechanisms for the recruitment of kinesin-1 to mitochondria include the motor adaptor syntabulin (Cai et al., 2005), Fasciculation and elongation protein zeta-1 (FEZ1) (Fujita et al., 2007) and Ran-binding protein 2 (RanBP2) (Patil et al., 2013). Recruitment of kinesin-3 to mitochondria has also been reported (Wozniak et al., 2005).

Mitochondrial retrograde transport has been less studied, but since TRAK1 and TRAK2 can also bind dynein, it is possible that the activity of anterograde and retrograde motors is coordinated. For instance, TRAK1 binds both kinesin-1 and dynein, and its mostly localised in axons, whilst TRAK2 preferentially binds dynein and is more abundant in dendrites (van Spronsen et al., 2013). Regarding mitochondrial docking, synaptic activity and high levels of calcium induce the recruitment of syntaphilin to axonal mitochondria, where it interacts with KIF5 and inhibits its ATPase activity, arresting mitochondrial transport (Chen and Sheng, 2013; Kang et al., 2008).

Signalling endosomes

Following endocytosis of activated receptors in the plasma membrane, some ligand-receptor complexes can persist actively engaged in signalling generation from the endosomal compartment. These “signalling endosomes” function as platforms for the compartmentalised regulation of signalling pathways, with neurotrophic signalling being one of the most frequently used as case study. In contrast to lysosomes and mitochondria, which move bidirectionally, neurotrophic signalling endosomes move preferentially towards the retrograde direction. Briefly, neurotrophins are a family of target-derived growth factors that are essential for neuronal development and survival (Segal, 2003). Members of the neurotrophic family include nerve growth factor (NGF), brain-derived neurotrophic factor (BDNF), neurotrophin 3 (NT-3) and neurotrophin-4/5 (NT-4/5). Neurotrophins bind two types of receptors: tropomyosin-related kinase

receptors (Trks) and the p75 neurotrophin receptor ($p75^{NTR}$), a member of the tumour necrosis factor receptor superfamily (Deinhardt and Chao, 2014). TrkA binds preferentially NGF, TrkB binds BDNF and NT-4/5, and TrkC binds NT-3. $p75^{NTR}$ can bind all members of the family, as well as regulate the affinity of Trk receptors for their ligands (Chao and Hempstead, 1995). Neurotrophins regulate neuronal survival, axonal/dendritic growth and branching, neuronal specification and synapse formation, through the activation of three main pathway: PI3K/AKT pathway, mitogen-activated protein kinases (MAPKs), in particular ERK1/2 and ERK5, and phospholipase C-gamma (PLCγ) (Reichardt, 2006).

The initial observation that target-derived factors promote the survival of neurons innervating the tissue, made by Rita Levi-Montalcini and Viktor Hamburger (Hamburger and Levi-Montalcini, 1949), together with findings showing that peripherally administrated NGF accumulates in neuronal cell bodies, (Angeletti et al., 1972), suggested that the neurotrophic signalling is retrogradely transported (Harrington and Ginty, 2013; Zweifel et al., 2005). Further evidence showing that activated TrkA and TrkB are transported from the axon terminal to the neuronal soma (Bhattacharyya et al., 1997; Ehlers et al., 1995), as well as the engagement of Trk receptors with specific signalling pathways from post-endocytic compartments (Zhang et al., 2000) prompted the formulation of the “signalling endosome” hypothesis, which states that internalised receptors bound to their ligands are transported in specialised endosomes which act as platforms for initiating signalling transduction, and that account for the retrograde transport of the neurotrophic signalling (Grimes et al., 1996, 1997).

Signalling endosomes are diverse, hence, the exact nature of the endosomal compartment and the determination of its associated transport machinery have not been straightforward (Villarroel-Campos et al., 2018). Some reports have shown NGF-TrkA is transported in early endosomes positive for Rab5 and for its effector early endosome antigen 1 (EEA1), in PC12 cells and DRGs (Delcroix et al., 2003). In agreement with this,

TrkB and AKT transport has been detected in Rab5-positive endosomes which were also positive for its effector Adaptor protein, phosphotyrosine interacting with PH domain and leucine zipper 1 (APPL1) in cultured hippocampal neurons (Goto-Silva et al., 2019). Other evidence indicate that in mouse cultured motor neurons, BDNF-TrkB is transported in Rab7 positive endosomes (Deinhardt et al., 2006). Interestingly, TrkB is not targeted for degradation during Rab7-dependent transport, since endosome acidification is impaired (Bohnert and Schiavo, 2005). In support of the Rab7-positive nature of signalling endosomes, recent evidence found NGF-TrkA being transported in multivesicular bodies positive for Rab7, RILP, LAMP1 and CD63 in cultured sympathetic neurons (Ye et al., 2018). Lastly, there is also evidence for TrkB transport in autophagosomes (Kononenko et al., 2017).

From the transport perspective, it is not fully clear whether signalling endosomes employ the same adaptors as other endosomes, and given their heterogeneity, it is likely that mechanisms driving the recruitment of specific motor complexes co-exist. For example, signalling endosomes containing BDNF-TrkB recruit dynein through the adaptor snapin in cultured cortical neurons (Zhou et al., 2012). Given that snapin is a member of the BORC complex (Niwa et al., 2017), it is possible that the entire complex participates on dynein recruitment, however this remains to be elucidated. In addition, BDNF-TrkB retrograde transport in sympathetic neurons is carried out at least in part by multivesicular bodies, and relies on Rab7-dependent RILP recruitment (Ye et al., 2018). Conversely, BDNF-TrkB signalling endosomes recruit dynein through the adaptor Hook1, in rat hippocampal neurons (Olenick et al., 2019).

Here we have provided just a few examples of how intracellular trafficking and axonal transport of specific organelles are regulated. More examples can be found in recent reiews (Guedes-Dias and Holzbaur, 2019; Maday et al., 2014).

1.8 Axonal transport defects during ALS

Early evidence linking axonal transport defects to ALS came from neuropathological post-mortem studies in patients. These studies showed accumulation of phosphorylated neurofilaments and organelles in the proximal axon of motor neurons (Hirano et al., 1984a, 1984b). Consistent with a dysfunction of the transport machinery, those axonal swellings (spheroids) were immunopositive for KHC, although cytoplasmic dynein was not detected (Toyoshima et al., 1998). Additionally, mRNA profiles on the motor cortex of sALS patients detected a reduction in the expression of KIF1Aβ and KIF1Bβ (Pantelidou et al., 2007). The advances in ALS genetics together with the generation of animal models of the disease allowed to expand the axonal transport phenotype. For instance, sciatic nerve ligation experiments carried out on $SOD1^{G93A}$ mice revealed reduced kinesin-1 activity. Strikingly, the axonal transport deficit were observed even at pre-symptomatic stages, suggesting they were not a consequence of neurodegeneration, but may be involved in its onset (Warita et al., 1999; Williamson and Cleveland, 1999).

One of the most frequently studied axonal cargoes are mitochondria, therefore, several ALS-linked mitochondrial axonal transport dysfunctions have been reported (Granatiero and Manfredi, 2019). Regarding this, anterograde mitochondrial transport is decreased in cultured motor neurons derived from $SOD1^{G93A}$ mouse (De Vos et al., 2007), whilst rat primary motor neurons transfected with $SOD1^{G93A}$ exhibit defects on retrograde mitochondrial transport, as well as reduced mitochondrial fusion, length and density (Magrané et al., 2012). Defects in mitochondrial shape and distribution along the axon also appear at pre-symptomatic stages in $SOD1^{G37R}$ and $SOD1^{G85R}$ mice models (Vande Velde et al., 2011). These mitochondrial axonal transport defects were corroborated *in vivo*, in sciatic nerve from $SOD1^{G93A}$ and TDP-43^{A315T} mice (Bilsland et al., 2010; Magrané et al., 2014).

Defects in mitochondrial axonal transport are not limited to SOD1 models, as can be concluded from the aforementioned *in vivo* studies. In fact, the overexpression of WT TDP-43 is enough to induce a reduction in mitochondrial length and density, as well as impaired mitochondrial transport, although this is exacerbated by ALS-linked mutations, such as Q331K and M337V (Wang et al., 2013). Cabeza (FUS *Drosophila* orthologue) P398L and C9ORF72 carrying the pathogenic hexanucleotide expansion (36 repeats) also disrupt mitochondrial transport in *Drosophila* motor axons (Baldwin et al., 2016). Interestingly, this defect can be rescued inhibiting HDAC6, in an iPSC model derived from FUS-ALS patients (Guo et al., 2017).

The molecular mechanisms underlying these defects are not fully clear, however, it has been shown that mutant SOD1 directly interacts with the dynein-dynactin complex, impairing its function (Ligon et al., 2005; Zhang et al., 2007a). In addition, mutant SOD1 accumulates in mitochondria, negatively affecting their function (Igoudjil et al., 2011).

ALS-linked axonal transport defects in other cargoes have been described as well. For example, TDP-43 associates with mRNP granules which move bidirectionally in axons, and ALS-associated TDP-43 mutations impair their transport (Alami et al., 2014).

ALS2 mutations reported in juvenile-onset ALS strongly suggest an involvement of the endolysosomal pathway in disease pathogenesis, since ALS2 encodes a GEF for Rab5 (Hadano et al., 2001). In agreement with this, a mechanism combining RNA and lysosomal transport was recently described. Annexin A11 acts as a tether between RNA and LAMP1-positive organelles, since its N-terminal low complexity domain phase separate into membraneless RNA granules, and its C-terminal domain binds to the organelle membrane. In this way, RNA granule transport is coupled to late endosome/lysosomal transport, a mechanisms disrupted by ALS-linked mutations in annexin A11 (Liao et al., 2019).

Impaired axonal transport of signalling endosomes is a good candidate to explain the mechanisms leading to neuronal death during ALS, given the role of the neurotrophic signalling on neuronal survival. In this regard, our group has taken advantage from the fact that the C-terminal, non-toxic fragment of the tetanus toxin (termed H_CT) is internalised and sorted into neurotrophin signalling endosomes (Lalli and Schiavo, 2002), to track these organelles in motor neurons from ALS mouse models. *In vitro* studies showed that primary motor neurons derived from $SOD1^{G93A}$ mouse display a disruption on retrograde axonal transport even at embryonic stages, manifested as increased frequency of pausing and oscillatory movement (Kieran et al., 2005). This was confirmed *in vivo*, in the sciatic nerve of pre-symptomatic $SOD1^{G93A}$ mice (Bilsland et al., 2010), hinting at a defect that precedes neurodegeneration. As mentioned before, this population of signalling endosomes is positive for Rab7 (Deinhardt et al., 2006), therefore, in an attempt to further understand how these carriers are transported back to the soma, we focused on the regulation of Rab7 activity.

1.9 Rab7 regulation

There are two Rab7 paralogues in mammals, Rab7a and Rab7b. Whilst Rab7b regulates the transport between late endosomes and the trans-Golgi network (TGN) (Progida et al., 2012), Rab7a regulates the trafficking from early to late endosomes, and from late endosomes to lysosomes (Bucci et al., 2000). Since Rab7a is the isoform involved in axonal transport of signalling endosomes, we will restrict to discuss the regulation of the activity of this Rab (henceforth called Rab7).

As other Rab GTPases, Rab7 cycles through a soluble GDP-bound state, and a membrane-associated GTP-bound state, which is regulated by GEFs and GAPs. Early evidence suggested that Vps39, a member of the HOPS complex acted as a GEF for Rab7 yeast homologue, Ypt7p (Wurmser et al., 2000). Nevertheless, studies carried out in *C. elegans* showed that the Mon1-Ccz1 complex fulfils the role of Rab7 GEF (Cabrera

et al., 2014; Nordmann et al., 2010). Interestingly, Mon1-Ccz1 acts as a Rab7 GEF only on late endosomes, since the complex dissociates from lysosomes (Yasuda et al., 2016). Given that Rab7 activity on lysosomes is Mon1-Ccz1-independent, this poses the question about whether additional uncharacterised GEFs for Rab7 exist. Regarding Rab7 activity during autophagosome-lysosome fusion, yeast Mon1-Ccz1 complex binds ATG8 on the autophagosome membrane via the LC3 interacting region (LIR) motif in Ccz1 (Gao et al., 2018). Mon1-Ccz1 association to LC3 in mammalian cells has not been described yet, although the LIR motifs are conserved.

Rab GAPs carry a Tre-2/Bub2/Cdc16 (TBC) domain originally identified in yeast, and present in more than 40 different proteins in mammals (Fukuda, 2011). The first Rab7 GAP reported, Armus/TBC1D2A, was identified as an effector of the rho GTPase Rac1 (Frasa et al., 2010), highlighting the coordination of GTPase cascades not only between Rab GTPases, but also with members of other GTPase families. Armus contains LIR motifs, and is able to bind LC3 and GABARAP on the autophagosome membrane (Popovic et al., 2012). Its recruitment to late endosomes likely depend on PtdIns(3)P recognition on the organelle membrane, via Armus pleckstrin homology (PH) domain (Jaber et al., 2016). Armus autoinhibited state is released by Leucine-rich repeat kinase 1 (LRRK1) phosphorylation (Toyofuku et al., 2015), a kinase closely related to LRRK2, which phosphorylates a subset of Rabs on the switch II domain.

TBC1D5 is another Rab7 GAP, which associates with the retromer complex (Seaman et al., 2009). Briefly, the retromer is a heteropentameric complex formed by a cargo-binding trimer composed of Vps35, Vps29 and Vps26, along with a membrane-binding dimer of Vps5 and Vps17, the yeast homologues of mammalian sortin-nexins 1/2 and 5/6 (Seaman, 2012). The retromer complex promotes the recycling of cargo proteins from endosomes to the TGN and the plasma membrane, (Gallon and Cullen, 2015). Rab7-GTP recruit the retromer complex to late endosomes through a direct interaction with Vps26 (Rojas et al., 2008), and TBC1D5 binds the complex via Vps29 (Jia et al., 2016).

TBC1D5 also associates with LC3 and its activity is required during mitophagy, since hyperactivated Rab7 impairs the correct sorting of membrane to the nascent autophagosome (Jimenez-Orgaz et al., 2018).

TBC1D15 is also a Rab7 GAP, which is recruited to mitochondria by the mitochondria outer membrane protein Fis1 (Onoue et al., 2013). TBC1D15 is required for mitophagy, but seems to be irrelevant for constitutive bulk autophagy (Yamano et al., 2014). In addition, TBC1D15-dependent Rab7 inactivation is required for mitochondria fission, takin place at mitochondria-lysosome contact sites (Wong et al., 2018).

Rab7 functions can be affected by pathogenic mutations. It is worth mentioning that Rab7 is not an ALS-linked gene, however, it is mutated in CMT disease, the most frequent hereditary peripheral neuropathy (Rossor et al., 2013). Specifically, Rab7 mutations are causative of CMT type 2B. Five missense point mutations have been described up to date (L129F, N161T/I, K157N and V162M), which lead to decreased nucleotide affinity, especially for GDP, and unregulated nucleotide exchange, without affecting Rab7 catalytic activity. As these mutants are predominantly in the GTP-bound state, they resemble constitutively active $Rab7^{Q67L}$; since they show increased interaction with a subset of effectors, and are abnormally retained on target membranes (De Luca et al., 2008; McCray et al., 2010; Spinosa et al., 2008). CMT-related Rab7 mutations affect the directionality of movement of Rab7-positive endosomes, as well as the transport of signalling endosomes containing NGF-TrkA in DRG cultures (Zhang et al., 2013). Deficits in transport have also been reported in animal models of the disease, for example, a *Drosophila* model expressing Rab7 L129F in sensory neurons showed reduced pausing of Rab7-positive endosomes, whilst tracking the same cargoes in zebrafish larvae expressing CMT-related Rab7 mutants revealed decreased speed for Rab7 K157N and reduced pausing for Rab7 N161T and V162M (Janssens et al., 2014; Ponomareva et al., 2016).

Rab7 is the target of post-translational modification which can affect its function (Modica and Lefrancois, 2017). For instance, Rab7 can be palmitoylated on cysteine 83 and 84, a modification required for the efficient recruitment of the retromer by Rab7 (Modica et al., 2017). Rab7 can be ubiquitinated by the E3-ubiquitin ligase Parkin on Lys38, Lys191 and Lys194, with a preference for Lys38 (Song et al., 2016b). In addition, Rab7 is deubiquitylated by ubiquitin-specific protease 32 (USP32) on Lys191 (Sapmaz et al., 2019). Rab7 ubiquitination on Lys191 regulates the recruitment of Rab7 effectors, since RILP binds preferentially to ubiquitination-deficient Rab7, whilst retromer-associated functions require an intact Rab7 ubiquitination/deubiquitination cycle. Finally, Rab7 can be phosphorylated on Ser72 and Tyr183, and phosphorylation at these sites impair the binding of Rab7 to the GDI (Shinde and Maddika, 2016), and to Rab7 effectors. Different studies assessing the effect of Ser72 phosphorylation have given conflicting results. Whilst p-Ser72 seems to inhibit Rab7 association to RILP (Shinde and Maddika, 2016), others have shown that p-Ser72 promotes RILP and dynein recruitment, facilitating the retrograde transport of epidermal growth factor receptor (EGFR) towards degradative compartments (Hanafusa et al., 2019). Regarding the identity of the enzymes mediating these modifications, Rab7 p-Ser72 and p-Tyr183 are targeted by the phosphatase phosphatidylinositol 3,4,5-trisphosphate 3-phosphatase and dual-specificity protein phosphatase (PTEN). Rab7 Tyr183 is phosphorylated by Src (Lin et al., 2017), and Ser72 has been shown to be targeted by LRRK1 and Tank-binding protein 1 (TBK1) (Hanafusa et al., 2019; Heo et al., 2018).

In an attempt to identify new Rab7 regulators that can impact on the axonal transport of signalling endosomes, our group carried out a screening using in vitro kinase assay on a library of kinases, and we identified two kinases which phosphorylate Rab7 in only one site: TBK1 and Inhibitor of nuclear factor kappa-B kinase subunit epsilon (IKKε) (Wallace, 2014).

1.10 TBK1

TBK1, also known as NF-κB-activating kinase (NAK), or T2K, is an ubiquitously expressed serine/threonine kinase, part of the 'noncanonical IkB kinases' (IKKs), which participate in the regulation of type-I interferon production during innate immunity (Fitzgerald et al., 2003). TBK1 is also involved in the control of autophagy and cell proliferation (Ahmad et al., 2016; Stolz et al., 2014).

TBK1 is formed by four domains: a serine/threonine kinase domain (KD, residues 1-307), an ubiquitin-like domain (ULD, residues 308-383), a coiled-coil domain 1 (CCD1, residues 407-657, also known as scaffold dimerisation domain (SDD)) and a coiled-coil domain 2 (CCD2, residues 658-713, also known as C-terminal domain (CTD)) (Larabi et al., 2013). TBK1 can forms homodimers or heterodimers with IKKε, which is mediated by interaction between the CCD1 domains. TBK1 dimerisation is thought to be necessary for activation, although recent evidence derived from ALS-mutants challenge this concept (Tu et al., 2013; Ye et al., 2019). Regarding this, the kinase domain contains an activation loop which includes the residue Ser172. This residue needs to be phosphorylated to ensure TBK1 activation. Structural studies have shown that TBK1 phosphorylates S172 in trans (Ma et al., 2012), and that the polyubiquitination of Lys30, Lys63 or Lys401 enhances TBK1 activity, possibly through a crowding effect that facilitates its transautophosphorylation (Li et al., 2011; Song et al., 2016a; Wang et al., 2009). TBK1 p-Ser172 is targeted by the phosphatase cell division cycle 25A (Cdc25A), thereby decreasing TBK1 activation during antiviral immune response (Qi et al., 2018).

TBK1 function is regulated by a group of adaptor proteins that alter its subcellular localisation and recruit TBK1 to specific signalling pathways. For instance, TRAF family member-associated NF-kappa-B activator (TANK), NAP1, and TANK-binding kinase 1-binding protein 1 (SINTBAD) all bind TBK1 CCD2 in a mutually exclusive manner (Goncalves et al., 2011). This organised alternative TBK1 recruitment ensures, for

example, that TBK1 activation during selective autophagy does not result in phosphorylation of its targets of the NF-κB pathway (Heo et al., 2015).

In the following sections, we will briefly present TBK1 roles on inflammation and autophagy, before discussing its involvement in ALS.

TBK1 roles in inflammation

The first function attributed to TBK1 after its discovery, consisted on a role during innate immune response. TBK1 is activated downstream to pattern-recognition receptors (PRRs), such as Toll-like receptor (TLR) 3 and TLR4, which initiate a signalling cascade in response to conserved molecular patterns associated to pathogens (Wallet et al., 2018). Specifically, TLR3 recognises double-stranded RNA (dsRNA), and TLR4 is activated by lipopolysaccharide (LPS) (Alexopoulou et al., 2001a; Lu et al., 2008). TLR3 signalling can also be triggered by dsRNA analogues, for example, low molecular weight polyinosinic:polycytidylic acid (LMW poly (I:C)) (Zhou et al., 2013). dsRNA also activates the intracellular receptors retinoic acid-inducible gene I (RIG-I) and melanoma differentiation-induced protein 5 (MDA5), which transduce the signalling through mitochondrial antiviral-signalling protein (MAVS) (Kato et al., 2006; Yoneyama et al., 2004). In addition, intracellular DNA is sensed by cyclic GMP-AMP synthase (cGAS), which in turn activates stimulator of interferon genes (STING). After that, both MAVS and STING activate TBK1 (Fang et al., 2017; Zhang et al., 2019). TLR3, TLR4, MAVS and STING pathways converge on TBK1 activation, inducing the formation of TBK1 dimers or TBK1/IKKε heterodimers which continue the signalling cascade, phosphorylating NF-κB and interferon regulatory factor 3 and 7 (IRF3/7). These transcription factors promote the expression of the interferon β (IFNβ) gene (Bakshi et al., 2017; Pomerantz and Baltimore, 1999). A scheme depicting TBK1 activation during innate immunity is presented in figure 1.5

TLR and NF-κB pathways are highly conserved through evolution. In fact, the first member of the TLR family was originally identified in *Drosophila*, as an homologue of the cytosolic domain of the transmembrane protein Toll (Gay and Keith, 1991). Toll promotes dorsoventral polarisation during *Drosophila* embryonic development, highlighting a feature also shared by the NF-κB pathway: these pathways emerged early during evolution as regulators of embryonic development and cellular patterning. From an evolutionary perspective canonical TLRs can be found in cnidaria, whilst TBK1 orthologues are present in porifera (Gilmore and Wolenski, 2012; Nie et al., 2018).

Consistent with the role of NF-κB during development, *TBK1* knockout mice die at E14.5 due to liver degeneration, since TBK1-dependent NF-κB-directed transcription is required for apoptosis inhibition in the liver at this stage (Bonnard et al., 2000).

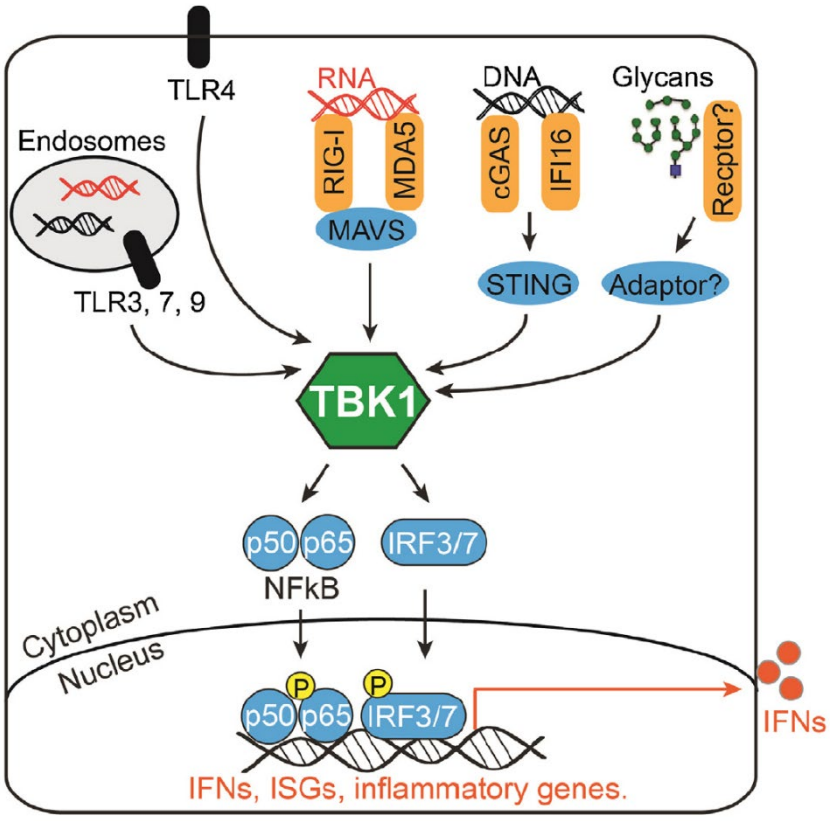

Figure 1.5. TBK1 activation during innate immunity. The figure shows the PRRs acting upstream to TBK1 and the ligands that activate them. TBK1 targets and transcribed responses are also presented. Modified from (Hasan and Yan, 2016).

TBK1 roles in autophagy

The involvement of TBK1 in autophagy has been mainly studied using the paradigm of mitochondria depolarisation with oligomycin A/antimycin A (OA), which induce mitophagy. Nevertheless, examples of TBK1 activity during xenophagy have also been reported (Minowa-Nozawa et al., 2017). Upon mitochondria depolarisation/damage, the serine/threonine kinase PTEN-induced kinase 1 (PINK1) accumulates on the mitochondrial outer membrane, phosphorylating the E3-ubiquitin ligase PARKIN, and Ser65 of ubiquitin (Sekine and Youle, 2018). This initiates PARKIN-dependent ubiquitination of many substrates on the mitochondria outer membrane, as well as the recruitment of cytosolic PARKIN, establishing a positive feedback loop of phosphorylation and ubiquitination (Harper et al., 2018). Those ubiquitin chains are recognised by autophagy receptors, such as p62, optineurin and NDP52, which link the damaged cargo to the autophagosome membrane via LC3 (Lazarou et al., 2015; Wong and Holzbaur, 2014). Optineurin and p62 phosphorylation by TBK1 enhances their affinity for ubiquitin, facilitating the autophagy process (Matsumoto et al., 2015). For instance, TBK1 phosphorylates optineurin Ser472 and Ser513, increasing its association with K63-ubiquitin chains (Richter et al., 2016). TBK1 also phosphorylates optineurin Ser177, promoting its interaction with LC3 (Wild et al., 2011). Regarding other autophagy receptors, TBK1 phosphorylates p62 Ser403, which is required for the elimination of pathogenic bacteria (Pilli et al., 2012), and promotes the interaction between NDP52 and the ULK1 complex, thereby facilitating the initiation of mitophagy (Vargas et al., 2019). This is not the only role of TBK1 during autophagy initiation, as TBK1-dependent phosphorylation on syntaxin 17 Ser202 has also been reported. This phosphorylation is required for the formation of the ULK1 complex, specifically for the interaction between ATG13 and FIP200 in the nascent autophagosome (Kumar et al., 2019).

In addition to its roles during autophagy initiation and phosphorylation of autophagy receptors, TBK1 also regulates autophagosome membrane expansion during mitophagy. OA-induced mitochondria depolarisation promotes the recruitment of TBK1 to the mitochondrial outer membrane, where it phosphorylates Rab7 Ser72. Rab7 p-Ser72 interacts with its effector folliculin (FLCN) and folliculin-interacting protein 1 (FNIP1). The FLCN-FNIP1 complex contains a DENN domain, hence it may act as a GEF for downstream Rab GTPases, however, the identity of these Rab proteins has not been elucidated yet. Rab7 p-Ser72 is also necessary for the recruitment of ATG9-positive vesicles which support the expansion of the autophagosome membrane (Heo et al., 2018).

TBK1 and ALS

TBK1 mutations leading to haploinsufficiency have been reported as disease-causative, in a group of patients affected by fALS, sALS or FTD (Cirulli et al., 2015; Freischmidt et al., 2015; Pottier et al., 2015). Additional studies have expanded the disease spectrum, to include progressive cerebellar ataxia (Wilke et al., 2018). To date, more than 90 TBK1 mutations have been described, distributed along the entire length of the protein. Some TBK1 mutations are nonsense mutations, therefore they trigger nonsense mediated RNA degradation, whilst others are missense, and impair phosphorylation of IRF3 or optineurin (Oakes et al., 2017). For instance, ALS-linked TBK1 E696K cannot interact with optineurin, hence OA-induced mitophagy is impaired when this TBK1 mutants is expressed in HeLa cells (Moore and Holzbaur, 2016). A scheme depicting the location of ALS-linked TBK1 mutations in the kinase structural domains is presented in figure 1.6.

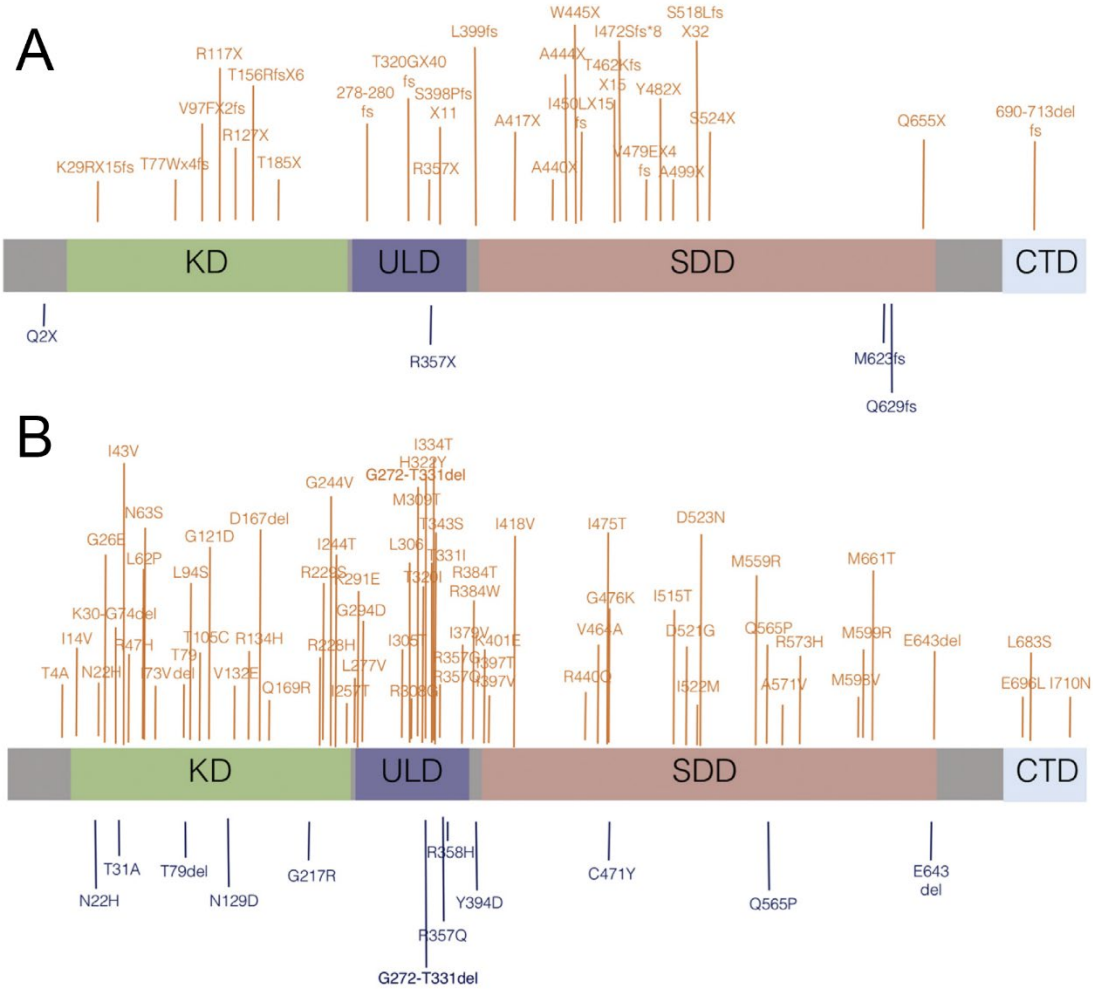

Figure 1.6 TBK1 structural domains and ALS-linked mutations. TBK1 kinase domain (KD), ubiquitin-like domain (ULD), scaffold dimerisation domain (SDD) and C-terminal domain (CTD) are depicted. The mutations shown in A correspond to nonsense mutation, including deletions, and frameshifts. The mutations shown in B are missense mutations. Mutations in orange have been reported elsewhere, whilst mutations in blue were reported in (de Majo et al., 2018), from where this image was modified.

Recent detailed analysis of ALS-linked TBK1 mutations has shown that TBK1 dimers with just one catalytically active subunit can still phosphorylate downstream targets, suggesting that TBK1 could be activated by any kinase targeting its S172 residue. In addition, some TBK1 mutants which were unable to dimerise retained their kinase activity, although protein stability was decreased (Ye et al., 2019). Finally, TBK1 heterozygosity on $SOD1^{G93A}$ background accelerated disease onset, which was linked to impaired autophagy, however, at later stages of the disease TBK1 deletion prolongs survival due to reduced microglial activation and neuroinflammation. Notably, the *TBK1*$^{+/-}$

mouse model with WT SOD1 background did not developed motor impairments, hinting that TBK1 may cause ALS onset only in the presence of a “second hit” (Brenner et al., 2019). It is worth noting, however, the similarities between this dual role on ALS progression, and the phenotype obtained after autophagy inhibition (ATG7 knock out) in the $SOD1^{G93A}$ strain (Rudnick et al., 2017).

Aims

The retrograde transport of signalling endosomes is negatively affected during ALS pathogenesis. The trafficking of these carriers relies on Rab7, a protein which can be regulated by TBK1 phosphorylation on Ser72. In addition, TBK1 itself is mutated in familial cases of ALS. Nevertheless, how Rab7 S72 phosphorylation impact on its function is not fully understood. Therefore, we asked whether Rab7 S72 phosphorylation or TBK loss of function affect signalling endosome retrograde transport.

The specific aims of this project are:

1. To assess the effect of Rab7 phosphorylation on axonal transport.

2. To investigate the role of TBK1 loss-of-function on axonal transport and neurotrophin signalling.

Chapter 2

Methods

2.1 Animals

All experiments were carried out following the guidelines of the UCL Institute of Neurology Genetic Manipulation and Ethic Committees, and in accordance with the European Community Council Directive of November 24, 1986 (86/609/EEC). Animal experiments were undertaken under license from the UK Home Office in accordance with the Animals (Scientific Procedures) Act 1986 (Amended Regulations 2012) and the GSK Policy on the Care, Welfare and Treatment of Animals. Wild-type (WT) mice from a C57BL/6 x SJL background were used in all experiments.

2.2 Reagents and DNA constructs

Canine Rab7 WT cloned in the mammalian expression vector pEGFF-C1 was kindly provided by Cecilia Bucci (Bucci et al., 2000). Site-directed mutagenesis was used by former members in our laboratory to generate the S72A and S72E mutants (Wallace, 2014). The three vectors were sequences before the start of this project (Source BioScience, UK). EB3-mCherry was a gift from Michael Davidson (Addgene plasmid # 55037). A set of four shRNAs directed against TBK1 plus a control sequence were purchased from GeneCopoeia (# MSH101526-LVRU6MP, with an U6 promoter and mCherry as reporter gene. Control sequence: GCTTCGCGCCGTAGTCTTA, shRNA 1: CCAGAATCAGAATTTCTCATT, shRNA 2: CCAGTTCTTGCAAACATACTT, shRNA 3: GGGTGAGATTTCAGACATACA, shRNA 4: GCTTATAATGAAGAACAGATC). LysoTracker Red DND-99, LysoTracker Deep Red and TMRE (T669) 1 mM stock were purchased from ThermoFisher. Poly I:C LMW was bought from Invitrogen and MRT67307 from Sigma.

2.3 Antibodies

The antibodies used are presented in table 2.1:

Antigen	Supplier/Clone	Species	Dilution
Acetylated tubulin	Santa Cruz sc-23950 Clone: 6-11 B-1	mouse	IF: 1:400
α-tubulin	Abcam ab6161	rat	WB: 1:2,000
βIII-tubulin (Tuj1)	Covance MMS-435P	mouse	IF: 1:1,000
Caspase-3 active	R&D systems	rabbit	IF: 1:750
GM-130	BD Transduction laboratories	mouse	IF: 1:100
LAMP2	DSHB Clone: ABL-93	rat	IF: 1:1,000
MAP2	Chemicon AB5622	rabbit	IF: 1:1,000
p-Rab7 (S72)	Home-made	rabbit	IF: 1:600
p-TBK1 (S172)	Cell Signaling mAb #5483 Clone: D52C2	rabbit	WB: 1:1,000 IF: 1:200
Rab7	Abcam ab50533	mouse	IF: 1:250
RFP	GenScript A00682	rabbit	WB: 1:2,000
SMI-31	Covance SMI-31R	mouse	IF: 1:1,000
TBK1	Abcam ab40676 Clone: EP611Y	rabbit	WB: 1:3,000 IF: 1:200
Tyrosinated tubulin	Millipore mab1864 Clone: YL 1/2	rat	IF: 1:500

Table 2.1. Details of the antibodies used, and dilutions for western blotting (WB) and immunofluorescence (IF).

2.3 H_CT labelling

3.3 mg of purified H_CT were incubated in reducing buffer (150 mM NaCl, 20 mM HEPES, pH = 7.4 plus 14.4 µl of tris(2-carboxyethyl)phosphine (TCEP) 10 mM to a final volume of 100 µl) for 30 min at 4°C. 1 mg of AlexaFluor 555 C_2 Maleimide (ThermoFisher) was reconstituted in 30 µl water-free dimethyl sulfoxide (DMSO). 5.5 µl of the fluorescent dye were added to the H_CT/TCEP mix, slowly but continuously under constant mild agitation. The reaction mixture was incubated at 4°C overnight protected from light. Next day, the reaction was stopped by adding 12.5 µl of STOP solution (40 mM reduced glutathione, 10 mM Tris-HCl, 100 mM NaCl, pH = 8.0) and incubated at 4°C, protected from light for 20 min. Labelled-H_CT was separated from free dye by loading the reaction product onto a PD-10 desalting column (GE Healthcare, 17-0851-01). Several eluted fractions were collected (~40 fractions) and tested for the presence of proteins by Ponceau staining. The fractions containing AlexaFluor 555-conjugated H_CT were combined and injected into a 10K dialysis cassette (Slide-A-Lyzer Dialysis cassette, 10000 MWCO, 3 ml), and dialysed against dialysis buffer (100 mM NaCl, 10 mM HEPES, pH = 7.4) at 4°C for 2 days (the dialysis buffer was changed after one day). Labelled H_CT was then concentrated using an Amicon Ultra-0.5 filter (50K), and its presence was checked by loading an aliquot onto a polyacrylamide gel and staining the gel with Coomassie blue staining, or by loading the aliquot onto a Mini-PROTEAN TGX Stain-Free gel (BioRad) and detecting protein bands with a ChemiDoc MP Imaging System (BioRad). Labelled H_CT concentration was measured with a nanodrop spectrophotometer. 2 µl aliquots were snap frozen and stored at -80°C.

2.3 Cell culture

Cell culture and primary motor neuron culture reagents were purchased from ThermoFisher, unless otherwise stated. Mouse neuroblastoma N2a cells and Lenti-HEK cells where maintained in DMEM 10% FBS supplemented with 1% GlutaMAX at 37°C

and 5% CO_2. Transfection of N2a cell was carried out using Lipofectamine 3000 (Invitrogen) following the manufacturer's instructions. Briefly, cells were seeded onto 13 mm coverslips and transfected at 70%-80% confluency. 500 ng of DNA and 0.75 µl of Lipofectamine were used per well. In experiments studying Rab7 intracellular distribution, transfection was carried out for 18 h.

Mouse NSC-34 cell line were differentiated as follows: 10,000 – 15,000 cells were seeded onto collagen coated coverslips and maintained in differentiation medium (DMEM 1% FBS, non-essential amino acids and penicillin/streptomycin). On day one, medium was changed to differentiation medium plus retinoic acid 1 µM. On day 3, medium was topped up and on day 6 cells were fixed as described in 2.6.

2.4 Primary motor neuron culture

Cultured primary motor neurons (MN) were obtained as previously described (Arce et al., 1999). Briefly, ventral spinal cords were dissected from E12.5 mice embryos, treated with trypsin 2.5% w/v (0.025% final concentration) for 10 min at 37°C, mechanically dissociated, treated with DNAse I 1 mg/ml (Sigma, 50 µg/ml final concentration), collected under a bovine serum albumin (BSA) cushion, and centrifugated at 380 x *g* for 5 min. Cells were resuspended in motor neuron medium (Neurobasal, 2% heat-inactivated horse serum, 2% B27 supplement, 1X GlutaMax, 25 µM β-mercaptoethanol, 1% penicillin/streptomycin, recombinant rat CNTF (R&D Systems, 10 ng/ml), recombinant rat GDNF (R&D Systems, 0.1 ng/ml) and recombinant human BDNF (R&D Systems, 1 ng/ml)). Cells were seeded onto poly-D-ornithine/laminin coated plates or coverslips. Magnetofection (NeuroMag, OZ Biosciences) was carried out following the manufacturer's instructions. Briefly, motor neuron medium was collected, stored at 37°C, and replaced with magnetofection medium (Neurobasal, 2% B27 supplement, 1X GlutaMAX, 25 µM β-mercaptoethanol, GDNF 10 ng/ml, CNTF 10 ng/ml and BDNF 10 ng/ml) for 1 h. The DNA-magnetic beads complexes were prepared as follows: for 24-

well plates, 500 ng of DNA and 1.75 µl of beads per well were separately dissolved into 50 µl of minimum essential medium (MEM). DNA-containing MEM was added to the beads-containing MEM, mixed and incubated at room temperature for 20 min. After this, the mix was added dropwise to the wells with motor neurons, the plate was returned to the incubator and was placed on a magnet for 20 min. Then, the magnet was removed and motor neurons were kept in the incubator for 40 min. Following this, transfection medium was discarded and replaced with a mix of the previously stored motor neuron medium and fresh motor neuron medium 1:1. Magnetofected neurons were incubated for 18-24 h and used for further experiments.

2.5 Western blotting

N2a cells and primary MN cultures were lysed in RIPA buffer: 50 mM Tris-HCl pH 7.5, 1 mM EDTA, 2 mM EGTA, 150 mM NaCl, 1% NP40, 0.5% sodium deoxycholate and 0.1% sodium dodecyl sulfate containing protease and phosphatase inhibitor cocktail (HALT, ThermoFisher), for 30 min at 4°C. Lysates were centrifugates at 14,000 rpm for 15 min at 4°C and protein concentration was determined using the BCA Protein Assay (ThermoFisher). Between 10 and 20 µg of total protein extract were loaded on 4-15% Mini-PROTEAN TGX precast gels (BioRad) and transferred into polyvinylidene difluoride (PVDF) membranes (BioRad). Membranes were blocked in Tris-buffered saline (TBS) containing 0.05% Tween-20 and 5% bovine serum albumin (BSA) for 1 h at room temperature, and then incubated with primary antibodies overnight at 4°C. Membranes were washed and incubated with horseradish peroxidase (HRP)-conjugated secondary antibodies (GE Healthcare) for 1 h at room temperature. Immunoreactivity was detected using Immobilon Classico ECL substrate (Millipore) and the ChemiDoc MP Imaging System (BioRad).

2.6 Immunofluorescence

N2a cells and cultured primary motor neurons were fixed in 4% paraformaldehyde/4% sucrose in phosphate-buffered saline (PBS) for 30 min at room temperature. Cells were washed three times with PBS, permeabilised with Triton X-100 0.2% in PBS for 5 min, washed again three times and blocked in 5% BSA in PBS for 1 h at room temperature. Primary antibodies were incubated overnight at 4°C in blocking solution. Coverslips were washed three times, incubated with AlexaFluor-conjugated secondary antibodies for 1 h at room temperature, washed again three times, stained with 4′,6-diamidino-2-phenylindole (DAPI) when indicated, washed once with water and mounted on Mowiol.

2.7 Live cell imaging and tracking

Cultured primary MN were transduced with viral particles on day *in vitro* (DIV) 3, or magnetofected on DIV 5, as specified earlier. On DIV 6, neurons were labelled with either 30 nM AlexaFluor-conjugated H_CT for 45 min, 50 nM Lysotracker Red for 30 min or 20 nM Tetramethylrhodamine, ethyl ester (TMRE) for 20 min. Cells were washed and imaged in motor neuron medium supplemented with 20 mM HEPES pH = 7.4 (for mitochondrial transport experiments, the imaging medium also contained 20 nM TMRE). Images were acquired every 500 ms, for a total of 400 images per time-lapse (300 frames for mitochondria experiments). Endosomes and lysosomes were tracked using the Fiji ImageJ plugin TrackMate (Tinevez et al., 2017) in manual mode. Mitochondria were tracked using the Fiji ImagJ plugin KymoAnalyzer (Neumann et al., 2017) with the following parameters: pixel size: 0.1 µm, frame rate: 2 frames/second, multiplication factor in “Segments” plugin (plugin 5): 2, threshold for the detection of mobile/stationary and switching tracks: 0.5 nm and threshold for the assignment of segments/pauses: 0.1. For the EB3-comets experiments, MN were magnetofected on DIV 2 and imaged after 6 h. Images were acquired every 500 ms, for a total of 100 images per time-lapse. Kymographs were generated with the Multi Kymographs analysis option in Fiji ImageJ.

2.8 Tyrosinated/Acetylated tubulin analysis

Cultured primary MN were magnetofected on DIV 2. After 24 h, neurons were simultaneously extracted and fixed, as previously described (Ahmad et al., 2000). Briefly, MN were washed with PBS and then extracted/fixed with a solution containing PHEM (60 mM PIPES, 25 mM HEPES, 10 mM EGTA and 2 mM $MgCl_2$, pH 6.9), 4% paraformaldehyde, 0.15% glutaraldehyde and 0.2% Triton X-100 for 15 min. After these steps, the immunofluorescence protocol was carried out as mentioned above. The analysis of fluorescence intensity profiles for both tyrosinated and acetylated tubulin was done using Fiji ImageJ. The profiles were measured starting at the axonal tip towards the cell body, until obtaining a profile of at least 50 µm in length. The ratio between both channels on the proximal and distal axon was determined: average measurement from segments of 5 µm in length, between 5 and 10 µm from the axon tip (shown as distal) and between 45 and 50 µm from the axonal tip (shown as proximal).

2.9 Viral particles preparation

Lenti-HEK cells were seeded onto 15 cm culture-treated plates and transfected with second generation lentiviral constructs VSV-G and PAX, as well as one of the TBK1 shRNA plasmids per condition. After 48 and 72 h of expression, supernatants were collected and centrifugated at 1,500 rpm (~ 500 x *g*) for 10 min at 4°C. LentiX concentrator (Clontech) was added to the supernatant in a proportion of 1:3, mixed and stored at 4°C for two days. Tubes were centrifugates at 3,000 rpm for 45 min at 4°C, the supernatant was discarded, the pellet resuspended in ~ 400 µl of Optimem (ThermoFisher), aliquoted and snap frozen in liquid nitrogen.

2.10 Statistical analysis

Statistical analysis was performed using GraphPad Prism software. Data is shown as mean ± SEM. We compared multiple groups by one-way ANOVA with Tukey's multiple

comparison test and grouped conditions by two-way ANOVA with Sidak's multiple comparison test. For cases when variances were non-comparable, Kruskal-Wallis non-parametric one-way ANOVA was used. We used D'Agostino-Pearson as a normality test. Statistical significance was considered as follows: *, $P < 0.05$, **, $P < 0.01$, and ***, $P < 0.001$.

Chapter 3

3.1 Rab7 intracellular localisation

The distribution of phosphorylated Rab GTPases has been addressed by subcellular fractionation and immunofluorescence (Steger et al., 2016). However, whether the consequences of Rab phosphorylation on the switch II region are the same for different Rab proteins is not clear. In addition, a cytosolic Rab7-S72E distribution has been reported in cell lines, such as HEK and HeLa (Heo et al., 2018; Shinde and Maddika, 2016), as well as in primary B-cells and A20 murine B-cell lymphoma (Satpathy et al., 2015). Nevertheless, its intracellular distribution in cells from neuronal lineages remains unexplored. In this regard, our first approach consisted in transfecting undifferentiated mouse neuroblastoma N2a cells with either GFP-Rab7 WT, GFP-Rab7 S72A (phospho-deficient mutant) or GFP-Rab7 S72E (phospho-mimetic mutant). Transfected cells were fixed after 8 h and stained for the late endosome and lysosome marker LAMP2 (Figure 3.1 A). Both GFP-Rab7 WT and GFP-Rab7 S72A show a vesicular pattern, which overlaps with the LAMP2 positive organelles in the perinuclear region. In contrast, GFP-Rab7 S72E exhibits a cytosolic distribution, suggesting that it is excluded from membranous compartments. The quantification of LAMP2 positive vesicles distribution (number and size) showed no difference between condition (data not shown). Next, we magnetofected cultured primary motor neurons (MN) after six days *in vitro* (DIV) with the three Rab7 constructs. Neurons were fixed after 8 h and imaged to assess GFP-Rab7 distribution (Figure 3.1 B). In agreement with the result obtained from N2a cells, both GFP-Rab7 WT and GFP-Rab7 S72A display a vesicular pattern whilst GFP-Rab7 S72E remains cytosolic.

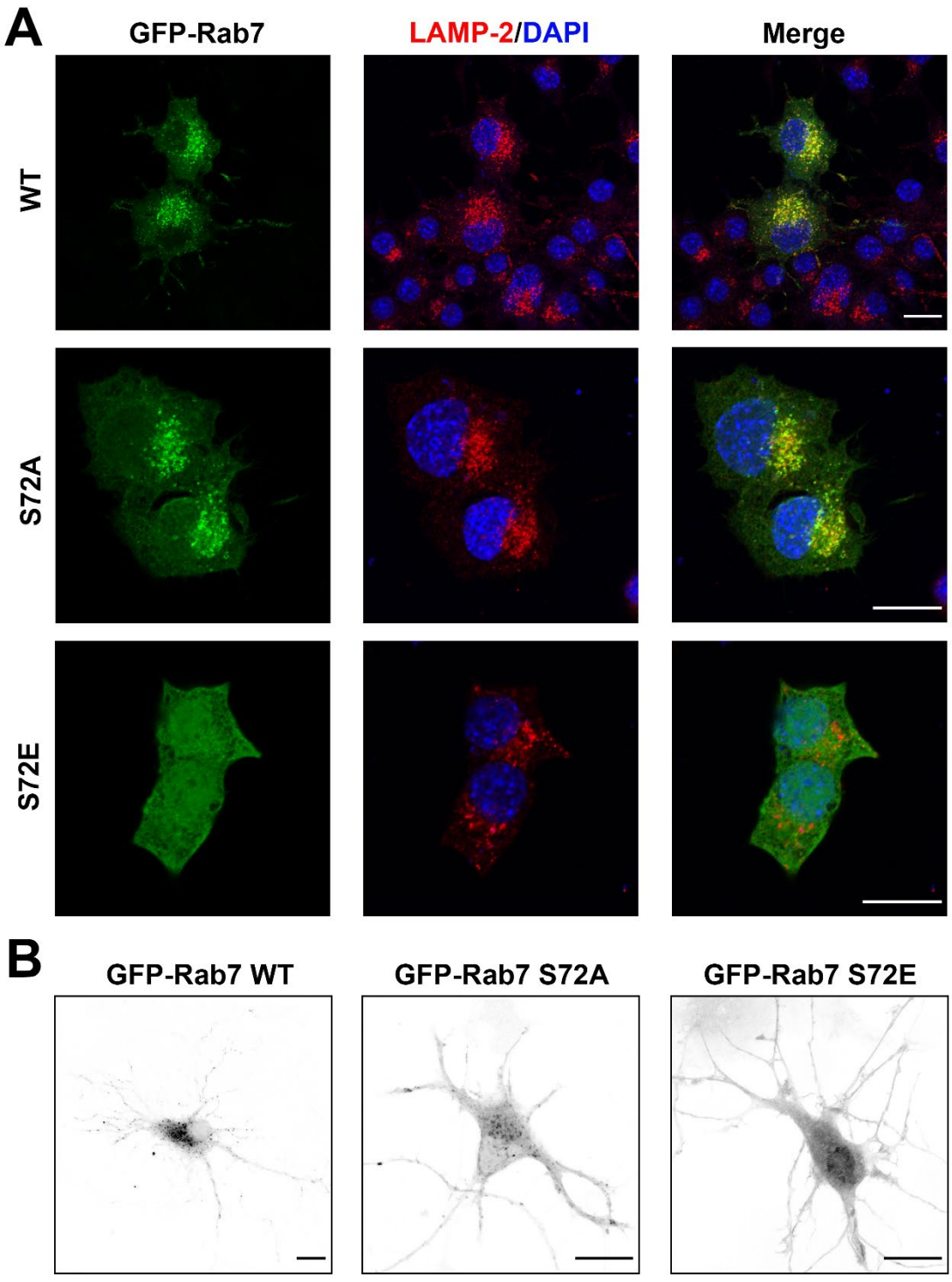

Figure 3.1. GFP-Rab7 distribution in neuronal cells. (A) Undifferentiated N2a cells were transfected with GFP-Rab7 WT, GFP-Rab7 S72A or GFP-Rab7 S72E, fixed after 8 h and stained as indicated. Rab7 WT and S72A show a punctate pattern, whilst the S72E mutant remains diffuse through the cytoplasm. Scale bar, 15 μm. **(B)** Primary motor neurons in culture were magnetofected after 6 DIV with GFP-Rab7 WT, GFP-Rab7 S72A or GFP-Rab7 S72E and fixed after 8 h. The Rab7 distribution pattern is consistent with that shown for N2a cells. Scale bar, 15 μm.

3.2 Rab7 effect on signalling endosomes axonal transport

The retrograde transport of signalling endosomes carrying neurotrophins and their receptors relies on Rab7 (Deinhardt et al., 2006). In this regard, we asked whether the phosphorylation state of Rab7 on S72 can alter the trafficking of these carriers. We wanted to express GFP-Rab7 WT and the mutants GFP-Rab7 S72A and GFP-Rab7 S72E in primary MN in culture, however, transfection by physicochemical methods (e.g. Lipofectamine, FuGENE, Calcium phosphate) are limited in this model due to the lack of efficient techniques. Nucleic acid delivery using magnetic beads (magnetofection) has emerged as an useful tool for inducing exogenous gene expression in cell types that are hard to transfect (Plank et al., 2011). Therefore, we transfected MN using magnetofection. Primary mouse MN in culture were magnetofected after 5 DIV, and one day later, the transport of signalling endosomes was monitored with fluorescently labelled H_CT, which is retrogradely transported in neurotrophin signalling endosomes (Lalli and Schiavo, 2002; Deinhardt et al., 2006). We detected two populations of cargoes: a pool double-positive for Rab7 and H_CT, and another single positive (labelled with H_CT but negative for Rab7), except upon expression of the Rab7 S72E mutant, where no double-positive cargoes were found. Hence, both double and single positive populations were analysed separately. First, we tested whether magnetofection itself has a detrimental effect on axonal transport. We compared single positive cargoes (H_CT positive cargoes, which were Rab7 WT negative in neurons expressing Rab7 WT, termed “No WT/H_CT”, and H_CT positive cargoes which were Rab7 S72A negative, in neurons expressing Rab7 S72A, termed “No S72A/ H_CT”) to H_CT-labelled endosomes from control neurons (no DNA or magnetic beads added). The speed profiles (Figure 3.2.1 A, retrograde transport is shown as positive) and the average speed per cargo, considering every single speed as positive (Figure 3.2.1 B) remain unchanged, indicating that axonal transport is not affected by magnetofection.

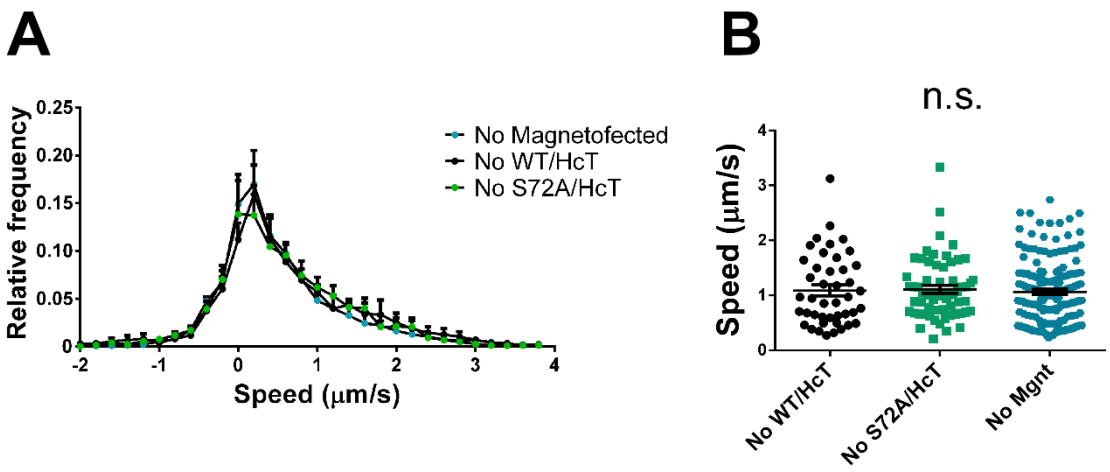

Figure 3.2.1. Magnetofection does not affect the axonal transport of H_CT-positive signalling endosomes. (A) Speed profiles for H_CT single positive carriers tracked in MN from No WT/H_CT, No S72A/H_CT and no magnetofected conditions. **(B)** Average speed per cargo, considering every displacement as positive. Magnetofection does not change the cargoes speed profile, nor their average speed. Data shown as mean ± SEM, n = (No WT/H_CT 43 cargoes and No S72A/H_CT 62 cargoes from 4 different cultures, and no magnetofected 169 cargoes from 3 independent cultures). One-way ANOVA with Tukey's multiple comparison test, n.s.= not significant.

Having confirmed that magnetofection does not affect axonal transport of signalling endosomes, we continued with the analysis of double and single positive cargoes. A representation of the movement of every cargo as a function of time (displacement graph) is shown in Figure 3.2.2 A. The majority of H_CT-positive cargoes move retrogradely in every condition analysed, except in neurons expressing the S72E mutant, where a subpopulation of carriers moves anterogradely. We also compared the average speed of the organelles, considering every displacement as positive (Figure 3.2.2 B), and observed that the speed of H_CT positive cargoes does not differ between conditions. The analysis of the cargoes speed profiles (Figure 3.2.2 C) shows that H_CT axonal transport is not affected by the expression of the S72A mutant, both for single and double positive carriers. Conversely, the speed profile of cargoes in neurons expressing the S72E mutant is shifted toward the left, in agreement with increased anterograde transport.

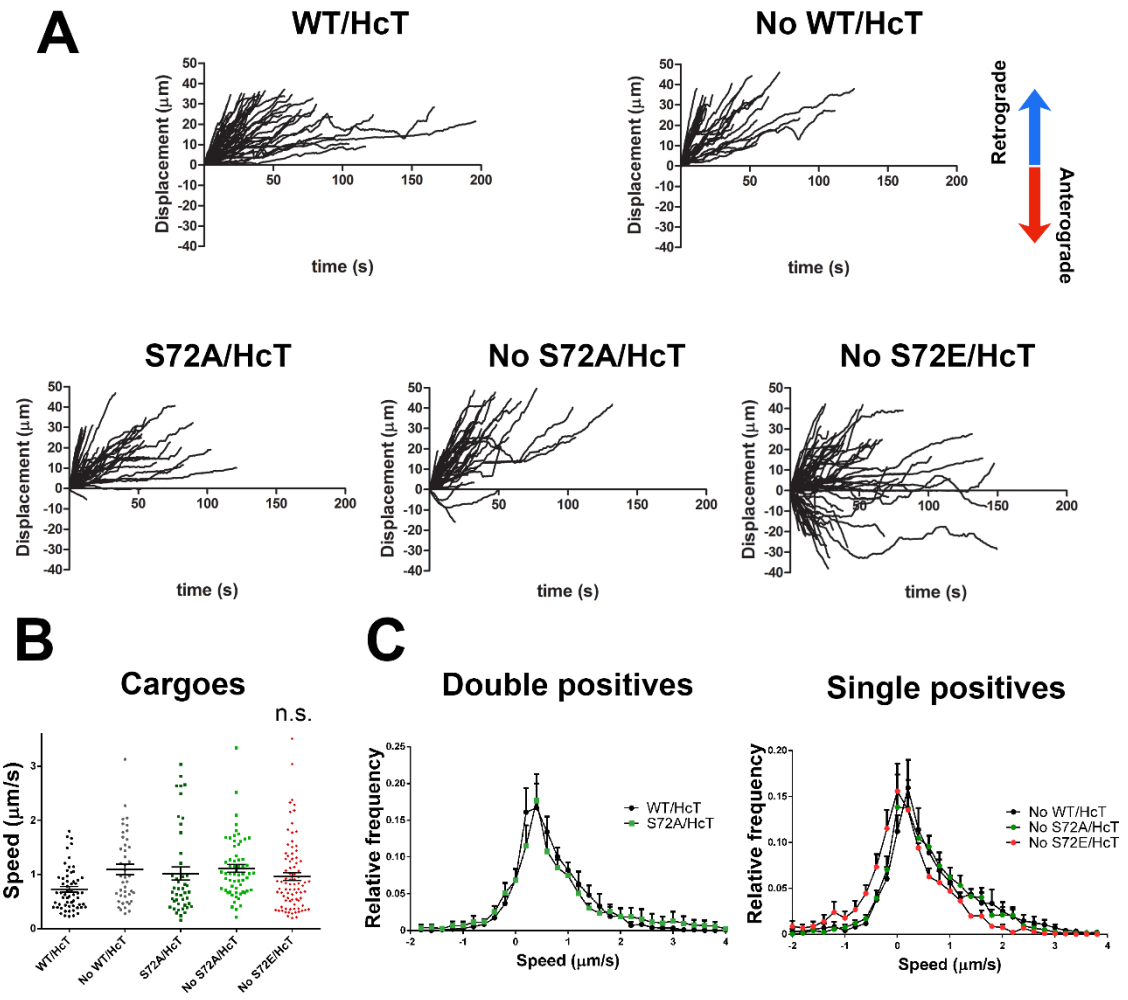

Figure 3.2.2. Rab7 S72E expression affects the transport of H_CT positive signalling endosomes. Primary MN were magnetofected with GFP-Rab7 WT, S72A or S72E after 5 DIV. 24 h later, the cells were labelled with AlexaFluor 555-conjugated H_CT 30 nM for 45 min, washed and imaged. Cargoes were tracked and classified as double positives for GFP-Rab7 and H_CT or single positives (just H_CT). **(A)** Displacement graphs for every condition, with retrograde movement considered positive. H_CT positive cargoes exhibit a preference for movement towards the retrograde direction, however a subpopulation of endosomes in the S72E condition moves anterogradely. **(B)** Average speed per cargo, considering every displacement as positive, regardless of its directionality. The speed of H_CT positive cargoes is not affected. **(C)** Speed profiles for double and single positive cargoes. The single positive cargo curve for the Rab7 S72E condition is shifted towards the left, reflecting the increase in anterograde movement. Data is shown as mean ± SEM, n = (WT/H_CT 59 cargoes, No WT/H_CT 43 cargoes, S72A/H_CT 45 cargoes, No S72A/H_CT 62 cargoes, No S72E/H_CT 85 cargoes) from 4 independent primary cultures, one-way ANOVA with Tukey's multiple comparison test, n.s.= not significant.

3.3 GFP-Rab7 constructs are expressed at equivalent levels in axons

Our results show that the expression of GFP-Rab7 S72E changes the directionality of transport of a subpopulation of H_CT positive cargoes. Regarding this, we wanted to rule out a possible adverse effect derived from differential over-expression of Rab7 variants. In order to do that, primary MN from the same cultures used in live-cell imaging experiments described in Figure 3.2.2, were fixed and immunolabelled for endogenous Rab7 (Figure 3.3 A), with an antibody which recognises both endogenous and the recombinant magnetofected Rab7 variant. Despite Rab7 signal in cell bodies from transfected neurons is increased, and allows to distinguish them from untransfected cells (Rab7 fluorescence signal is 2-3 times higher in the soma of transfected cells), the intensity in the axon is similar between transfected and untransfected neurons. Therefore, we measured Rab7 fluorescent intensity in axons of transfected MN and compared them to untransfected MN in the same coverslip (Figure 3.3 B). This analysis revealed that axonal Rab7 levels in transfected MN are comparable to untransfected MN, and that all three constructs are expressed at similar levels.

Additional experimental methods, such as western blotting, cannot be used in this case, given the low magnetofection efficiency and the heterogeneity of magnetofected cells, which include neurons and glial cells. In conclusion, the effect of Rab7 S72E on axonal transport is unlikely to be due to differential transfection efficiency or expression levels in the axons. Nevertheless, we cannot rule out completely the effect the accumulation of Rab7 in the soma may exert on Rab7-dependent mechanisms taking place in the axon.

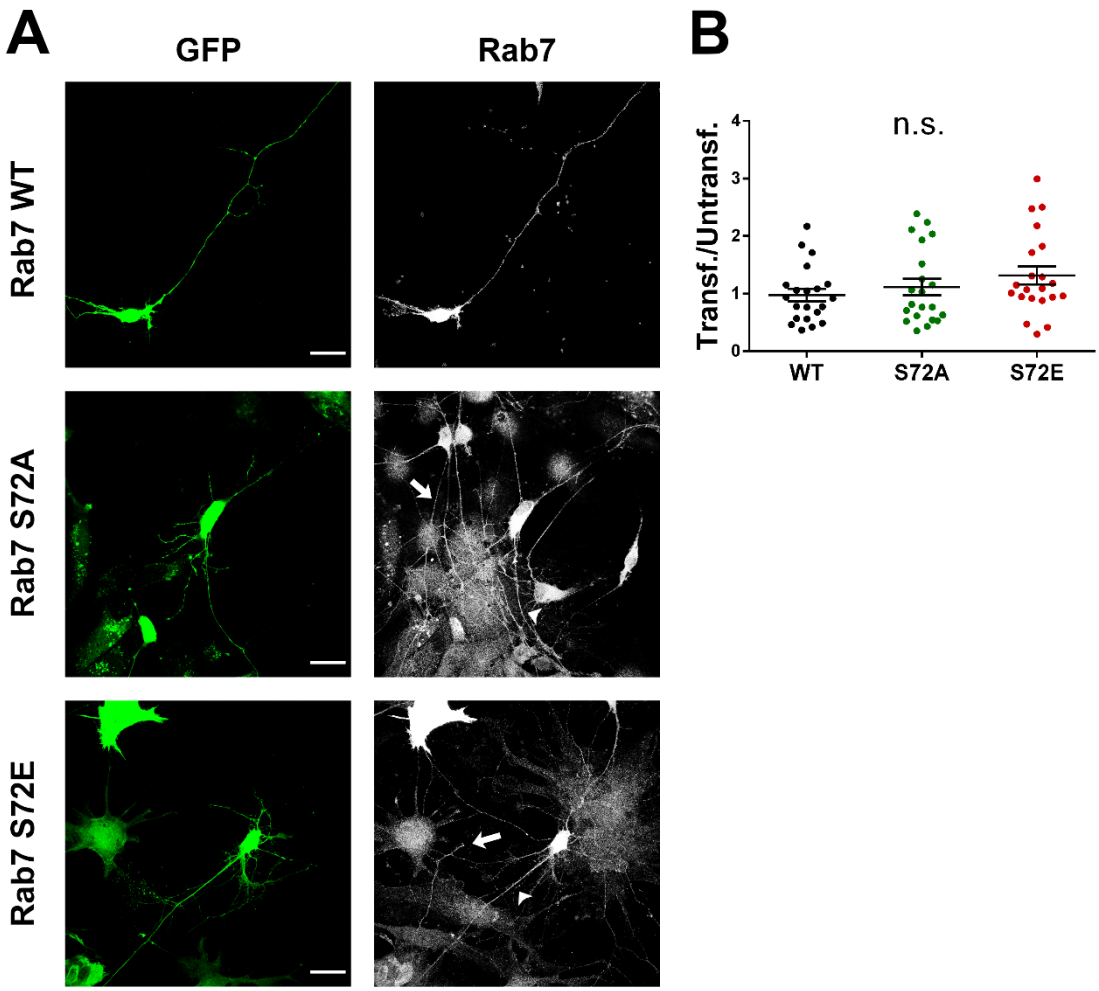

Figure 3.3. GFP-Rab7 WT, S72A and S72E are expressed at similar levels in axons. **(A)** Primary MN in culture were magnetofected after 5 DIV with either GFP-Rab7 WT, GFP-Rab7 S72A or GFP-Rab7 S72E, fixed 24 h later, and stained for Rab7. Whilst the cell body of transfected neurons exhibits higher levels of Rab7 compared to untransfected neurons, the axon (arroehead) is comparable to untransfected neurons (arrows). Scale bar, 25 μm **(B)** Axonal Rab7 fluorescent intensity, expressed as the radio between transfected and untransfected MN. Data is shown as mean ± SEM, n = 21 neurons for the three conditions, from 3 independent primary cultures, one-way ANOVA with Tukey's multiple comparison test, n.s.= not significant.

3.4 GFP-Rab7 S72E expression does not affect neuronal polarity

After showing that the different conditions of magnetofected MN express similar levels of Rab7 WT or mutant, we sought to evaluate whether this phenotypic change is the consequence of a general disruption on neuronal polarity. Given that the identification of individual processes is less complex in low density primary MN cultures, we evaluated changes in neuronal polarity at 2 DIV. Cultured primary MN were magnetofected with either GFP-Rab7 WT or GFP-Rab7 S72E and fixed after 8 h. Neurons were stained with the somatodendritic marker MAP2 and the axonal marker SMI-31 (Figure 3.4 A). In both conditions MN exhibited a clearly identifiable polarisation, and their axons were immunolabelled by a SMI-31 specific antibody, indicating that their axonal identity has not been lost.

The retrograde transport of signalling endosomes relies on the polarised array of microtubules in axons (Baas et al., 1988). Therefore, changes in the directionality of transport might emerge not only from neuronal polarity defects, but also from microtubule polarity rearrangements. In this regard, we tested if GFP-Rab7 S72E expression induces loss of microtubule polarity in the axon, by monitoring the movement of end-binding (EB) protein EB3. EB3 belongs to the group of plus-end tracking proteins (+TIPS), which accumulate at the plus-end of growing microtubules (Akhmanova and Hoogenraad, 2005). Primary MN in culture were co-magnetofected with EB3-mCherry and either GFP-Rab7 WT or GFP-Rab7 S72E at 2 DIV, and imaged 6 h later. Figure 3.4 B shows selected frames from representative videos, as well as their respective kymographs for the EB3-mCherry channel. We found that approximately 98% of EB3 comets move anterogradely in axons from MN expressing GFP-Rab7 WT, and this percentage remains unchanged in Rab7 S72E expressing neurons. Altogether, these results suggest that the changes induced by GFP-Rab7 S72E on the axonal transport of H_CT carriers, are not due to an alteration of neuronal polarity.

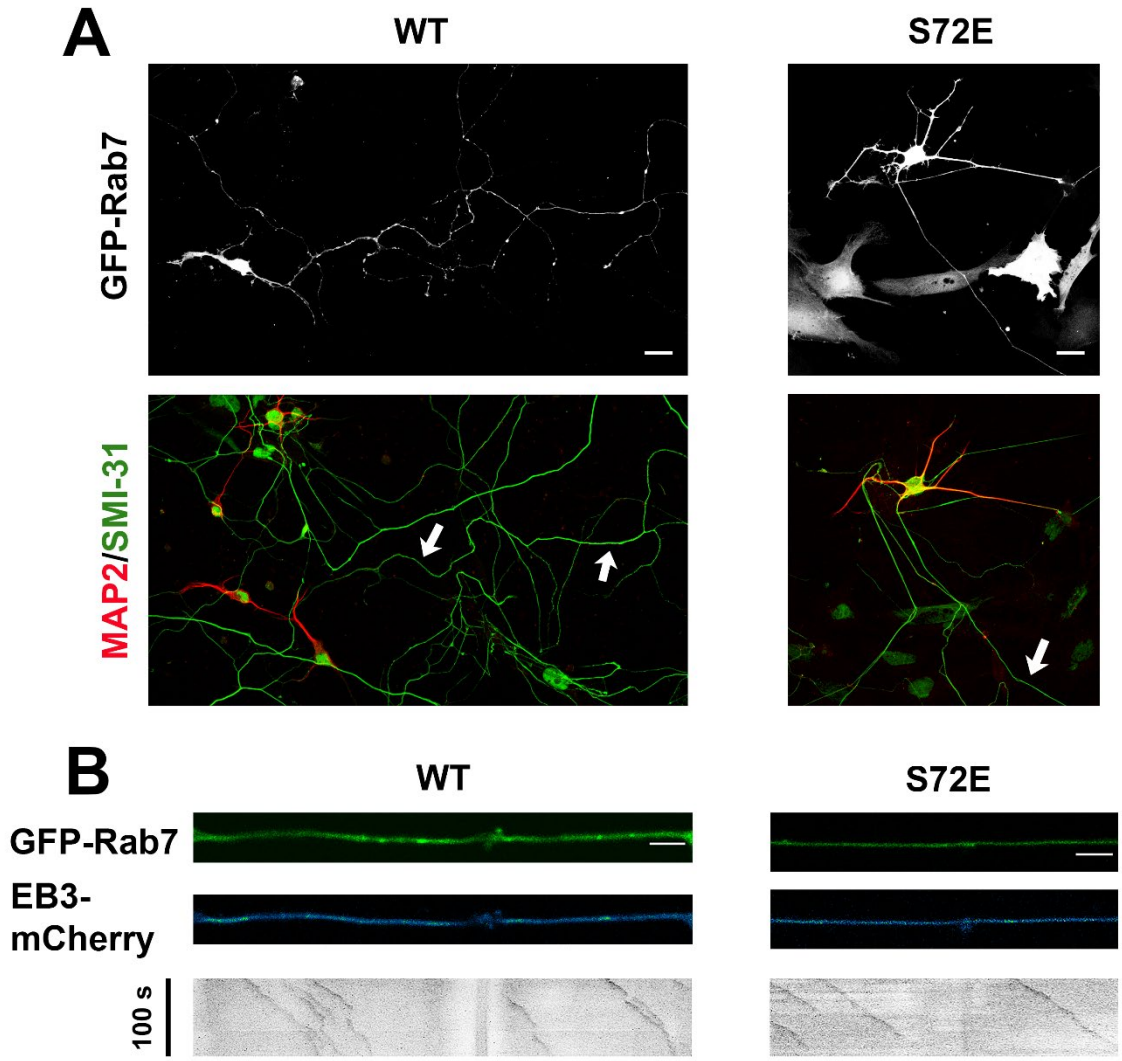

Figure 3.4. Neuronal polarity and axonal microtubule polarity are not affected in MN expressing GFP-Rab7 S72E. (A) Primary MN were magnetofected at DIV 2 with either GFP-Rab7 WT or S72E, fixed after 8 h and stained as indicated. Arrows show the axon of the transfected neuron in the merged image. Scale bar, 20 µm. **(B)** Primary MN were co-magnetofected with EB3-mCherry and either GFP-Rab7 WT or S72E on DIV 2 and imaged after 6 h. Number of retrogradely moving comets: WT first experiment = 1/39, S72E first experiment = 3/133, WT second experiment = 2/98, S72E second experiment = 1/89. Scale bar, 5 µm.

3.5 Rab7 S72E expression does not alter the ratio of tyrosinated/acetylated tubulin along the axon

Even though microtubule orientation along the axon appears unchanged, other cytoskeletal dynamics alterations may still be responsible for the changes in directionality of transport of H_CT signalling endosomes. Microtubules are not uniform arrays of polimerised tubulin, but mosaic polymers composed of α and β tubulin bearing several different post-translational modifications, which are assymetrically distributed across microtubules (Park and Roll-Mecak, 2018). These tubulin post-translational modifications can control microtubule dynamics and interaction with microtubule associated proteins, including the molecular motor cytoplasmic dynein (McKenney et al., 2016). Regarding this, we asked whether GFP-Rab7 S72E expression modifies the distribution of tyrosinated (Tyr) and acetylated (Ac) tubulin along axonal microtubules. The analysis of tubulin post-translational modification distribution requires the extraction of the soluble fraction of the cytoskeleton, hence, we first visualised of Tyr-tubulin and Ac-tubulin staining in extracted neurons. Cultured primary MN at 2 DIV were magnetofected with GFP-Rab7 WT and 24 h later, simultaneously extracted and fixed as described in the methods section. Figure 3.5.1 A shows an unextracted neuron, where the GFP-Rab7 WT fluorescent signal can be detected in both the somatodendritic and axonal compartments. On the other hand, extracted neurons lose the GFP-Rab7 signal in the axon, although it is still detectable in the soma (Figure 3.5.1 B, arrow). Using this protocol, we were able to see a pattern of enriched Tyr-tubulin at the axon tip, as previously described in the literature (Witte et al., 2008). Next, we magnetofected primary MN in culture at 2 DIV, with either GFP-Rab7 WT, GFP-Rab7 S72A or GFP-Rab7 S72E, and used the simultaneous extraction/fixation protocol after 24 h of expression (Figure 3.5.2 A). Fluorescent intensity profiles along the axon were measured for both Tyr-tubulin and Ac-tubulin staining, starting at the axon tip towards the cell body, until obtaining a profile of at least 50 μm in length. Fluorescent intensity profiles show that Ac-tubulin is

enriched in the proximal region, whilst Tyr-tubulin predominates in the distal axon. This pattern is conserved among the three conditions. We also compared the ratio of Tyr/Ac tubulin in the proximal and distal axon for these conditions (Figure 3.5.2 B), and found no statistically signficant differences between GFP-Rab7 WT and Rab7 mutants.

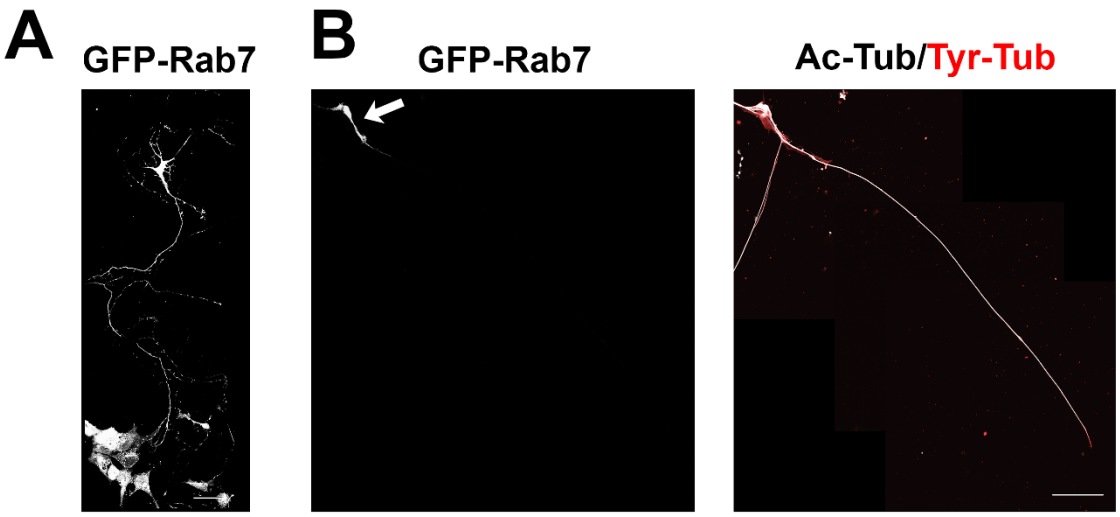

Figure 3.5.1. Testing the extraction of the soluble fraction of the cytoskeleton. Cultured primary MN at 2 DIV were magnetofected with GFP-Rab7 WT and 24 h later, neurons were fixed **(A)** or simultaneously extracted, fixed and stained as indicated. **(B)** Arrow shows the GFP-Rab7 WT signal that remains in the cell body, arrowhead shows Tyr-Tub enrichement on the distal axon. Scale bar, 50 µm. Images in A and B were acquired under the same conditions.

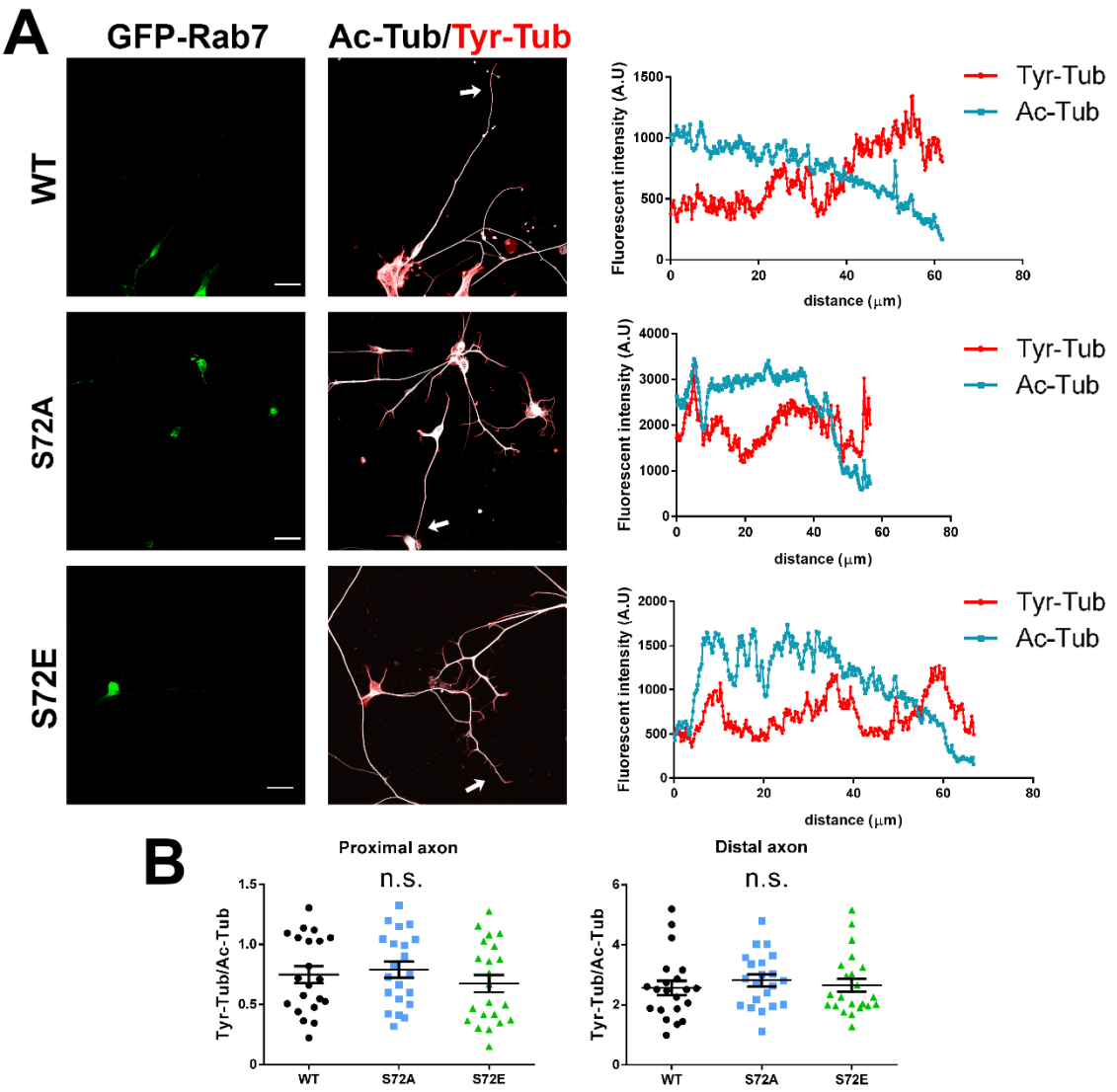

Figure 3.5.2. Tyr/Ac-tubulin distribution along the axon is not modified by Rab7 S72E expression. (A) Cultured primary MN at 2 DIV were magnetofected with GFP-Rab7 WT, GFP-Rab7 S72A or GFP-Rab7 S72E, simultaneously extracted and fixed after 24 h of expression, and stained. Fluorescence intensity profiles were measured starting at the axon tip until collecting profiles of at least 50 μm in length. In the fluorescence intensity profiles, the cell bodies are on the left. Arrows indicate the axon corresponding to the magnetofected neuron. Scale bar, 25 μm. **(B)** The ratio between Tyr-tubulin/Ac-tubulin on the proximal and distal axon was determined (average measurement from segments of 5 μm in length, between 5 and 10 μm from the axon tip (distal) and between 45 and 50 μm from the axonal tip (proximal)). Data shown as mean ± SEM, n = (WT 21 neurons, S72A 21 neurons, S72E 22 neurons, from 3 independent primary cultures). One-way ANOVA with Tukey's multiple comparison test, n.s.= not significant.

3.6 Rab7 S72E expression does not affect lysosomal transport

Our results show that the change in directionality of transport of H_CT positive cargoes is not linked to alterations in neuronal polarity or to modifications in microtubule orientation. We then asked whether this is a global effect on axonal transport or a specific change in signalling endosome dynamics. In addition to mediate signalling endosome transport, Rab7 also regulates late endosome and lysosome trafficking (Cabukusta and Neefjes, 2018; Guerra and Bucci, 2016), hence, we monitored the effect of GFP-Rab7 S72E expression on lysosomal transport. Cultured primary MN were magnetofected on DIV 5 with either GFP-Rab7 WT, GFP-Rab7 S72A or GFP-Rab7 S72E, and after 24 h of expression, labelled with LysoTracker Red for 30 min, washed and imaged. Figure 3.6 A shows the displacement graph for every condition, including the untreated group (Unt). Lysosomes move bidirectionally in control conditions, although with a bias towards the retrogarde direction. This remain unchanged upon expression of GFP-Rab7 WT, S72A and S72E (Figure 3.6 A). The analysis of the average speed per cargo, considering every speed as positive (Figure 3.6 B) indicates that this parameter is also unaffected. In agreement with this, the speed profiles for all conditions (Figure 3.6 C) overlaps, confirming that lysosomal transport is not altered by GFP-Rab7 S72E expression. Lastly, we quantified the percentage of cargoes moving on each direction (Figure 3.6 D), and found that about 80% of LysoTracker positive carriers moves retrogradely, a fraction that remained unchanged upon expression of Rab7 WT and its variants.

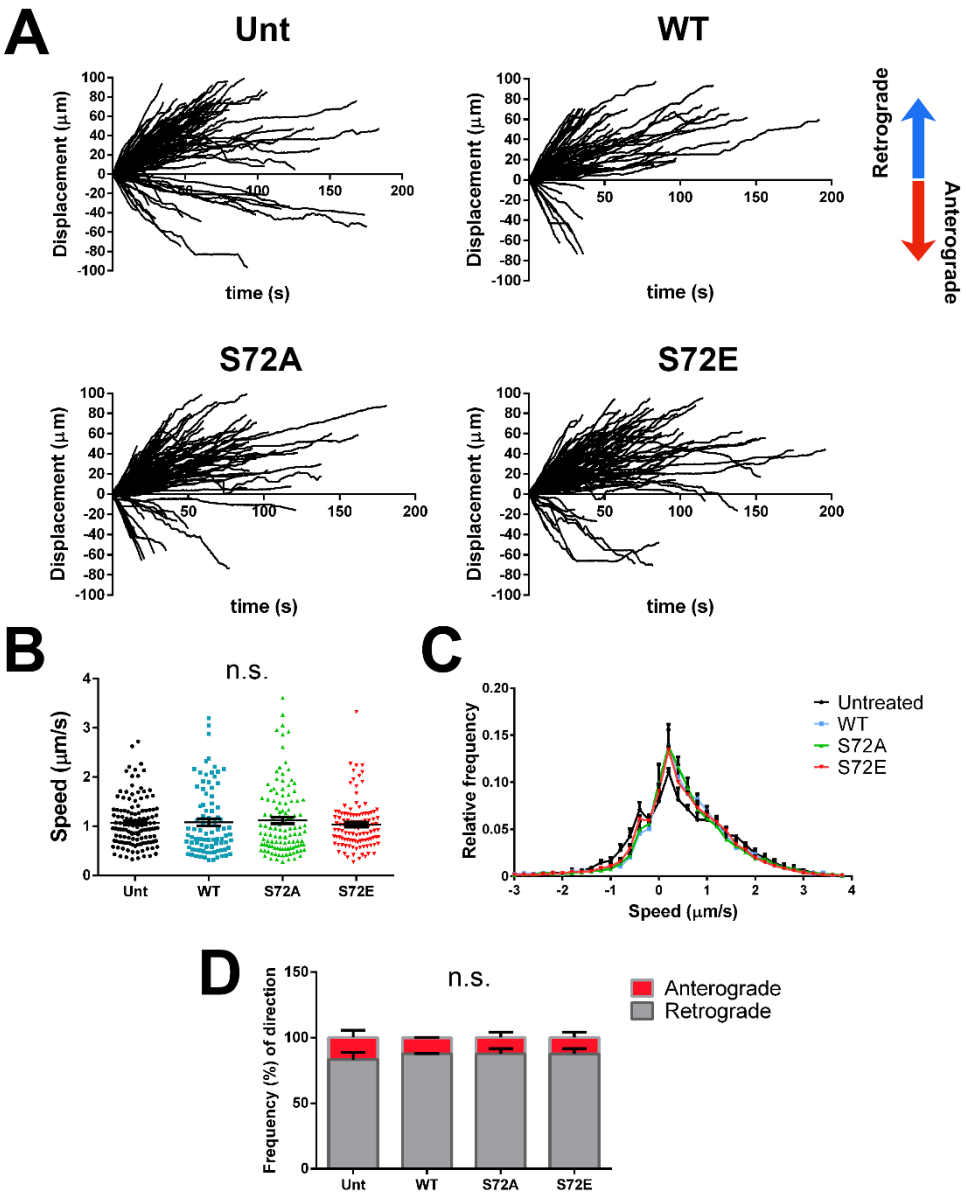

Figure 3.6. Lysosomal transport is not affected by Rab7 S72E expression. Cultured primary MN were magnetofected with either Rab7 WT, S72A or 72E on DIV 5 and 24 h later, labelled with LysoTracker Red (50 nM, 30 min), washed and imaged. **(A)** Displacement graphs for the untreated (Unt) and magnetofected conditions, with retrograde transport shown as positive. Despite lysosomal bidirectional movement, carriers exhibit biased retrograde trajectories, which are not modified by Rab7 WT or the mutant forms. **(B)** Average speed per cargo, considering every speed as positive. No statistically significant differences were observed for this parameter. Data shown as mean ± SEM, n = (Unt 127, WT 89, S72A 117, S72E 111, from 3 independent primary cultures), one-way ANOVA with Tukey's multiple comparison test, n.s.= not significant. **(C)** Speed profiles for the untreated and magnetofected conditions. Speed profiles overlap and confirm that lysosomal transport is not affected by Rab72E expression. **(D)** Quantification of the directionality of transport. About 80% of LysoTracker positive carriers move retrogradely, and this remains constant for all conditions. Data shown as mean ± SEM, n = 3 for each condition, two-way ANOVA with Sidak's multiple comparison test, n.s.= not significant.

3.7 Rab7 S72E expression does not affect mitochondrial transport

Since GFP-Rab7 S72E expression did not affect lysosomal trafficking, we decided to expand the analysis to an additional cargo, in order to further rule out a global defect on axonal transport. In particular, we chose to include mitochondria, because their bidirectional movement relies on the recruitment of motors through mechanisms which do not involve Rab7 (Mandal and Drerup, 2019; Saxton and Hollenbeck, 2012). Given the nature of mitochondrial transport, where a high proportion of organelles are not motile, we decided to analyse their trafficking with a kymograph-based protocol, instead of frame-to-frame tracking. We adopted the Fiji ImageJ plugin KymoAnalyzer (Neumann et al., 2017). Primary MN in culture were magnetofected on DIV 5 with either GFP-Rab7 WT, GFP-Rab7 S72A or GFP-Rab7 S72E, and after 24 h of expression, labelled with tetramethylrhodamine ethyl ester (TMRE) for 20 min, washed and imaged in medium containing TMRE. This cationic probe accumulates as a function of the mitochondrial membrane potential, allowing us to track polarised mitochondria (Scaduto and Grotyohann, 1999). This is relevant, since the proportion of motile and non motile mitochondria changes as a result of physiological stimuli, such as calcium influx (Chen and Sheng, 2013). Figure 3.7.1 A shows the distribution of the cargo population. In our experimental conditions, about 75% of mitochondria are static, whilst the rest are split almost equally between anterograde and retrograde transport. The expression of GFP-Rab7 WT or the two mutants does not alter the proportion of mitochondria moving, or their directionality. The speed profiles for each condition are depicted in Figure 3.7.1 B. Compared to H_CT-positive signalling endosomes and lysosomes, mitochondria move slower, with a maximum speed well below 2 μm/s in both directions. In addition, the speed profiles for every condition overlap, suggesting that mitochondrial transport is not affected. The average speeds for retrograde and anterograde transport are shown in Figures 3.7.1 C and 3.7.1 D, respectively. In agreement with the speed profiles, the average mitochondrial speed is between 0.4 – 0.6 μm/s, around half of the average value

for signalling endosomes and lysosomes. Despite a variation on the dispersion of the samples for the retrograde transport (untreated and GFP-Rab7 WT conditions in Figure 3.7.1 C), no statistically significant change was detected for any condition, neither on the retrograde nor the anterograde mitochondrial speeds.

Given the emerging role of Rab7 during Parkin-mediated mitophagy (Heo et al., 2018; Jimenez-Orgaz et al., 2018), we also checked whether GFP-Rab7 S72E affects mitochondrial axonal density. Figure 3.7.2 A shows representative images, with GFP-Rab7 fluorescent signal in green and TMRE in red. Mitochondrial density (expressed as mitochondria/μm, Figure 3.7.2 B) remains unchanged in every condition analysed. During this quantification, we noted an increased frequency for elongated mitochondria upon expression of Rab7 S72A (arrows in Figure 3.7.2 A). Therefore, we measured mitochondrial length (Figure 3.7.2 C) and found a significant increase of this parameter upon expression of GFP-Rab7 WT and S72A, whilst GFP-Rab7 S72E-expressing MN were unaffected. This change can be also appreciated in the cumulative frequency graph for mitochondrial length (Figure 3.7.2 D), where the untreated control and S72E groups behaves similarly and reach the pleateu faster, indicating a reduction in mitochondrial length, which is suggestive of a change in fusion and fission dynamics.

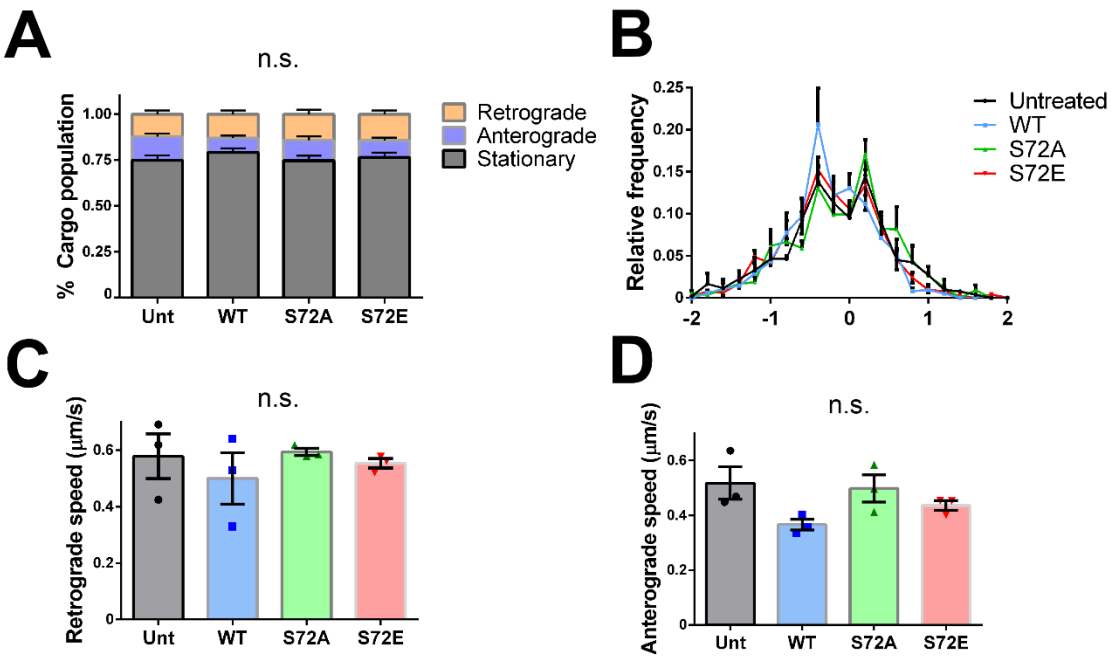

Figure 3.7.1. Mitochondrial axonal transport is not affected by Rab7 S72E expression. Primary MNs in culture were magnetofected with either Rab7 WT, S72A or 72E on DIV 5 and 24 h later, labelled with TMRE (20 nM, 20 min), washed and imaged in medium containing 20 nM TMRE. **(A)** Cargo population distribution. Between 70% - 80% of mitochondria are static, whilst the rest is split equally between retrograde and anterograde movement. No significant changes were detected in any condition. Data shown as mean ± SEM, n = (Unt 21, WT 20, S72A 18, S72E 20 neurons from 3 independent primary cultures), two-way ANOVA with Sidak's multiple comparison test, n.s.= not significant. **(B)** Speed profiles for every condition. The overlapping speed profiles shows that mitochondrial axonal transport is not affected by Rab72E expression. **(C)** Average retrograde speed per experiment. Average speeds remain unchanged between conditions, although there is a reduction on the dispersion of the samples for S72A and S72E, hence, a non-parametric test was used. Data shown as mean ± SEM, n = 3, Kruskal-Wallis one-way ANOVA with Dunn's multiple comparison test, n.s.= not significant. **(D)** Average anterograde speed per experimental replica. No statistically significant differences were detected between conditions. Data shown as mean ± SEM, n = 3, one-way ANOVA with Tukey's multiple comparison test, n.s.= not significant.

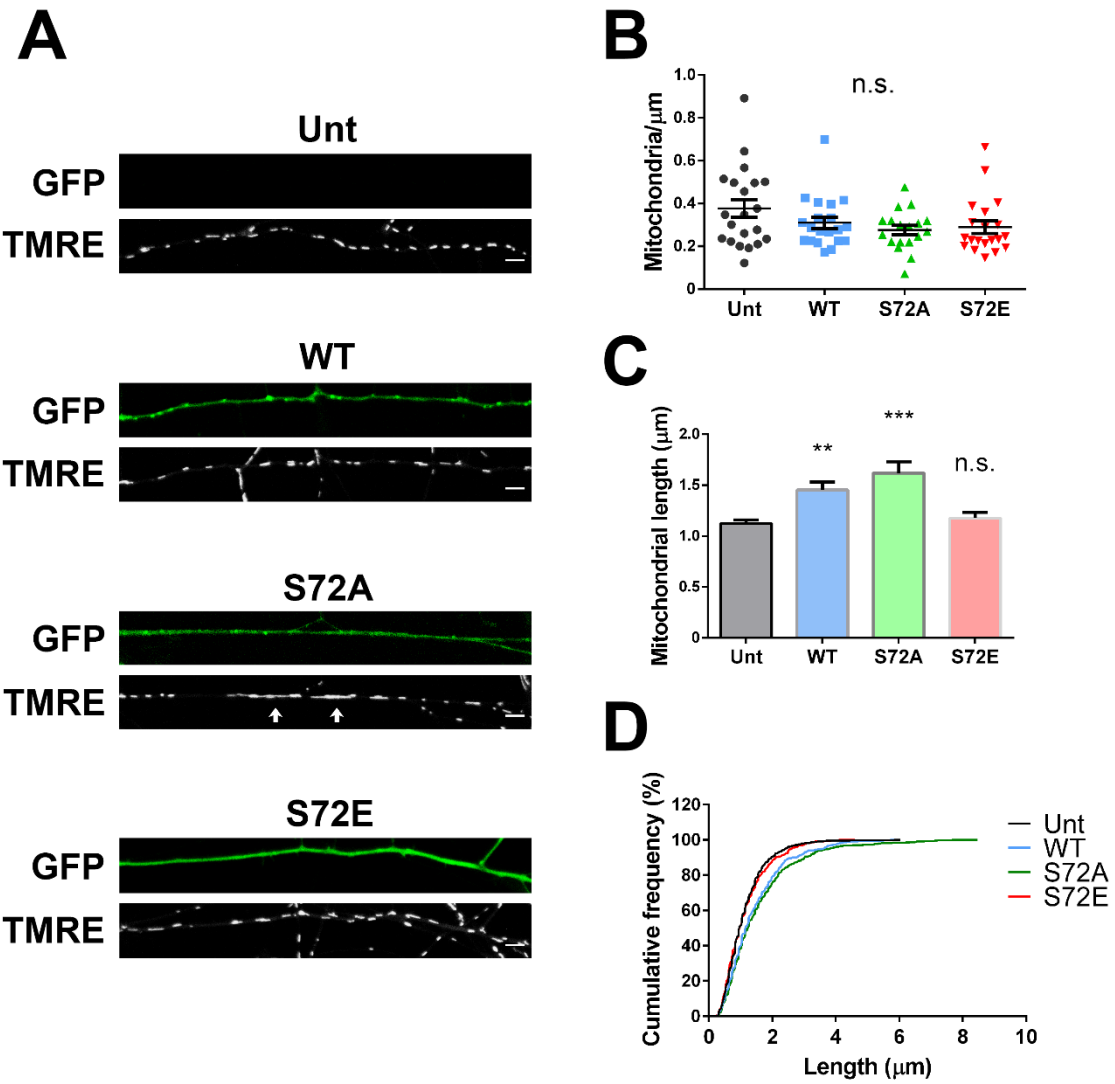

Figure 3.7.2. Rab7 increases mitochondrial length in axons. (A) Representative images from live-cell imaging experiments, with cultured MN expressing the indicated Rab7 constructs. GFP-Rab7 fluorescent signal is depicted in green and TMRE in red. Arrows show elongated mitochondria in the S72A condition. Scale bar, 5 µm. **(B)** Mitochondrial axonal density for every condition. No statistical changes were detected between conditions. Data shown as mean ± SEM, n = (Unt 21, WT 20, S72A 18, S72E 20 neurons from 3 independent primary cultures), one-way ANOVA with Tukey's multiple comparison test, n.s.= not significant. **(C)** Mitochondrial length in axons. Rab7 WT induced a significant increase in length, which was even more evident in the S72A condition, whilst the S72E group remained indistinguishable from the untreated control. Data shown as mean ± SEM, n = (Unt 21, WT 20, S72A 18, S72E 20 neurons from 3 independent primary cultures), one-way ANOVA with Tukey's multiple comparison test, ** $P < 0.01$, *** $P < 0.001$, n.s.= not significant. **(D)** The cumulative frequency for mitochondrial length shows similar distributions for S72E and the untreated control. Conversely, both WT and S72A conditions are shifted toward higher length values.

3.8 Summary of results

The results presented in this chapter suggest that the phosphorylation on Rab7 S72 is mechanistically relevant for the axonal transport of signalling endosomes carrying neurotrophins and their receptors, since the phospho-mimetic mutant Rab7 S72E affects their directionality of transport. Interestingly, this effect is specific for these organelles, as lysosomal and mitochondrial axonal transport is not compromised. It is worth noting that Rab7 S72E does not transition through a Rab GTP-bound/Rab GDP-bound cycle (Shinde and Maddika, 2016), and does not seem to exert the same effect as Rab7 WT, at least for the phenotypic change on mitochondrial length.

With this in mind, we hypothesised that kinases responsible for the Rab7 S72 phosphorylation should also regulate the axonal transport of signalling endosomes. If Rab7 S72E is in fact mimicking the phosphorylated Rab7 variant, then reducing the upstream kinase activity will promote the retrograde transport of H_CT carriers. On the other hand, if Rab7 S72E is unable to engage on phosphorylation-dependent Rab7 pathways, a reduced upstream kinase activity should phenocopy Rab7 S72E expression.

We focused on TBK1, since its phosphorylation on Rab7 S72 has been described previously in other cell types (Heo et al., 2018; Ritter et al., 2020), and because defects on both signalling endosomes axonal transport and TBK1 activity are relevant for the pathogenesis of ALS. The experiments on axonal transport after TBK1 loss of function are described in the next chapter.

Chapter 4

4.1 TBK1 knockdown efficiency

Rab7 S72E expression modifies the directionality of transport of signalling endosomes, in a manner that is independent from alterations in neuronal polarity and microtubule orientation. This effect is specific, since the axonal transport of lysosomes and mitochondria is unaffected. Since Rab7 S72 phosphorylation is carried out by the ALS-related kinase TBK1 (Wallace., 2014; Heo et al., 2018; Ritter et al., 2020), we wanted to address how TBK1 dysfunction might affect signalling endosome trafficking. Given that some cases of fALS are caused by TBK1 haploinsufficiency (Cirulli et al., 2015; Freischmidt et al., 2015), we proceeded with a loss of function strategy, using shRNAs directed against TBK1. To test the efficiency of this approach, undifferentiated N2a cells were transfected with a set of 4 shRNAs bearing mCherry as reporter gene, and TBK1 expression levels were determined by western blotting 48 h later (Figure 4.1.1 A). All shRNAs had a similar knockdown efficiency (about 50%), whilst the control shRNA (shC) did not alter TBK1 expression levels. We chose shRNAs 1 and 2 (sh1 and sh2) for further testing, as they consistently achieved the highest knockdown levels. Undifferentiated N2a cells were transfected with the selected shRNAs, fixed after 48 h of expression and stained for endogenous TBK1. As shown in Figure 4.1.1 B, both shRNAs 1 and 2 reduce the expression of endogenous TBK1.

Next, we tested shRNAs 1 and 2 knockdown efficiency in primary MNs in culture. We packed the selected shRNAs plus the shRNA control shC into viral particles and transduced primary MN at DIV 3. Neurons were fixed at DIV 6 and stained for endogenous TBK1, as well as for the neuronal marker Tuj1 (Figure 4.1.2 A). In agreement with the result obtained in N2a cells, shRNAs 1 and 2 reduce TBK1 expression whilst shC does not significantly alter TBK1. We quantified the endogenous

TBK1 fluorescence intensity (Figure 4.1.2 B) and found a knockdown efficiency of ~ 65%. TBK1 knockdown was also tested by western blotting (Figures 4.1.2 C and D), where we found even higher knockdown levels (sh1 ~ 90%, sh2 almost a complete knockdown).

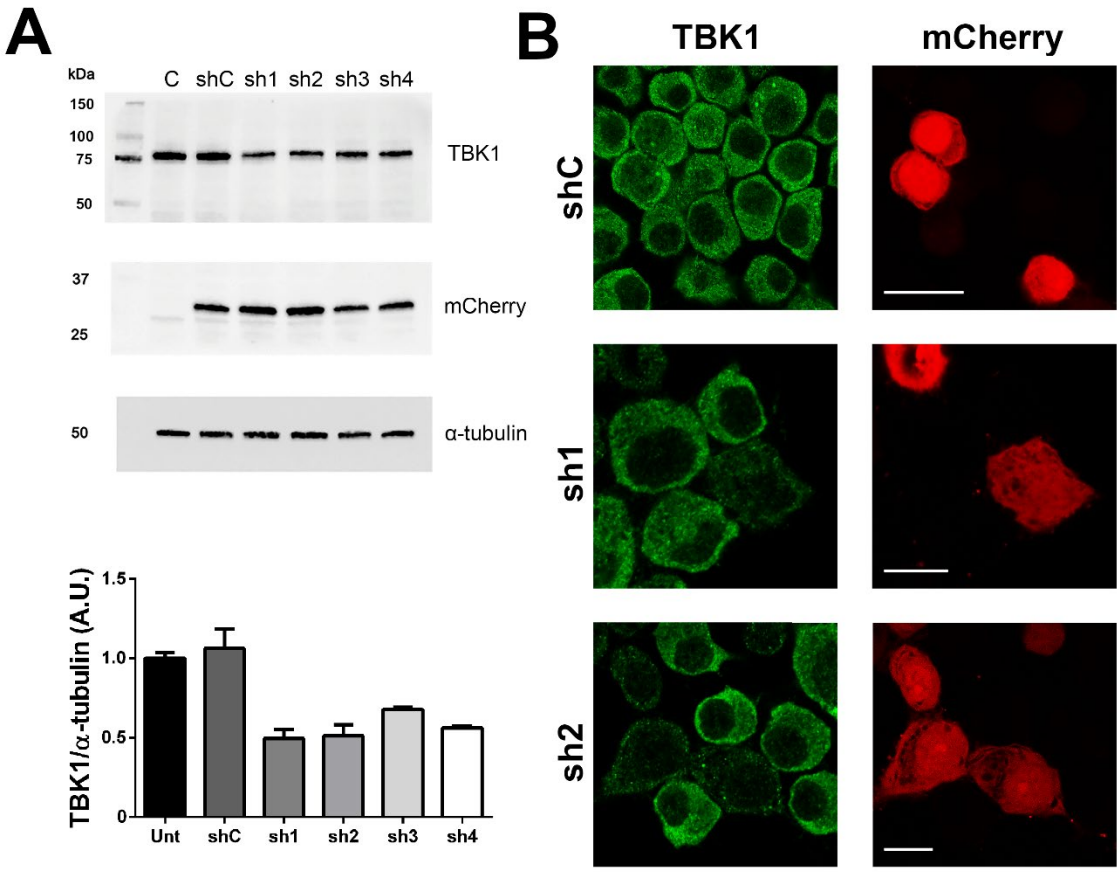

Figure 4.1.1. Knockdown efficiency assessment for TBK1 shRNAs in N2a cells. (A) Undifferentiated N2a cells were transfected with a set of 4 shRNAs against TBK1 plus a control shRNA (shC), and TBK1 expression levels were determined by western blotting after 48 h of expression. The bands quantification normalised to untreated levels, shows 50% knockdown. Data presented as mean ± SEM, n = 3. **(B)** shRNAs 1 and 2 were transfected in undifferentiated N2a cells. After 48 h, cells were fixed and stained for endogenous TBK1, (mCherry expression is a reporter of transfection). We obtained around 50% transfection efficiency. Scale bar, 20 μm.

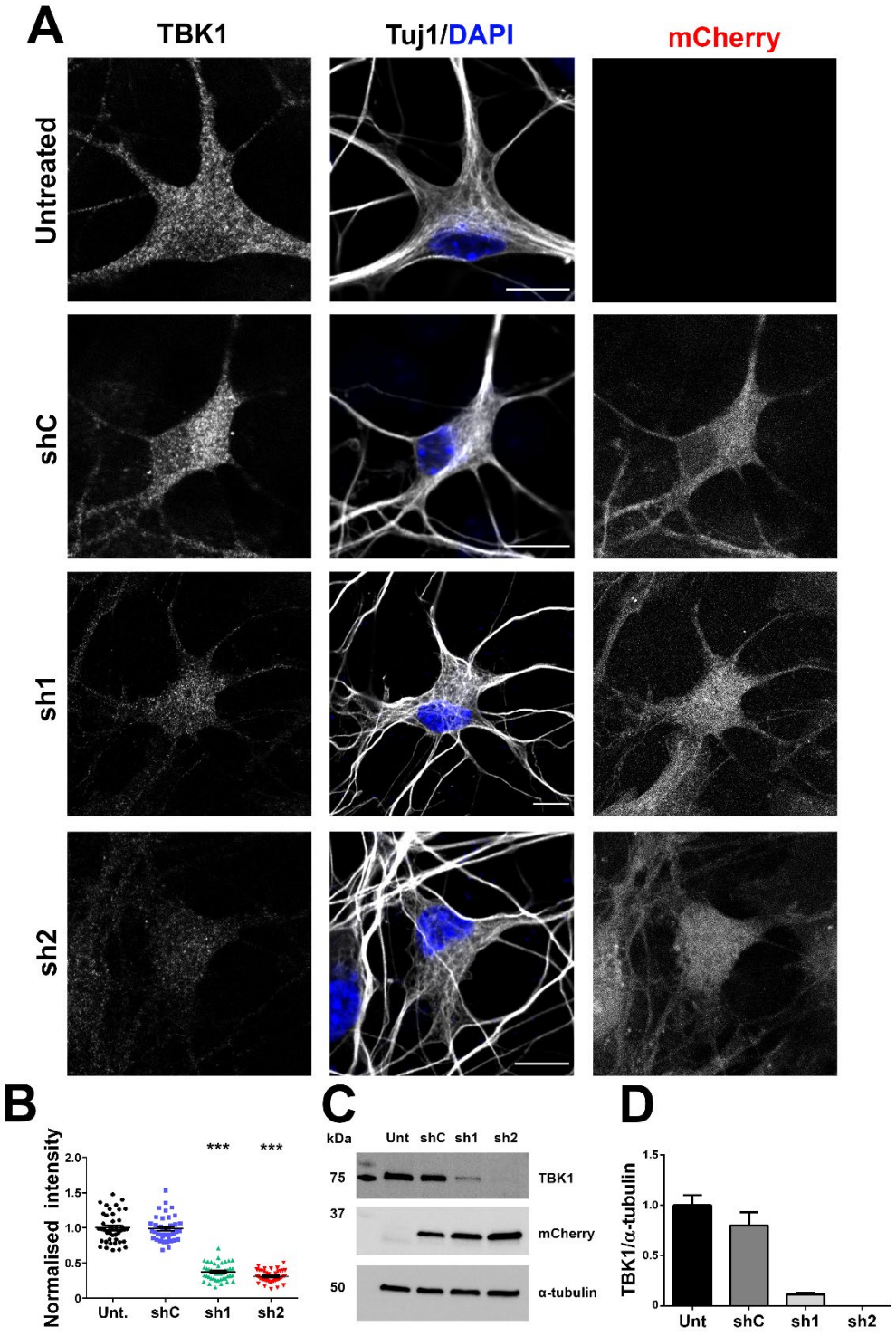

Figure 4.1.2. TBK1 knockdown efficiency in MN. (A) Cultured primary MN were transduced with viral particles containing either shC, sh1 or sh2 on DIV 3. Neurons were fixed 72 h later and stained as indicated. Scale bar, 10 µm. **(B)** Fluorescence intensity quantification from transduced MN. We observed a knockdown efficiency of ~ 65% for both shRNAs. Data shown as mean ± SEM, n = (Unt 41 neurons, shC 40 neurons, sh1 43 neurons, sh2 44 neurons, from 3 independent cultures), one-way ANOVA with Tukey's multiple comparison test, ***P<0.001. **(C)** Cultured primary MN were transduced as in A, and TBK1 expression leveles were determined by western blotting. **(D)** TBK1 knockdown quantification from C, normalised to untreated levels. We obtained ~ 90%

knockdown with sh1 and almost complete silencing with sh2, whilst shC effect is not significantly different from untreated cells. Data shown as mean ± SEM, n = 3, one-way ANOVA with Tukey's multiple comparison test, ***P<0.001.

Recent studies uncovered an inhibitory role for TBK1 on receptor-interacting serine/threonine-protein kinase (RIPK1)-mediated apoptosis, in MEFs and mouse fetal liver (Xu et al., 2018). Therefore, we also tested whether TBK1 knockdown induces apoptosis in our model. Cultured primary MN were transduced with viral particles carrying either shC, sh1 or sh2 on DIV 3 and fixed after 72 h. As a positive control for cell death, we treated neurons with staurosporine, a cell permeable alkaloid which induces apoptosis (Kabir et al., 2002; Zhang et al., 2004). Figure 4.1.3 shows representative images from this experiment. Whilst the cleaved caspase-3 fluorescent signal is absent from cell treated with vehicle (DMSO), this apoptotic marker is visible in MN treated with staurosporine. In agreement with this, blebbing can be seen on the Tuj1/DAPI panel for this condition (arrowheads), confirming the detrimental effect. Interestingly, we did not find evidence of cell death on MN transduced with the TBK1 shRNAs up to 3 days of expression.

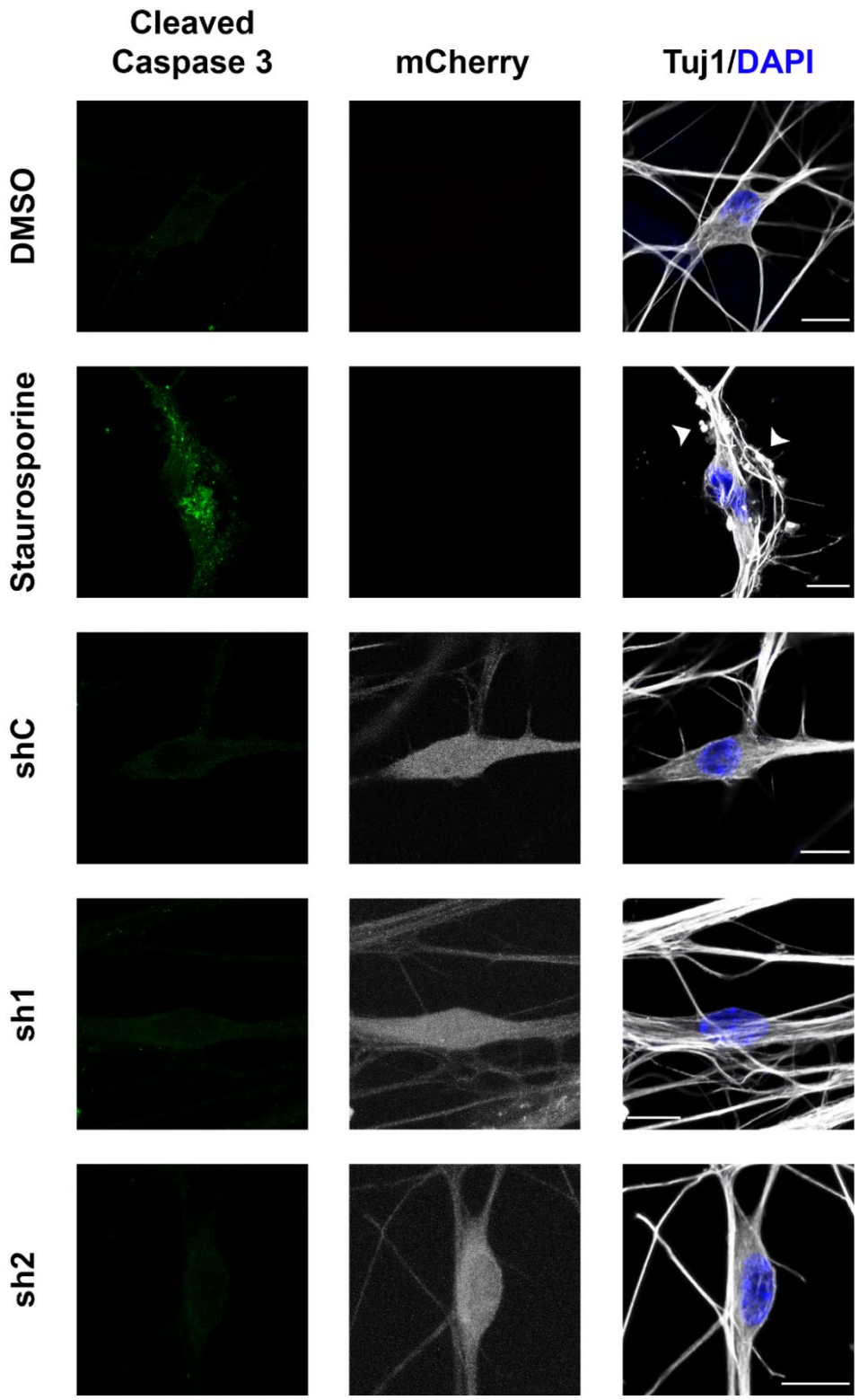

Figure 4.1.3. TBK1 knockdown does not induce cell death in MN. (A) Cultured MN were transduced with viral particles containing either shC, sh1 or sh2 on DIV 3 and fixed after 72 h. Alternatively, untransduced 6 DIV MN were treated with DMSO or staurosporine 1 μM for 5 h and fixed. Cells were then stained for cleaved caspase-3 and Tuj1, as depicted. MN expressing TBK1 shRNAs were negative for the apoptotic marker. Scale bar, 10 μm. Arrowheads show blebbing in the staurosporine condition.

4.2 TBK1 knockdown affects signalling endosomes transport

Having validated our shRNAs against TBK1, we proceeded to evaluate how reducing TBK1 expression levels impact on signalling endosome trafficking. Cultured primary MN were transduced with viral particles containing either shC, sh1 or sh2 on DIV 3. 72 h later, MN were labelled with fluorescent H_CT for 45 min, washed and imaged. Figure 4.2 A shows the displacement graphs for every condition, including the untreated control. The vast majority of H_CT-positive carriers move retrogradely in the untreated and shC conditions, however a significant subpopulation of cargoes is transported anterogradely in both the sh1 and sh2 groups. The analysis of the average speed per cargo, considering every displacement as positive (Figure 4.2 B), reveals that neurons expressing sh1 and sh2 display a similar behaviour. Additionally, untreated and shC conditions were equivalent in terms of average speed. Interestingly, both sh1 and sh2 groups present increased average speeds per cargo when compared to the untreated control. The speed profiles for the sh1 and sh2 conditions (Figure 4.2 C) is shifted towards the left, reflecting the increased frequency in anterograde movement, recapitulating the phenotype found after GFP-Rab7 S723E expression.

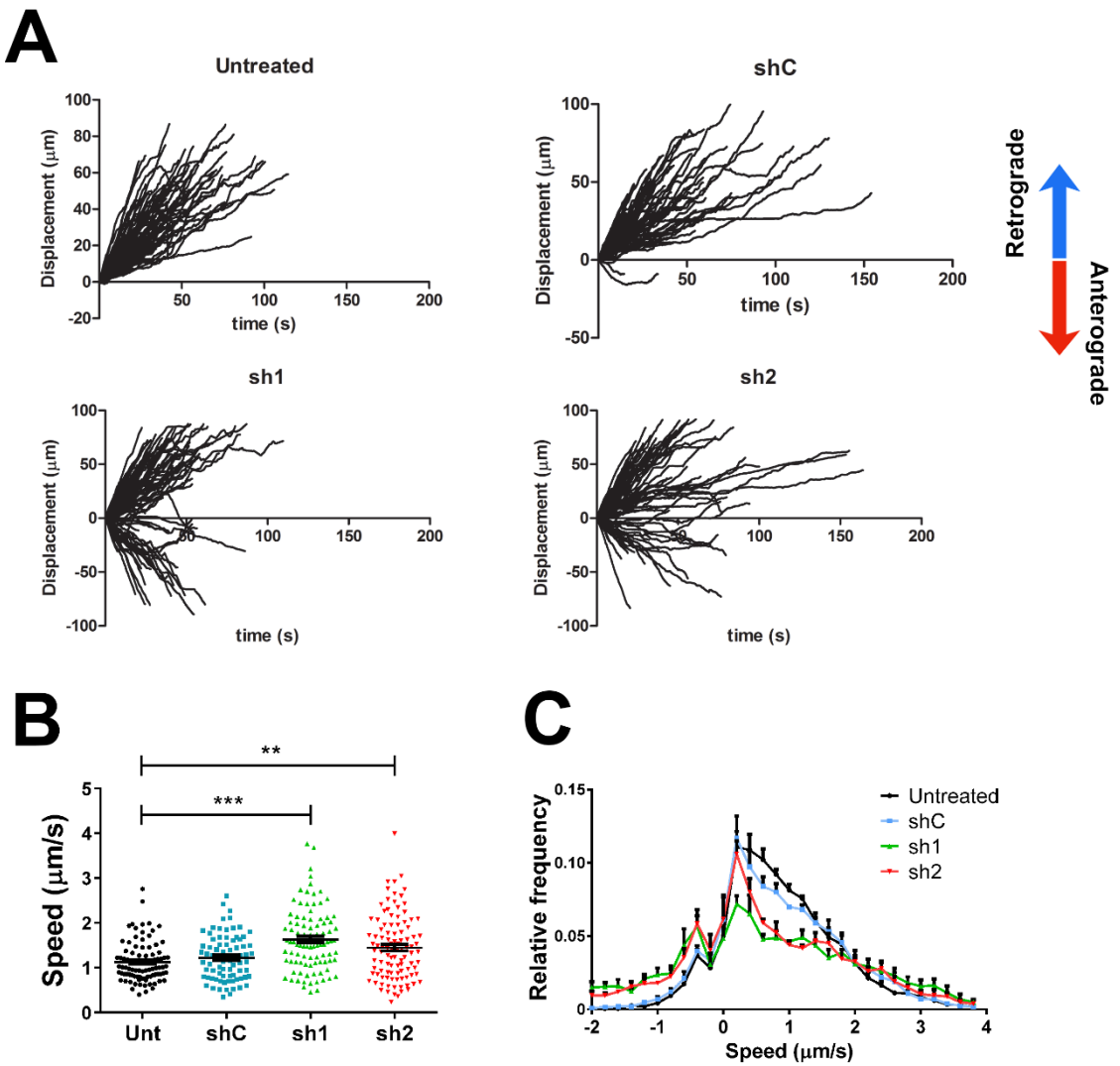

Figure 4.2. TBK1 knockdown increases signalling endosome anterograde transport. Cultured primary MN were transduced with viral vectors encoding shC, sh1 or sh2 on DIV 3. After 72 h, cells were labelled with 30 nM AlexaFluor 647-conjugated H_CT for 45 min, washed and imaged. **(A)** Displacement graphs for untreated (Unt) and shC conditions, as well as sh1 and sh2, where retrograde transport is shown as positive. A subpopulation of carriers moves anterogradely for both sh1 and sh2. **(B)** Average speed per cargo, considering every displacement as positive. There is an increase on the speed of movement for sh1 and sh2 when compared to the untreated condition. Data shown as mean ± SEM, n = (Unt 92, shC 79, sh1 92, sh2 103, from 3 independent cultures), one-way ANOVA with Tukey's multiple comparison test, **P<0.01, ***P<0.001. **(C)** Speed profiles for each condition, both sh1 and sh2 curves are shifted towards the left, indicating increased frequency of anterograde movement.

4.3 Inefficient TBK1 activation by dsRNA analogue poly I:C in primary MN

Since reduced TBK1 expression alters the axonal transport of H_CT positive cargoes, we decided to activate TBK1 in primary MN, to test whether its activity is required for this effect. TLR3 initiates type-I IFN response via IKKε and TBK1 during viral infection (Fitzgerald et al., 2003). TLR3 recognises viral dsRNA and can also be activated by dsRNA analogues, such as polyinosinic:polycytidylic acid (poly I:C, or p-I:C) (Alexopoulou et al., 2001b). We checked the ability of MN to respond after poly I:C stimulation and used the phosphorylation on TBK1 Ser 172 as a read out. 6 DIV cultured primary MN were treated with poly I:C at a low (10 µg/ml) or high (100 µg/ml) concentration for 2 h, and the levels of p-TBK1 and total TBK1 were determined by western blotting. Figure 4.3 A shows a representative image of the results. We quantified the levels of phosphorylated and total TBK1 (Figure 4.3 B) and found no TBK1 activation in the range of poly I:C concentration used, despite previous results from our group showing 10 µg/ml were effective for TBK1 activation in MEF cells (Wallace, 2014). We also tested the effect of poly I:C on cultured MN by immunofluorescence. 6 DIV primary MN were treated with poly I:C 100 µg/ml for 2 h, fixed and stained as indicated in Figure 4.3 C. The Golgi marker GM130 was included as it has been reported that following TLR3 activation, TBK1 is recruited to the Golgi apparatus in HEK cells, a process that promotes its trans-autophosphorylation and activation (Pourcelot et al., 2016). We detected a punctuate pattern for p-TBK1, which was not altered by poly I:C treatment. Interestingly, the antibody detected a high intensity pool of p-TBK1 associated to centrosomes in dividing non-neuronal cells, as shown in Figure 4.3 D.

After the unsuccessful attempt to activate TLR3 and TBK1 in primary MN, we turned to treatments with a TBK1 inhibitor as a complementary approach. Primary MN were treated with the IKKε/TBK1 inhibitor MRT67307 at 2 µM for 3 h. We included one condition where poly I:C 100 µg/ml was added 1 h after MRT67307 treatment, for 2 h. p-

TBK1 and total TBK1 levels were determined by western blotting. Figure 4.3 A shows a representative result, with lines 5 and 6 corresponding to the treatment with the inhibitor. Unexpectedly, we obtained a trend toward TBK1 activation in MN treated with the inhibitor. We reasoned this might be a cell-specific effect, hence we designed a pilot study using a different cell type, to confirm or discard the result. Undifferentiated N2a cells were treated with the same conditions than primary MN in Figure 4.3 A, and the p-TBK1 and total TBK1 levels were assessed by western blotting (Figure 4.3 A, two bottom panels). Our pilot experiment showed two main results: first, p-TBK1 levels in N2a cells are considerably higher and less difficult to detect than in primary MN, and second, it confirmed TBK1 activation induced by the inhibitor.

We also tested an antibody against phosphorylated Rab7 S72 (p-Rab7), previously generated and characterised in our laboratory (Wallace, 2014). Supplementary figure S4.1 A shows the p-Rab7 pattern on differentiated NSC-34 cells, a hybrid cell line generated by fusion of MN from the spinal cord of mouse embryos with mouse neuroblastoma cells N18TG2 (Cashman et al., 1992). We used NSC-34 cells since they resemble MN better than N2a cells, when subjected to differentiation protocols. The fluorescent signal shows a mix of punctuate and cytosolic patterns, equally distributed around the cell body. The puncta are more evident on neurites (Figure S4.1 B) and are also present in primary MN in culture (Figure S4.1 C). In agreement with these previous results, p-Rab7 fluorescent signal also remains unaffected by poly I:C treatment.

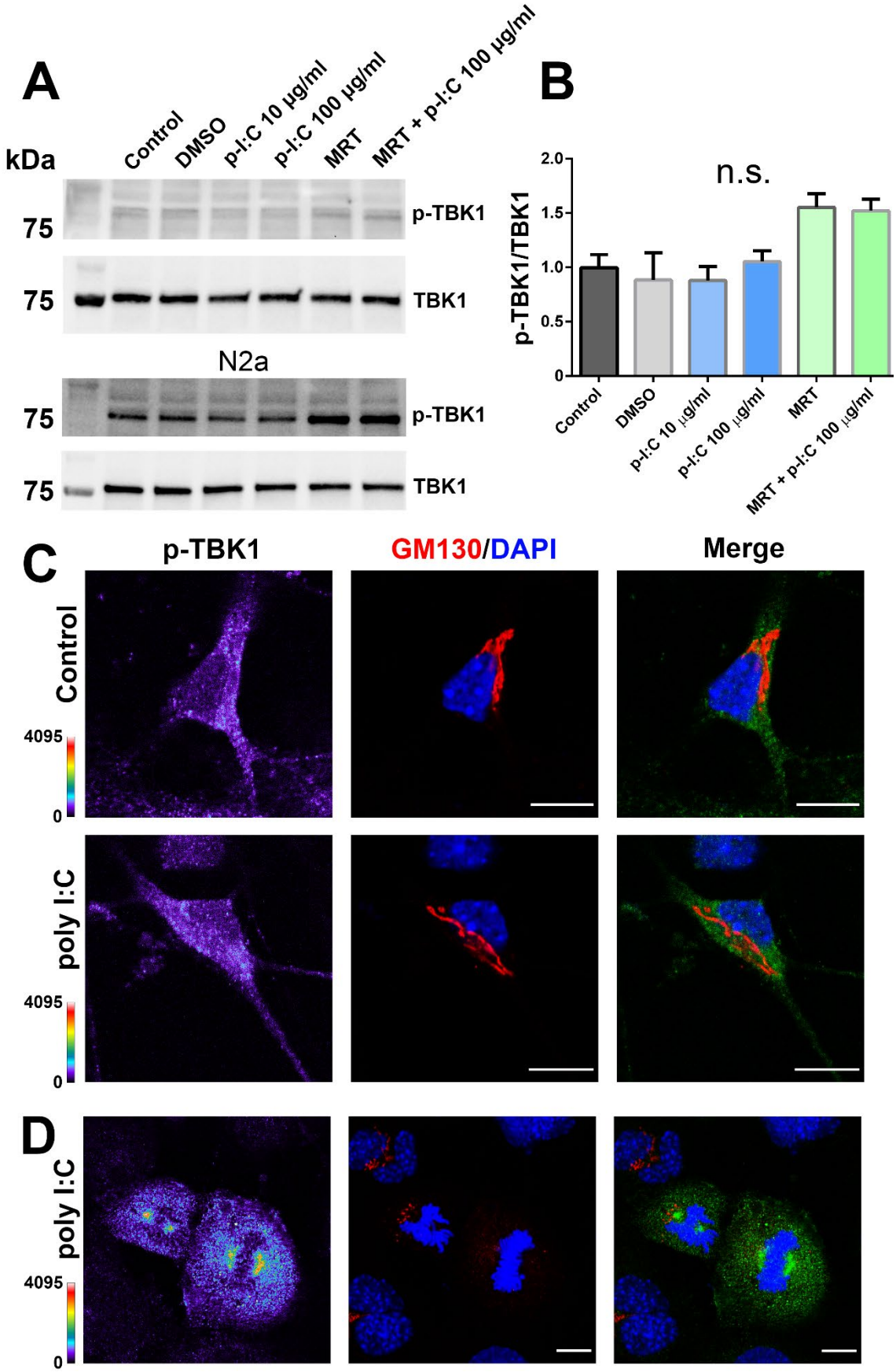
A
kDa
Control
DMSO
p-I:C 10 μg/ml
p-I:C 100 μg/ml
MRT
MRT + p-I:C 100 μg/ml
75
p-TBK1
75
TBK1
N2a
75
p-TBK1
75
TBK1
B
n.s.
p-TBK1/TBK1
2.0
1.5
1.0
0.5
0
Control
DMSO
p-I:C 10 μg/ml
p-I:C 100 μg/ml
MRT
MRT + p-I:C 100 μg/ml
C
p-TBK1
GM130/DAPI
Merge
Control
poly I:C
4095
0
D
poly I:C
4095
0

Figure 4.3. Poly I:C does not activate TBK1 in cultured primary MN. (A) 6 DIV primary MN were stimulated with poly I:C 10 µg/ml or 100 µg/ml for 2 h. An additional group was treated with the TBK1 inhibitor MRT67307 2 µM for 3 h, or MRT67307 2 µm for 1 h and poly I:C 100 µg/ml for two more hours in the presence of the inhibitor. p-TBK1 and TBK1 levels were determined by western blotting. The same conditions applied to MN were used to stimulate undifferentiated N2a cells (bottom two panels, n = 1). **(B)** Quantification from MN treatments in (A) normalised to untreated control levels. No statistically significant differences were observed. Data shown as mean ± SEM, n = 3, one-way ANOVA with Tukey's multiple comparison test, n.s. = not significant. **(C)** 6 DIV primary MN were stimulated with poly I:C 100 µg/ml for 2 h, fixed and stained as indicated. p-TBK1 fluorescent intensity levels are shown with a rainbow look up table (intensity scale provided). Poly I:C did not change p-TBK1 levels, nor its distribution in relation to the Golgi marker GM130. Scale bar, 10 µm. **(D)** An example of non-neuronal cells undergoing mitosis in the same primary culture from (C). Centrosomes show a clear p-TBK1 accumulation. Scale bar, 5 µm.

4.4 TBK1 knockdown does not affect lysosomal transport

After confirming that stimulation with the dsRNA analogue poly I:C is not a suitable way to activate TLR3, and consequently TBK1 in primary MN, we examined the specificity of the modulation of TBK1 knockdown on axonal transport. Reduced TBK1 expression levels phenocopy GFP-Rab7 S72E expression, as both conditions change the directionality of transport of a subpopulation of H_CT positive signalling endosomes. The Rab7 S72E effect is specific for that population of cargoes, since lysosomes and mitochondria are not affected. In this regard, we checked whether TBK1 knockdown impairs lysosomal transport. Cultured primary MN were transduced with viral particles containing either shC or sh1 on DIV3. 72 h later, cells were labelled with LysoTracker Deep Red for 30 min, washed and imaged. The displacement graphs for all conditions are depicted in Figure 4.4 A. The untreated condition shows bidirectional transport, with a bias towards the retrograde directions, just as in the experiment described on the previous chapter (Figure 3.6). This was not modified by the control shRNA nor by sh1 expression. The speed profiles for all three conditions overlap, ruling out an effect of TBK1 downregulation on lysosomal trafficking (Figure 4.4 B). This result is further supported by the unaltered average speed per cargo, considering every displacement as positive (Figure 4.4 C). Finally, we quantified the percentage of carriers moving in

each direction, finding that about 80% is transported retrogradely, a proportion that remains unchanged for all conditions.

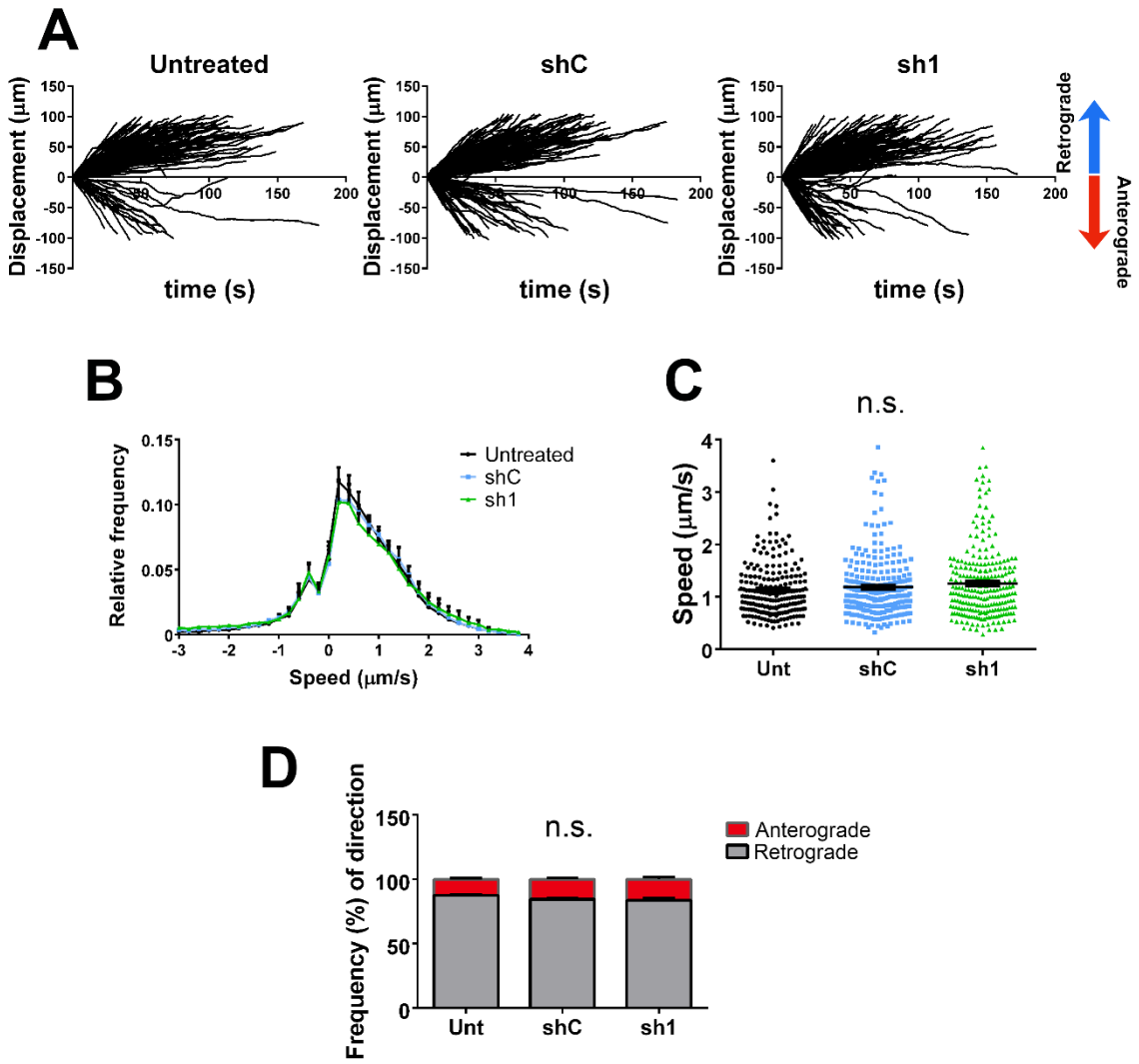

Figure 4.4. TBK1 knockdown does not impair lysosomal transport. Cultured primary MN were transduced with viral particles containing either shC or sh1 on DIV3. Three days later, MN were labelled with LysoTracker Deep Red (50 nM) for 30 min, washed and imaged. **(A)** Displacement graphs for every condition analysed. Cargoes move bidirectionally, with a bias toward the retrograde direction (blue arrow). **(B)** Speed graphs for each condition, showing overlapping profiles. **(C)** Average speed per cargo, considering every displacement as positive. Statistically significant differences were not detected. Data shown as mean ± SEM, n = (Unt 207, shC 252, sh1 244 from 3 independent primary cultures), one-way ANOVA with Tukey's multiple comparison test, n.s.= not significant. **(D)** Quantification of the directionality of transport. Around 80% of LysoTracker positive carriers move retrogradely, a percentage that remained constant for all conditions. Data shown as mean ± SEM, n = 3 for each condition, two-way ANOVA with Sidak's multiple comparison test, n.s.= not significant.

4.5 TBK1 knockdown does not affect mitochondrial axonal transport

Hitherto, we have confirmed that Rab7 S72E expression and TBK1 knockdown modify signalling endosome axonal transport, leaving lysosome trafficking unchanged. We wanted to know if this specificity might extend to mitochondria, as is the case for Rab7 S72E. This constitutes an interesting case, as Rab7 WT and S72A expression changed mitochondrial length, possible due to a differential regulation on mitochondrial fission and/or fusion, therefore we analysed not only mitochondrial transport, but their morphology as well. Cultured primary MN were transduced with viral particles containing either shC or sh1 on DIV 3. After 72 h, MN were labelled with TMRE 20 nM for 20 min, washed, and imaged in medium containing TMRE. The distribution of the cargo population is depicted in Figure 4.5 A. In agreement with the experiments described previously (Figure 3.7), around 75% of mitochondria were static, with the rest split equally between retrograde and anterograde movement. This distribution was unaffected by TBK1 knockdown. Additionally, we generated speed graphs for the three conditions, which are shown in Figure 4.5 B. There is a slight shift towards the left for shC, however TBK1 knockdown overlaps completely with the untreated samples, suggesting that mitochondrial movement is in fact, not affected. We obtained a similar result for the average speed per experiment, both in the retrograde and anterograde direction (Figures 4.5 C and 4.5 D respectively), confirming that shC and sh1 expression do not affect mitochondrial axonal transport. Finally, we analysed mitochondrial density and length. Representative images of axonal mitochondria for each condition are presented in Figure 4.5 E. Our results show a density of about 0.4 mitochondria/μm, similar to what we obtained in the previous chapter. As expected, the density was not affected by TBK1 knockdown (Figure 4.5 F). Regarding mitochondrial length, this parameter also remained unchanged between conditions (Figure 4.5 G, and cumulative frequency in Figure 4.5 H). Altogether, these results show that TBK1 knockdown does not affect mitochondrial axonal transport, nor their density and length.

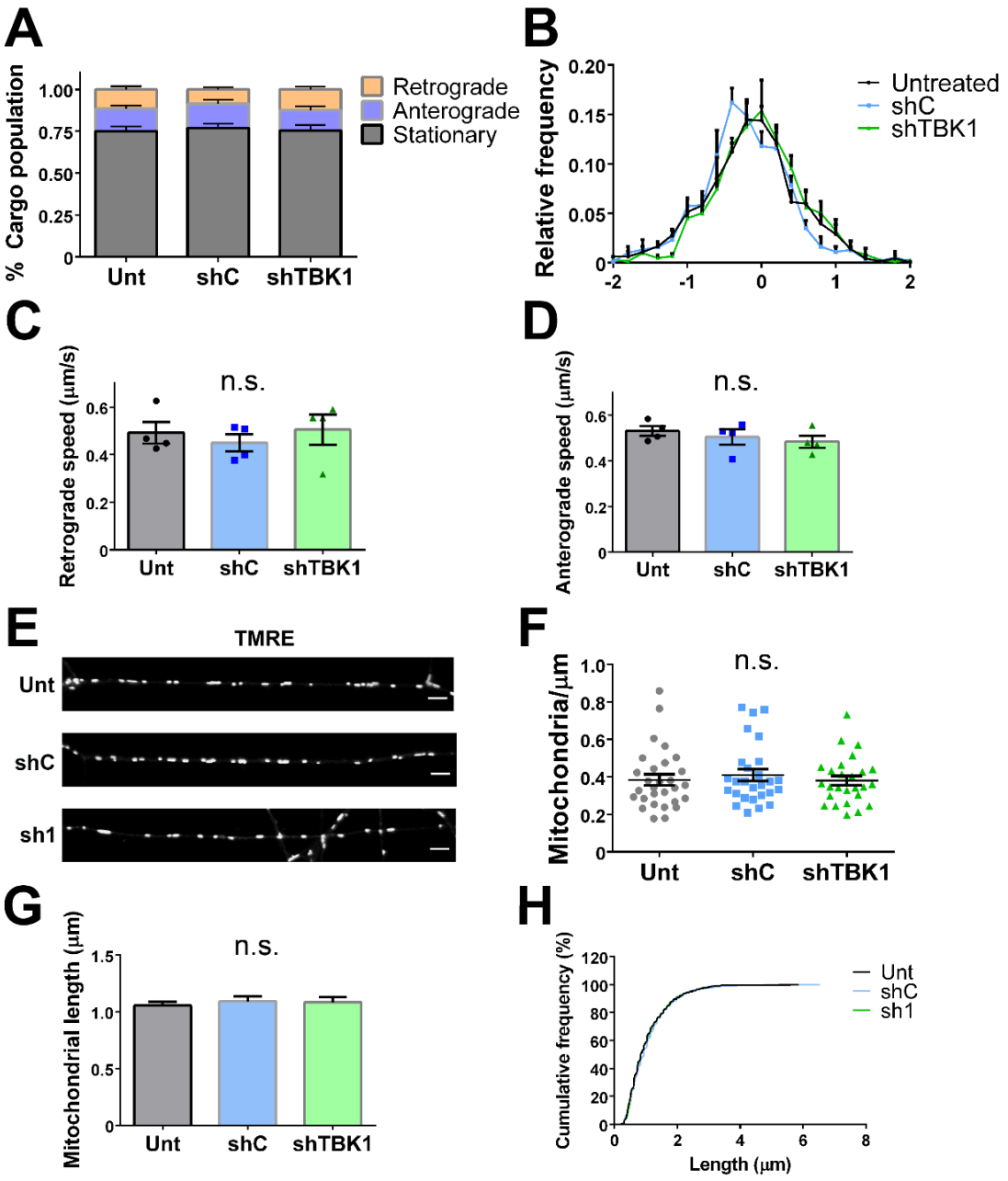

Figure 4.5. TBK1 knockdown does not affect the axonal transport of mitochondria. 3 DIV cultured primary MN were transduced with shC and sh1. 72 h later, MN were labelled with TMRE 20 nM for 20 min, washed and imaged in medium containing TMRE 20 nM. **(A)** Cargo population distribution. About 75% of mitochondria are static, whilst the rest is split evenly between anterograde and retrograde movement. **(B)** Speed profiles for the three conditions. The untreated and sh1 condition overlap almost completely, whilst shC exhibits a slight shift towards the left. **(C)** and **(D)** Average retrograde and anterograde speed per experiment, respectively. No statistically significant changes were detected. Data shown as mean ± SEM, n = 4, one-way ANOVA with Tukey's multiple comparison test, n.s.= not significant. **(E)** Representative images showing axonal mitochondria labelled with TMRE. Scale bar, 5 µm **(F)** Mitochondrial density for each group. No significant changes were detected. Data shown as mean ± SEM, n = (Unt 29, shC 27, sh1 26 neurons from 4 independent cultures), one-way ANOVA with Tukey's multiple comparison test, n.s.= not significant. **(G)** Quantification of

mitochondrial length. No significant changes between conditions were detected. Data shown as mean ± SEM, n = (Unt 29, shC 27, sh1 26 neurons from 4 independent cultures), one-way ANOVA with Tukey's multiple comparison test, n.s.= not significant. **(H)** Mitochondrial length cumulative frequency, showing similar distributions for all conditions.

4.6 Summary of results

In this chapter we addressed the effect of TBK1 knockdown on axonal transport. We took this approach since TBK1 haploinsufficiency cause fALS, therefore reducing TBK1 expression is relevant to the disease. We successfully knocked down TBK1 levels by ~ 65% in primary MN in culture, which was detectable both by western blotting and immunofluorescence techniques. We also ruled out a detrimental effect of TBK1 knockdown on cell survival in our model, as MN did not present evidence of apoptosis upon TBK1 downregulation. Having validated our shRNAs, we checked whether TBK1 knockdown affects the axonal transport of H_CT positive signalling endosomes. We found that reducing TBK1 levels induce changes in the directionality of transport of these endosomes, phenocopying the effect of Rab7 S72E described in Chapter 3. The disruption in axonal transport observed in the TBK1 knockdown condition is not a general phenomenon, since the trafficking of other organelles studied was not impaired.

Chapter 5

Discussion

Throughout this work we have shown the phosphorylation state of Rab7 Ser72 is relevant for the axonal transport of signalling endosomes. Now we will discuss the effect of this modification on Rab7 localisation and function, the implications for the trafficking of signalling endosomes, lysosomes and mitochondria, and will comment on further questions that arise from these results.

5.1 The subcellular localisation of phosphorylated Rab7

Rab GTPase phosphorylation on the switch II region modifies their association to interactors and may alter their cellular distribution. In this work we found that Rab7-S72E shows a cytosolic localisation in MNs, in contrast to Rab7 WT and S72A variants, which exhibit a mixed cytosolic and membrane-bound pattern. This confirms previous reports in cell lines, where Rab7-S72E was not found associated to membrane compartments (Wallace, 2014; Heo et al., 2018; Shinde and Maddika, 2016).

Rab8-T72E and Rab10-T72E are correctly destined to their target membrane, however, this is not the case for Rab7-S72E. The evidence indicates that these three Rab variants cannot interacts with the GDIs, however Rab8 and Rab10 must be able to bind REP and start the Rab cycle (introduced in figure 1.4), whilst Rab7 is probably defective in this initial step as well. This suggest that Rab phosphorylation on this conserved residue does not impact all Rab proteins equally. It would be interesting to analyse whether phospho-mimetic Rabs from other subfamilies remain cytosolic or manage to reach their target organelles.

Phospho-proteomic analyses from purified mitochondria after A/O depolarisation have shown that about 0.06% of total Rab7 is phosphorylated in Ser 72 (Heo et al., 2018). This suggest that although Rab7-S72E remains cytosolic, p-Ser72 Rab7 is found

associated to membranes. In agreement with this, the antibody directed against p-Ser72 Rab7 generated in our group stains a punctuate pattern in NSC-34 cells and MNs, indicating that endogenous p-Ser72 Rab7 is in fact, associated to membrane compartments. A possible explanation for this localisation considers the phosphorylation taking place after Rab7 reaches its target membrane. As discussed before, TBK1 signalling is modulated by localisation, for example, during *Salmonella enterica* infection NDP52 recruits TBK1 to the autophagosome through its adaptors NAP1 and SINTBAD (Thurston et al., 2009), and during Sendai virus infection, optineurin recruits TBK1 to the Golgi apparatus (Pourcelot et al., 2016). Therefore, TBK1 might be recruited to signalling endosomes by one of its adaptors, catalysing there the phosphorylation of Rab7 at Ser72. The identity of the adaptor recruiting TBK1 to signalling endosomes and whether this depends on neurotrophic signalling remains to be verified.

5.2 Rab7-S72E and TBK1 knockdown effect on axonal transport of signalling endosomes

Signalling endosomes rely on Rab7 for their axonal transport in primary MNs. Here we have shown Rab7 phospho-mimetic mutant disrupts the axonal transport of signalling endosomes, increasing the frequency of anterograde displacement. A higher frequency of oscillatory movements had been described for signalling endosomes in cultured MN derived from $SOD1^{G93A}$ mouse (Kieran et al., 2005), as well as for mRNA granules in patient-derived iPS cells bearing ALS-linked TDP-43 mutations (Alami et al., 2014). Interestingly, bidirectional displacement is also the effect observed on NGF-TrkA signalling endosomes in DRGs expressing CMT-associated Rab7 mutants (Zhang et al., 2013), therefore, disrupting the directionality of transport in cargoes which normally move unidirectionally in neurons, might be a common pathogenic mechanism in *in vitro* models of neurodegenerative diseases. It is relevant to make the distinction between *in vitro* and *in vivo* systems for the study of axonal transport, since axonal transport defects *in vivo*

frequently manifest as reduced cargo speed and increased pausing, rather than as changes in directionality (Sleigh et al., 2019). In this regard, future studies addressing the effect of Rab7 Ser72 phosphorylation on the axonal transport of signalling endosomes *in vivo,* would shed light on the different mechanisms impairing their retrograde trafficking.

TBK1 knockdown phenocopies Rab7-S72E effect on the axonal transport of signalling endosomes. This is the first evidence linking TBK1 to a role on axonal trafficking, since the vast majority of experiments reported in the literature focus on inflammation and autophagy. The result is, however, counterintuitive: knocking down the kinase has the same effect as mimicking the phosphorylation of its substrate. We have considered two possible models explaining the observation. The first model envisages that TBK1 activity must be tightly regulated within an optimal physiological range, hence both significantly reduced or overactivated TBK1 will be detrimental for axonal transport of signalling endosomes. Alternatively, it is possible that Rab7-S72E does not correctly mimic p-Ser72 Rab7. The substitution of a Ser or Thr residue for Asp or Glu is a strategy frequently used to generate phospho-mimetic mutants, and from a structural perspective Rab7-S72E would fulfil this role, however, since it does not localise to the correct compartment and its Rab cycle is impaired, the recruitment of effectors is expected to be affected as well. If the second model is correct, it is tempting to hypothesise that Rab7-S72E variant behaves as a dominant negative mutant. Despite *bona fide* dominant negative Rab7 (T22N or N125I mutants) consist of variants persistently in the GDP-bound state or which cannot bind nucleotides at all, Rab7 S72E might also exert this role, impairing the association of GEFs, GAPs and effectors to endogenous Rab7, although further experiments are required to confirm this. Consequently, Rab7-S72E is likely to be a loss of function mutant that cannot engage with the pathways which are normally regulated by p-Rab7 Ser72, and that might act as a dominant negative mutant.

According to the different steps in the Rab cycle, cytosolic Rab7-S72E should not be able to bind Rab7 effectors. Nevertheless, our group and others have shown that whilst Rab7-S72E cannot recruit RILP, ORP1L interaction is not affected (Wallace, 2014; Shinde and Maddika, 2016). This can be explained by the fact ORP1L binds an additional Rab7 domain, not located in the switch II region, thus is not affected by S72 phosphorylation. Interestingly, during selective mitophagy, Rab7-S72E binds its effector folliculin, despite not being associated to the mitochondrial membrane (Heo et al., 2018). The binding of Rab7-S72E to ORP1L and folliculin, plus the preliminary data from our laboratory showing that Rab7-S72E retains the ability to interacts with $p150^{Glued}$ (Wallace, 2014) indicates that although this variant is incapable of associate with membranous compartments, somehow retains the ability to bind a subset of its effectors. The association of GDP-bound, cytosolic Rab7 to some of its effectors is in conflict with the Rab cycle, since Rab localisation and activation are tightly intertwined. Nevertheless, Rab11-GDP has been reported to bind its “effector” protrudin during neurite elongation (Shirane and Nakayama, 2006), and recent evidence has shown that both Rab7 T22N and Q67L can be found associated to membranes or cytosolic, and both can bind the GDI, suggesting a four-state transition model where active or inactive Rab7 can reach its target membrane and then being extracted by the GDI (Kanemitsu-Fujita et al., 2018). Therefore, it is plausible that Rab7 S72E enhances the uncoupling between Rab7 localisation and activation. Further experiments are required to clarify this point.

Some groups consider Rab7-S72E a dominant-negative mutant (Ritter et al., 2020), whilst others desisted of using it as a tool, since its altered subcellular localisation complicated the interpretation of results (Heo et al., 2018). In our opinion, it is a mutant unable to engage with pathways which require Rab7 phosphorylation, and that may act as a dominant negative variant. Besides, it is a useful mutant to assess whether p-Rab7 S72 is relevant for certain phenotypes, like we have done in this work. In conclusion, Rab7-S72E is not a bona-fide phospho-mimetic mutant but is still a reliable tool to

question the effect of Rab phosphorylation during axonal transport. The effect of Rab7 phosphorylation and Rab7-S72E localisation on the Rab cycle are presented in figure 5.1.

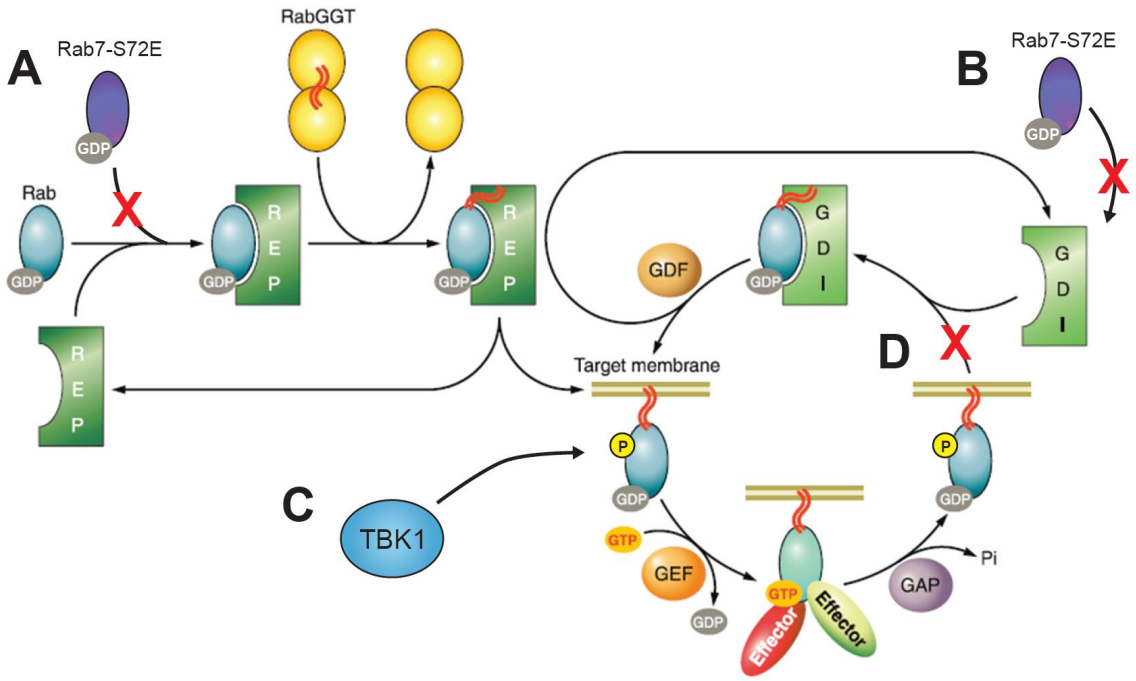

Figure 5.1. Phosphorylation of Rab7 Ser72 impacts on its cycling. Rab7-S72E is defective on REP (A) and GDI (B) binding, hence it fails to be delivered to its target membrane. TBK1-dependent Rab7 phosphorylation likely takes place after Rab7 is membrane-bound (C). Rab7 p-Ser72 exhibits reduced interaction with the GDI, therefore it stays in the target organelle for longer periods, as it is not efficiently extracted from the membrane (D). Image modified from (Hutagalung and Novick, 2011).

5.3 Modulation of TBK1 activity

We addressed whether the transport of signalling endosomes depends on tightly regulated TBK1 activity, by characterising tools to activate TBK1 in our model. The dsRNA analogue poly I:C is routinely employed to activate TBK1 downstream to TLR3 in immune system cells. Interestingly, our group has previously achieved this in MEFs (Wallace, 2014). Despite the evidence in other cells types, we could not activate TBK1 upon treatment of MNs with poly I:C, using the phosphorylation of TBK1 Ser172 as a read out. A possible explanation is that MNs do not express TLR3 or given that ventral

spinal cord cultures are a mixed culture, MNs and their associated glia do not express TLR3. Previous reports provided evidence that TLRs are expressed in peripheral nerves. The highest expression in Schwann cells correspond to TLR3 and TLR4, whilst MNs express TLR3 and TLR5 as the highest TLR variants. Nevertheless, TLR3 expression in MNs is about an order of magnitude lower than in peripheral macrophages (Goethals et al., 2010). This is the reason why we used poly I:C 100 µg/ml instead of the 10 µg/ml commonly used to stimulate macrophages and dendritic cells. We also assessed the downstream phosphorylation of IRF3 on Ser396, without any success (data not shown). It is possible that whilst TLR3 pathway is active in immune-derive cells and cell lines, it is not active in primary MN. This does not mean TLRs are irrelevant for ALS, for instance, TLR4 and its endogenous ligand high-mobility group box 1 (HMGB1) increase their expression in activated microglia and astrocytes isolated from the ventral spinal cord of $SO1^{G93A}$ mice during disease progression, and TLR4 ablation extends survival in this model (Lee et al., 2015).

An additional method to trigger the IFN response consist in stimulating cells with poly I:C and lipofectamine, in order to promote poly I:C internalisation and activation of the RIG-I/MDA5 intracellular receptors. This is unfeasible in our model, given that MN are not easily amenable to this physicochemical method.

Considering the difficulties to increase TBK1 activity in MN, we turned our strategy towards TBK1 inhibition. The most widely used TBK1 inhibitor is BX795, a potent and non-selective kinase inhibitor. Given the high number of BX795 off targets, its structure has been used as a starting point to generate more specific inhibitors, such as MRT67307 (Wang et al., 2012). We used MRT67307 in primary MN without any success. Intriguingly, MRT67307 enhances poly I:C-dependent TBK1 activation. This result has been observed before in the human keratinocyte cell line HACAT, in bone marrow-derived macrophages, and in the macrophage cell line RAW264.7; and was used as an

argument for proposing that an unidentified kinase phosphorylates TBK1 at S172 (Bakshi et al., 2017; Clark et al., 2011). Further studies have shown MRT67307 inhibits TBK1 downstream targets even in cells double knockout for TBK1 and IKKε, demonstrating that MRT67307 has additional targets (Lork et al., 2018). The development of new TBK1 inhibitors with increased specificity is absolutely required to advance our understanding of the physiological roles of this kinase.

5.4 The axonal transport defect is not due to a polarity problem

Here we have shown that Rab7-S72E does not affect neuronal polarity. Previous reports have linked Rab7 activity to neuritogenesis, for example, dominant-negative Rab7 T22N enhances NGF-induced neurite outgrowth in PC12 cells. Conversely, CMT-associated Rab7 mutants inhibit neurite elongation (Saxena et al., 2005; Cogli et al., 2010). Despite this evidence, Rab7 has not been linked to defect on the acquisition of neuronal polarity, and our results further support this conclusion.

Interestingly, microtubule orientation is also spared. This is relevant because TBK1 loss of function in Drosophila has been related to cytoskeletal defects. Drosophila IK2 is the orthologue of TBK1 and IKKε. Embryos lacking *ik2* exhibit patterning defects i.e. impaired determination of the antero-posterior axis, therefore, they develop two posterior ends, phenocopying *Bicaudal D* insufficiency (Mohler and Wieschaus, 1986; Shapiro and Anderson, 2006). IK2 is required for the correct positioning of the mRNA oskar, which determine the posterior region during oogenesis. Although IK2 regulates oskar transport, the phenotype is not mediated by kinesin and dynein dysfunction. Instead, IK2 loss of function induce abnormalities on microtubule minus-ends, and in this way negatively affects minus-end directed transport. However, we did not find defects in microtubule orientation in the axon, suggesting this might be a mechanism specific for oogenesis polarity determination.

5.5 Lysosomal transport is not affected by Rab7-S72E expression or TBK1 knockdown

After describing the defect on axonal transport of signalling endosomes, we wanted to investigate whether this was a general phenotype affecting the transport of many different cargoes, or specific for signalling endosomes. We chose lysosomes because they key features with signalling endosomes, the main one being the presence of Rab7 on their membrane. In agreement with previous reports, lysosomes move bidirectionally in our primary cultures (Cabukusta and Neefjes, 2018), and their transport was not affected by TBK1 knockdown or Rab7-S72E expression. Given the many different mechanisms for lysosomal transport, it is likely that compensatory mechanisms arise if one pathway is altered, occluding an effect on individual lysosomal trafficking routes.

It may be argued that not all five lysosomal transport mechanisms described in chapter 1 (Rab7/RILP, TRPML1/ALG-2, TMEM55B/JIP4, BORC/Arl8/SKIP, and Rab7/FYCO1) have been found in neurons. In this regard, Rab7, RILP, JIP1, JIP3 and the late endosome/autophagosome dynein adaptor snapin have been reported as dynein-dynactin adaptors acting in the axonal compartment (Ferguson, 2019), hence, there are several different ways by which neuronal lysosomes can be transported. Some of these routes include the recruitment of kinesins to mediate anterograde axonal transport. For instance, experiments carried out in cortical neurons seeded onto microfluidic devices reported delivery of functional lysosomes from the soma toward the distal axon (Farfel-Becker et al., 2019). This point is relevant, since much of the studies in the field use lysosomal markers such as LAMP1, however, recent reports tracking LAMP1 in neurons show a significant subpopulation of LAMP1-positive organelles lacking lysosomal hydrolases. In addition, LAMP1 intensity variations does not correlate with lysosomal deficit in $SOD1^{G93A}$ mice (Cheng et al., 2018). We used LysoTracker to follow lysosomes in axons, instead of LAMP1, therefore we relied on the acidification of endosomes as a criterion to define what population of cargoes would be tracked. Our LysoTracker

analysis would benefit from further labelling with probes detecting active lysosomal hydrolases, as a complementary way to confirm that functional lysosomes are not affected by TBK1 knockdown.

5.6 Mitochondrial transport is not affected by Rab7-S72E expression or TBK1 knockdown

The main mechanism controlling mitochondrial transport differs from lysosomes and signalling endosomes, as it depends on Miro/TRAK for the recruitment of motors. Hence, a defect in mitochondrial movement would have suggested a more general phenotype, possible a dysregulation at the level of motor function. This was not the case, since our experiments ruled out a disruption on this mechanism in both TBK1 knockdown conditions and after expressing Rab7-S72E.

Interestingly, we observed an unexpected increase in mitochondrial length induced by Rab7-S72A and to a lesser extent, by Rab7 WT. Regarding this, mitochondrial fission often occurs at mitochondria-lysosome contact sites, which are also frequently contacted by ER-tubules. Mitochondrial fission is regulated by Rab7 GTP hydrolysis (promoted by TBC1D15), hence, constitutively active Rab7 Q67L or the CTM-related mutant Rab7 V162M prolong the duration of the contact, inhibiting mitochondrial untethering (Wong et al., 2018, 2019). Here we now describe that this process is also regulated by Rab7 phosphorylation. Although the details of the mechanism are not clear, our findings are consistent with reports showing mitochondria escape autophagic degradation by enhancing fusion, and that mitophagy is impaired in cells expressing Rab7 S72A (Heo et al., 2018; Rambold et al., 2011). The fact that Rab7-S72E does not alter mitochondrial length suggest this variant face defects to engage in pathways modulated by Rab7 phosphorylation, supporting the second model proposed in section 5.2, on how Rab7-S72E function in cells.

We did not detect any change in mitochondrial dynamics upon TBK1 knockdown. This poses the question about how knocking down a protein with major roles in selective mitophagy does not impact on mitochondrial transport or density. There are several possible explanations for this apparent contradiction. First, the same phospho-proteomic study who described the stoichiometry of p-Rab7 S72 present on mitochondria, reported that after mitochondria depolarisation with A/O, 0.12% of TBK1 is activated (measured as levels of p-TBK1 S172), therefore, only a small cytosolic pool of TBK1 is involved in PARKIN-dependent mitophagy, and it is likely that with the 65% TBK1 knockdown we achieved here, the remaining protein levels are enough to carry out its mitophagy-related functions. Second, it might be a cell type- or compartment-specific effect, since most of the mitophagy studies are done in HeLa or HEK cells. Unlike the reticular network that mitochondria form in fibroblast-like cells and in neuronal cell bodies, axonal mitochondria are discrete “bean-shaped” entities (Pilling et al., 2006). This may affect their fusion/fission dynamics, as well as their degradation. Third, studies using *in vivo* models have shown PARKIN-dependent mitophagy rarely occurs in axons (Sung et al., 2016). It is possible that in TBK1 knockdown conditions mitophagy still takes place, but by different mechanisms, such as the exposure of the phospholipid cardiolipin on the mitochondrial outer membrane, a signal that directly recruits LC3 in neurons (Chu et al., 2013).

Standing questions and future perspectives

5.7 How Rab7-S72E expression and TBK1 knockdown alter signalling endosome axonal transport?

Given that both Rab7-S72E expression and TBK1 knockdown affect the directionality of transport of signalling endosomes, and that there is a causal relation between them (substrate/kinase), we hypothesise TBK1 regulates signalling endosome retrograde transport by directly phosphorylating Rab7. Nevertheless, we cannot rule out the TBK1-

dependent phosphorylation of a different substrate, such as a molecular motor or adaptor. For example, ALS-related mutant SOD1 activates p38α MAP kinase, which in turn phosphorylates kinesin-1. This is an inhibitory phosphorylation; thus, anterograde transport becomes inhibited (Morfini et al., 2013). However, the specificity of the axonal transport defect described here, which affect only signalling endosomes, suggest a modulation at the motor level is highly unlikely.

We have shown that knocking down TBK1 promotes signalling endosome bidirectional movement, hinting at a defect on the adaptors which recruit motors, rather than motors themselves. In this regard, it is currently unknown what adaptor is used by signalling endosomes in their route to the MN cell body. As mentioned in Chapter 1, BDNF TrkB-containing signalling endosomes use Hook1 in hippocampal neurons and snapin in cortical neurons (Olenick et al., 2019; Zhou et al., 2012). Additionally, we consider RILP as a possible candidate to mediate the axonal transport of signalling endosomes. Rab7-S72E interaction with its effector RILP is impaired (Wallace, 2014; Shinde and Maddika, 2016), therefore, this could be the way by which retrograde motors fail to be recruited to signalling endosomes. Another hypothesis that may explain our results consist in signalling endosomes typically bearing both dynein and kinesin. TBK1 may inhibit one of them, for example kinesin, hence ensuring unidirectional transport. A similar mechanism operates in autophagosomes moving retrogradely towards the cell body. Autophagosome-associated JIP1 binds both dynein and kinesin-1 but maintains kinesin-1 in its autoinhibited form. JIP1 function is also affected by phosphorylation, although in this case, dephosphorylated JIP1 promotes retrograde transport (Fu et al., 2014). This example illustrates why identifying the adaptor which recruit motors to signalling endosomes is a priority to elucidate the molecular mechanism.

An alternative mechanism to explain our observations include aberrant fusion between signalling endosomes and lysosomes, and the generation of hybrid organelles. This mechanism might present analogies to how autophagosomes formed at the distal axon

regulate their movement. Autophagosomes move unidirectionally in the retrograde direction, but as they reach the soma, they become increasingly acidified and start moving bidirectionally, which is characteristic of lysosomes (Maday et al., 2012).

From an experimental perspective, novel TBK1 substrates regulating axonal transport can be identified by phospho-proteomic approaches, using purified H_CT-positive signalling endosomes isolated in TBK1 knockdown and control conditions. Signalling endosome/lysosome fusion could be assessed by tracking H_CT-positive signalling endosomes and checking whether TBK1 knockdown induce a subpopulation that can be labelled by both LysoTracker and probes detecting active cathepsins, such as Magic Red. Finally, the identity of the motor adaptor can be addressed by checking changes in their interaction with Rab7 in TBK1 knockdown or control conditions, and in Rab7 WT or Rab7-S72E expressing cells. Additionally, constructs encoding dominant-negative adaptor mutants could be magnetofected into MN, in order to check if any of them induce signalling endosome bidirectional transport. For example, RILP-C33 is a truncated form of the adaptor, which lacks the N-terminal region, thus exerting a dominant-negative effect (Cantalupo et al., 2001), which might be useful to dissect whether the mechanism depends on this Rab7 effector.

5.8 What are the consequences of TBK1 loss of function for ALS?

TBK1 heterozygosity in the $SOD1^{G93A}$ mice background accelerates disease onset, but extend their lifespan (Brenner et al., 2019). Late stages of the disease are undoubtedly linked to neuroinflammatory processes, where TBK1 is likely to play a role, possibly on activated microglia and astrocytes. Nevertheless, TBK1 contribution to disease onset is less clear.

Many ALS defects on axonal transport precede the apparition of symptoms, in agreement with a “dying back” hypothesis, where motor neuron degeneration starts at the NMJ and progress towards the soma (Kiernan et al., 2011). In this regard, we

propose a role for TBK1 during the retrograde transport of neurotrophic signalling. TBK1 haploinsufficiency would result in reduced retrograde transport of signalling endosomes, ultimately impacting on neuronal survival and motor neuron degeneration.

References

Ahmad, F.J., J. Hughey, T. Wittmann, A. Hyman, M. Greaser, and P.W. Baas. 2000. Motor proteins regulate force interactions between microtubules and microfilaments in the axon. *Nat Cell Biol*. 2:276–280. doi:10.1038/35010544.

Ahmad, L., Zhang, S.-Y., Casanova, J.-L., and Sancho-Shimizu, V. (2016). Human TBK1: A Gatekeeper of Neuroinflammation. Trends Mol Med *22*, 511–527.

Akhmanova, A., and Hoogenraad, C.C. (2005). Microtubule plus-end-tracking proteins: mechanisms and functions. Curr. Opin. Cell Biol. *17*, 47–54.

Akhmanova, A., and Hoogenraad, C.C. (2015). Microtubule minus-end-targeting proteins. Curr. Biol. *25*, R162-171.

Akhmanova, A., and Steinmetz, M.O. (2015). Control of microtubule organization and dynamics: two ends in the limelight. Nat. Rev. Mol. Cell Biol. *16*, 711–726.

Alami, N.H., Smith, R.B., Carrasco, M.A., Williams, L.A., Winborn, C.S., Han, S.S.W., Kiskinis, E., Winborn, B., Freibaum, B.D., Kanagaraj, A., et al. (2014). Axonal transport of TDP-43 mRNA granules is impaired by ALS-causing mutations. Neuron *81*, 536–543.

Al-Chalabi, A., and Hardiman, O. (2013). The epidemiology of ALS: a conspiracy of genes, environment and time. Nat Rev Neurol *9*, 617–628.

Al-Chalabi, A., Hardiman, O., Kiernan, M.C., Chiò, A., Rix-Brooks, B., and van den Berg, L.H. (2016). Amyotrophic lateral sclerosis: moving towards a new classification system. Lancet Neurol *15*, 1182–1194.

Alers, S., Löffler, A.S., Wesselborg, S., and Stork, B. (2012). Role of AMPK-mTOR-Ulk1/2 in the regulation of autophagy: cross talk, shortcuts, and feedbacks. Mol. Cell. Biol. *32*, 2–11.

Alexopoulou, L., Holt, A.C., Medzhitov, R., and Flavell, R.A. (2001a). Recognition of double-stranded RNA and activation of NF-kappaB by Toll-like receptor 3. Nature *413*, 732–738.

Alexopoulou, L., Holt, A.C., Medzhitov, R., and Flavell, R.A. (2001b). Recognition of double-stranded RNA and activation of NF-kappaB by Toll-like receptor 3. Nature *413*, 732–738.

Anderson, P., and Kedersha, N. (2008). Stress granules: the Tao of RNA triage. Trends Biochem. Sci. *33*, 141–150.

Angeletti, R.H., Aneletti, P.U., and Levi-Montalcini, R. (1972). Selective accumulation of (125 I) labelled nerve growth factor in sympathetic ganglia. Brain Res. *46*, 421–425.

Arai, T., Hasegawa, M., Akiyama, H., Ikeda, K., Nonaka, T., Mori, H., Mann, D., Tsuchiya, K., Yoshida, M., Hashizume, Y., et al. (2006). TDP-43 is a component of ubiquitin-positive tau-negative inclusions in frontotemporal lobar degeneration and amyotrophic lateral sclerosis. Biochem. Biophys. Res. Commun. *351*, 602–611.

Arce, V., Garces, A., de Bovis, B., Filippi, P., Henderson, C., Pettmann, B., and deLapeyrière, O. (1999). Cardiotrophin-1 requires LIFRbeta to promote survival of mouse motoneurons purified by a novel technique. J. Neurosci. Res. *55*, 119–126.

Arimoto, M., Koushika, S.P., Choudhary, B.C., Li, C., Matsumoto, K., and Hisamoto, N. (2011). The Caenorhabditis elegans JIP3 protein UNC-16 functions as an adaptor to link kinesin-1 with cytoplasmic dynein. J. Neurosci. *31*, 2216–2224.

Arnold, E.S., Ling, S.-C., Huelga, S.C., Lagier-Tourenne, C., Polymenidou, M., Ditsworth, D., Kordasiewicz, H.B., McAlonis-Downes, M., Platoshyn, O., Parone, P.A., et al. (2013). ALS-linked TDP-43 mutations produce aberrant RNA splicing and adult-onset motor neuron disease without aggregation or loss of nuclear TDP-43. Proc. Natl. Acad. Sci. U.S.A. *110*, E736-745.

Arthur, K.C., Calvo, A., Price, T.R., Geiger, J.T., Chiò, A., and Traynor, B.J. (2016). Projected increase in amyotrophic lateral sclerosis from 2015 to 2040. Nat Commun *7*, 12408.

Avendaño-Vázquez, S.E., Dhir, A., Bembich, S., Buratti, E., Proudfoot, N., and Baralle, F.E. (2012). Autoregulation of TDP-43 mRNA levels involves interplay between transcription, splicing, and alternative polyA site selection. Genes Dev. *26*, 1679–1684.

Ayloo, S., Lazarus, J.E., Dodda, A., Tokito, M., Ostap, E.M., and Holzbaur, E.L.F. (2014). Dynactin functions as both a dynamic tether and brake during dynein-driven motility. Nat Commun *5*, 4807.

Baas, P.W., and Lin, S. (2011). Hooks and comets: The story of microtubule polarity orientation in the neuron. Dev Neurobiol *71*, 403–418.

Baas, P.W., Deitch, J.S., Black, M.M., and Banker, G.A. (1988). Polarity orientation of microtubules in hippocampal neurons: uniformity in the axon and nonuniformity in the dendrite. Proc. Natl. Acad. Sci. U.S.A. *85*, 8335–8339.

Bailly, E., McCaffrey, M., Touchot, N., Zahraoui, A., Goud, B., and Bornens, M. (1991). Phosphorylation of two small GTP-binding proteins of the Rab family by p34cdc2. Nature *350*, 715–718.

Bakshi, S., Taylor, J., Strickson, S., McCartney, T., and Cohen, P. (2017). Identification of TBK1 complexes required for the phosphorylation of IRF3 and the production of interferon β. Biochem. J. *474*, 1163–1174.

Baldwin, K.R., Godena, V.K., Hewitt, V.L., and Whitworth, A.J. (2016). Axonal transport defects are a common phenotype in Drosophila models of ALS. Hum. Mol. Genet. *25*, 2378–2392.

Barr, F., and Lambright, D.G. (2010). Rab GEFs and GAPs. Curr. Opin. Cell Biol. *22*, 461–470.

Barthelme, D., Jauregui, R., and Sauer, R.T. (2015). An ALS disease mutation in Cdc48/p97 impairs 20S proteasome binding and proteolytic communication. Protein Sci. *24*, 1521–1527.

Beaulieu, J.M., Nguyen, M.D., and Julien, J.P. (1999). Late onset of motor neurons in mice overexpressing wild-type peripherin. J. Cell Biol. *147*, 531–544.

Bennett, C.L., Dastidar, S.G., Ling, S.-C., Malik, B., Ashe, T., Wadhwa, M., Miller, D.B., Lee, C., Mitchell, M.B., van Es, M.A., et al. (2018). Senataxin mutations elicit motor neuron degeneration phenotypes and yield TDP-43 mislocalization in ALS4 mice and human patients. Acta Neuropathol. *136*, 425–443.

Bhattacharyya, A., Watson, F.L., Bradlee, T.A., Pomeroy, S.L., Stiles, C.D., and Segal, R.A. (1997). Trk receptors function as rapid retrograde signal carriers in the adult nervous system. J. Neurosci. *17*, 7007–7016.

Bieling, P., Kandels-Lewis, S., Telley, I.A., van Dijk, J., Janke, C., and Surrey, T. (2008). CLIP-170 tracks growing microtubule ends by dynamically recognizing composite EB1/tubulin-binding sites. J. Cell Biol. *183*, 1223–1233.

Bilsland, L.G., Sahai, E., Kelly, G., Golding, M., Greensmith, L., and Schiavo, G. (2010). Deficits in axonal transport precede ALS symptoms in vivo. Proc. Natl. Acad. Sci. U.S.A. *107*, 20523–20528.

Birsa, N., Bentham, M.P., and Fratta, P. (2019). Cytoplasmic functions of TDP-43 and FUS and their role in ALS. Semin. Cell Dev. Biol.

Bodakuntla, S., Jijumon, A.S., Villablanca, C., Gonzalez-Billault, C., and Janke, C. (2019). Microtubule-Associated Proteins: Structuring the Cytoskeleton. Trends Cell Biol. *29*, 804–819.

Bodakuntla, S., Schnitzler, A., Villablanca, C., Gonzalez-Billault, C., Bieche, I., Janke, C., and Magiera, M.M. (2020). Tubulin polyglutamylation is a general traffic control mechanism in hippocampal neurons. J. Cell. Sci.

Bohnert, S., and Schiavo, G. (2005). Tetanus toxin is transported in a novel neuronal compartment characterized by a specialized pH regulation. J. Biol. Chem. *280*, 42336–42344.

Boillée, S., Yamanaka, K., Lobsiger, C.S., Copeland, N.G., Jenkins, N.A., Kassiotis, G., Kollias, G., and Cleveland, D.W. (2006). Onset and progression in inherited ALS determined by motor neurons and microglia. Science *312*, 1389–1392.

Bonnard, M., Mirtsos, C., Suzuki, S., Graham, K., Huang, J., Ng, M., Itié, A., Wakeham, A., Shahinian, A., Henzel, W.J., et al. (2000). Deficiency of T2K leads to apoptotic liver degeneration and impaired NF-kappaB-dependent gene transcription. EMBO J. *19*, 4976–4985.

Bosco, D.A., Lemay, N., Ko, H.K., Zhou, H., Burke, C., Kwiatkowski, T.J., Sapp, P., McKenna-Yasek, D., Brown, R.H., and Hayward, L.J. (2010). Mutant FUS proteins that cause amyotrophic lateral sclerosis incorporate into stress granules. Hum. Mol. Genet. *19*, 4160–4175.

Boutry, M., Branchu, J., Lustremant, C., Pujol, C., Pernelle, J., Matusiak, R., Seyer, A., Poirel, M., Chu-Van, E., Pierga, A., et al. (2018). Inhibition of Lysosome Membrane Recycling Causes Accumulation of Gangliosides that Contribute to Neurodegeneration. Cell Rep *23*, 3813–3826.

Boutry, M., Pierga, A., Matusiak, R., Branchu, J., Houllegatte, M., Ibrahim, Y., Balse, E., El Hachimi, K.-H., Brice, A., Stevanin, G., et al. (2019). Loss of spatacsin impairs cholesterol trafficking and calcium homeostasis. Commun Biol *2*, 380.

Brenner, D., Yilmaz, R., Müller, K., Grehl, T., Petri, S., Meyer, T., Grosskreutz, J., Weydt, P., Ruf, W., Neuwirth, C., et al. (2018). Hot-spot KIF5A mutations cause familial ALS. Brain *141*, 688–697.

Brenner, D., Sieverding, K., Bruno, C., Lüningschrör, P., Buck, E., Mungwa, S., Fischer, L., Brockmann, S.J., Ulmer, J., Bliederhäuser, C., et al. (2019). Heterozygous Tbk1 loss has opposing effects in early and late stages of ALS in mice. J. Exp. Med. *216*, 267–278.

Brouhard, G.J. (2015). Dynamic instability 30 years later: complexities in microtubule growth and catastrophe. Mol. Biol. Cell *26*, 1207–1210.

Brouhard, G.J., and Rice, L.M. (2018). Microtubule dynamics: an interplay of biochemistry and mechanics. Nat. Rev. Mol. Cell Biol. *19*, 451–463.

Bruijn, L.I., Becher, M.W., Lee, M.K., Anderson, K.L., Jenkins, N.A., Copeland, N.G., Sisodia, S.S., Rothstein, J.D., Borchelt, D.R., Price, D.L., et al. (1997). ALS-linked SOD1 mutant G85R mediates damage to astrocytes and promotes rapidly progressive disease with SOD1-containing inclusions. Neuron *18*, 327–338.

Bryantseva, S.A., and Zhapparova, O.N. (2012). Bidirectional transport of organelles: unity and struggle of opposing motors. Cell Biol. Int. *36*, 1–6.

Bucci, C., Thomsen, P., Nicoziani, P., McCarthy, J., and van Deurs, B. (2000). Rab7: a key to lysosome biogenesis. Mol. Biol. Cell *11*, 467–480.

Buratti, E. (2018). TDP-43 post-translational modifications in health and disease. Expert Opin. Ther. Targets *22*, 279–293.

Burrell, J.R., Kiernan, M.C., Vucic, S., and Hodges, J.R. (2011). Motor neuron dysfunction in frontotemporal dementia. Brain *134*, 2582–2594.

Cabrera, M., Nordmann, M., Perz, A., Schmedt, D., Gerondopoulos, A., Barr, F., Piehler, J., Engelbrecht-Vandré, S., and Ungermann, C. (2014). The Mon1-Ccz1 GEF activates the Rab7 GTPase Ypt7 via a longin-fold-Rab interface and association with PI3P-positive membranes. J. Cell. Sci. *127*, 1043–1051.

Cabukusta, B., and Neefjes, J. (2018). Mechanisms of lysosomal positioning and movement. Traffic *19*, 761–769.

Cai, Q., Gerwin, C., and Sheng, Z.-H. (2005). Syntabulin-mediated anterograde transport of mitochondria along neuronal processes. J. Cell Biol. *170*, 959–969.

Cairns, N.J., Bigio, E.H., Mackenzie, I.R.A., Neumann, M., Lee, V.M.-Y., Hatanpaa, K.J., White, C.L., Schneider, J.A., Grinberg, L.T., Halliday, G., et al. (2007). Neuropathologic diagnostic and nosologic criteria for frontotemporal lobar degeneration: consensus of the Consortium for Frontotemporal Lobar Degeneration. Acta Neuropathol. *114*, 5–22.

Cantalupo, G., Alifano, P., Roberti, V., Bruni, C.B., and Bucci, C. (2001). Rab-interacting lysosomal protein (RILP): the Rab7 effector required for transport to lysosomes. EMBO J. *20*, 683–693.

Cashman, N.R., Durham, H.D., Blusztajn, J.K., Oda, K., Tabira, T., Shaw, I.T., Dahrouge, S., and Antel, J.P. (1992). Neuroblastoma x spinal cord (NSC) hybrid cell lines resemble developing motor neurons. Dev. Dyn. *194*, 209–221.

Cavalli, V., Kujala, P., Klumperman, J., and Goldstein, L.S.B. (2005). Sunday Driver links axonal transport to damage signaling. J. Cell Biol. *168*, 775–787.

Celetti, G., Paci, G., Caria, J., VanDelinder, V., Bachand, G., and Lemke, E.A. (2020). The liquid state of FG-nucleoporins mimics permeability barrier properties of nuclear pore complexes. J. Cell Biol. *219*.

Chang, L., and Monteiro, M.J. (2015). Defective Proteasome Delivery of Polyubiquitinated Proteins by Ubiquilin-2 Proteins Containing ALS Mutations. PLoS ONE *10*, e0130162.

Chao, M.V., and Hempstead, B.L. (1995). p75 and Trk: a two-receptor system. Trends Neurosci. *18*, 321–326.

Chavrier, P., Parton, R.G., Hauri, H.P., Simons, K., and Zerial, M. (1990). Localization of low molecular weight GTP binding proteins to exocytic and endocytic compartments. Cell *62*, 317–329.

Chen, Y., and Sheng, Z.-H. (2013). Kinesin-1-syntaphilin coupling mediates activity-dependent regulation of axonal mitochondrial transport. J. Cell Biol. *202*, 351–364.

Chen, Y.-Z., Bennett, C.L., Huynh, H.M., Blair, I.P., Puls, I., Irobi, J., Dierick, I., Abel, A., Kennerson, M.L., Rabin, B.A., et al. (2004). DNA/RNA helicase gene mutations in a form of juvenile amyotrophic lateral sclerosis (ALS4). Am. J. Hum. Genet. *74*, 1128–1135.

Cheng, X.-T., Xie, Y.-X., Zhou, B., Huang, N., Farfel-Becker, T., and Sheng, Z.-H. (2018). Characterization of LAMP1-labeled nondegradative lysosomal and endocytic compartments in neurons. J. Cell Biol. *217*, 3127–3139.

Chiò, A., Logroscino, G., Traynor, B.J., Collins, J., Simeone, J.C., Goldstein, L.A., and White, L.A. (2013). Global epidemiology of amyotrophic lateral sclerosis: a systematic review of the published literature. Neuroepidemiology *41*, 118–130.

Chitiprolu, M., Jagow, C., Tremblay, V., Bondy-Chorney, E., Paris, G., Savard, A., Palidwor, G., Barry, F.A., Zinman, L., Keith, J., et al. (2018). A complex of C9ORF72 and p62 uses arginine methylation to eliminate stress granules by autophagy. Nat Commun *9*, 2794.

Chowdhury, S., Ketcham, S.A., Schroer, T.A., and Lander, G.C. (2015). Structural organization of the dynein-dynactin complex bound to microtubules. Nat. Struct. Mol. Biol. *22*, 345–347.

Chu, C.T., Ji, J., Dagda, R.K., Jiang, J.F., Tyurina, Y.Y., Kapralov, A.A., Tyurin, V.A., Yanamala, N., Shrivastava, I.H., Mohammadyani, D., et al. (2013). Cardiolipin externalization to the outer mitochondrial membrane acts as an elimination signal for mitophagy in neuronal cells. Nat. Cell Biol. *15*, 1197–1205.

Cirulli, E.T., Lasseigne, B.N., Petrovski, S., Sapp, P.C., Dion, P.A., Leblond, C.S., Couthouis, J., Lu, Y.-F., Wang, Q., Krueger, B.J., et al. (2015). Exome sequencing in amyotrophic lateral sclerosis identifies risk genes and pathways. Science *347*, 1436–1441.

Clark, K., Peggie, M., Plater, L., Sorcek, R.J., Young, E.R.R., Madwed, J.B., Hough, J., McIver, E.G., and Cohen, P. (2011). Novel cross-talk within the IKK family controls innate immunity. Biochem. J. *434*, 93–104.

Cogli, L., Progida, C., Lecci, R., Bramato, R., Krüttgen, A., and Bucci, C. (2010). CMT2B-associated Rab7 mutants inhibit neurite outgrowth. Acta Neuropathol. *120*, 491–501.

Cogli, L., Progida, C., Thomas, C.L., Spencer-Dene, B., Donno, C., Schiavo, G., and Bucci, C. (2013). Charcot-Marie-Tooth type 2B disease-causing RAB7A mutant proteins show altered interaction with the neuronal intermediate filament peripherin. Acta Neuropathol. *125*, 257–272.

Colucci, A.M.R., Campana, M.C., Bellopede, M., and Bucci, C. (2005). The Rab-interacting lysosomal protein, a Rab7 and Rab34 effector, is capable of self-interaction. Biochem. Biophys. Res. Commun. *334*, 128–133.

Corbo, M., and Hays, A.P. (1992). Peripherin and neurofilament protein coexist in spinal spheroids of motor neuron disease. J. Neuropathol. Exp. Neurol. *51*, 531–537.

Couthouis, J., Hart, M.P., Erion, R., King, O.D., Diaz, Z., Nakaya, T., Ibrahim, F., Kim, H.-J., Mojsilovic-Petrovic, J., Panossian, S., et al. (2012). Evaluating the role of the FUS/TLS-related gene EWSR1 in amyotrophic lateral sclerosis. Hum. Mol. Genet. *21*, 2899–2911.

Coyne, A.N., Siddegowda, B.B., Estes, P.S., Johannesmeyer, J., Kovalik, T., Daniel, S.G., Pearson, A., Bowser, R., and Zarnescu, D.C. (2014). Futsch/MAP1B mRNA is a translational target of TDP-43 and is neuroprotective in a Drosophila model of amyotrophic lateral sclerosis. J. Neurosci. *34*, 15962–15974.

Cross, J.A., and Dodding, M.P. (2019). Motor-cargo adaptors at the organelle-cytoskeleton interface. Curr. Opin. Cell Biol. *59*, 16–23.

Da Cruz, S., Bui, A., Saberi, S., Lee, S.K., Stauffer, J., McAlonis-Downes, M., Schulte, D., Pizzo, D.P., Parone, P.A., Cleveland, D.W., et al. (2017). Misfolded SOD1 is not a primary component of sporadic ALS. Acta Neuropathol. *134*, 97–111.

De Luca, A., Progida, C., Spinosa, M.R., Alifano, P., and Bucci, C. (2008). Characterization of the Rab7K157N mutant protein associated with Charcot-Marie-Tooth type 2B. Biochem. Biophys. Res. Commun. *372*, 283–287.

De Vos, K.J., and Hafezparast, M. (2017). Neurobiology of axonal transport defects in motor neuron diseases: Opportunities for translational research? Neurobiol. Dis. *105*, 283–299.

De Vos, K.J., Chapman, A.L., Tennant, M.E., Manser, C., Tudor, E.L., Lau, K.-F., Brownlees, J., Ackerley, S., Shaw, P.J., McLoughlin, D.M., et al. (2007). Familial amyotrophic lateral sclerosis-linked SOD1 mutants perturb fast axonal transport to reduce axonal mitochondria content. Hum. Mol. Genet. *16*, 2720–2728.

Deinhardt, K., and Chao, M.V. (2014). Trk receptors. Handb Exp Pharmacol *220*, 103–119.

Deinhardt, K., Salinas, S., Verastegui, C., Watson, R., Worth, D., Hanrahan, S., Bucci, C., and Schiavo, G. (2006). Rab5 and Rab7 control endocytic sorting along the axonal retrograde transport pathway. Neuron *52*, 293–305.

DeJesus-Hernandez, M., Mackenzie, I.R., Boeve, B.F., Boxer, A.L., Baker, M., Rutherford, N.J., Nicholson, A.M., Finch, N.A., Flynn, H., Adamson, J., et al. (2011). Expanded GGGGCC hexanucleotide repeat in noncoding region of C9ORF72 causes chromosome 9p-linked FTD and ALS. Neuron *72*, 245–256.

del Aguila, M.A., Longstreth, W.T., McGuire, V., Koepsell, T.D., and van Belle, G. (2003). Prognosis in amyotrophic lateral sclerosis: a population-based study. Neurology *60*, 813–819.

Delcroix, J.-D., Valletta, J.S., Wu, C., Hunt, S.J., Kowal, A.S., and Mobley, W.C. (2003). NGF signaling in sensory neurons: evidence that early endosomes carry NGF retrograde signals. Neuron *39*, 69–84.

Deng, H.-X., Chen, W., Hong, S.-T., Boycott, K.M., Gorrie, G.H., Siddique, N., Yang, Y., Fecto, F., Shi, Y., Zhai, H., et al. (2011). Mutations in UBQLN2 cause dominant X-linked juvenile and adult-onset ALS and ALS/dementia. Nature *477*, 211–215.

Desai, A., and Mitchison, T.J. (1997). Microtubule polymerization dynamics. Annu. Rev. Cell Dev. Biol. *13*, 83–117.

Di Giorgio, F.P., Carrasco, M.A., Siao, M.C., Maniatis, T., and Eggan, K. (2007). Non-cell autonomous effect of glia on motor neurons in an embryonic stem cell-based ALS model. Nat. Neurosci. *10*, 608–614.

Dienstbier, M., Boehl, F., Li, X., and Bullock, S.L. (2009). Egalitarian is a selective RNA-binding protein linking mRNA localization signals to the dynein motor. Genes Dev. *23*, 1546–1558.

Dikic, I. (2017). Proteasomal and Autophagic Degradation Systems. Annu. Rev. Biochem. *86*, 193–224.

Dikic, I., and Elazar, Z. (2018). Mechanism and medical implications of mammalian autophagy. Nat. Rev. Mol. Cell Biol. *19*, 349–364.

Dong, X., Shen, D., Wang, X., Dawson, T., Li, X., Zhang, Q., Cheng, X., Zhang, Y., Weisman, L.S., Delling, M., et al. (2010). PI(3,5)P(2) controls membrane trafficking by direct activation of mucolipin Ca(2+) release channels in the endolysosome. Nat Commun *1*, 38.

Ederle, H., and Dormann, D. (2017). TDP-43 and FUS en route from the nucleus to the cytoplasm. FEBS Lett. *591*, 1489–1507.

Ehlers, M.D., Kaplan, D.R., Price, D.L., and Koliatsos, V.E. (1995). NGF-stimulated retrograde transport of trkA in the mammalian nervous system. J. Cell Biol. *130*, 149–156.

Engelender, S., Sharp, A.H., Colomer, V., Tokito, M.K., Lanahan, A., Worley, P., Holzbaur, E.L., and Ross, C.A. (1997). Huntingtin-associated protein 1 (HAP1) interacts with the p150Glued subunit of dynactin. Hum. Mol. Genet. *6*, 2205–2212.

van Es, M.A., Hardiman, O., Chio, A., Al-Chalabi, A., Pasterkamp, R.J., Veldink, J.H., and van den Berg, L.H. (2017). Amyotrophic lateral sclerosis. Lancet *390*, 2084–2098.

Evans, C.S., and Holzbaur, E.L.F. (2019). Autophagy and mitophagy in ALS. Neurobiol. Dis. *122*, 35–40.

Even, A., Morelli, G., Broix, L., Scaramuzzino, C., Turchetto, S., Gladwyn-Ng, I., Le Bail, R., Shilian, M., Freeman, S., Magiera, M.M., et al. (2019). ATAT1-enriched vesicles promote microtubule acetylation via axonal transport. Sci Adv *5*, eaax2705.

Fang, R., Jiang, Q., Zhou, X., Wang, C., Guan, Y., Tao, J., Xi, J., Feng, J.-M., and Jiang, Z. (2017). MAVS activates TBK1 and IKKε through TRAFs in NEMO dependent and independent manner. PLoS Pathog. *13*, e1006720.

Farfel-Becker, T., Roney, J.C., Cheng, X.-T., Li, S., Cuddy, S.R., and Sheng, Z.-H. (2019). Neuronal Soma-Derived Degradative Lysosomes Are Continuously Delivered to Distal Axons to Maintain Local Degradation Capacity. Cell Rep *28*, 51-64.e4.

Farhan, S.M.K., Howrigan, D.P., Abbott, L.E., Klim, J.R., Topp, S.D., Byrnes, A.E., Churchhouse, C., Phatnani, H., Smith, B.N., Rampersaud, E., et al. (2019). Exome sequencing in amyotrophic lateral sclerosis implicates a novel gene, DNAJC7, encoding a heat-shock protein. Nat. Neurosci. *22*, 1966–1974.

Farías, G.G., Guardia, C.M., De Pace, R., Britt, D.J., and Bonifacino, J.S. (2017). BORC/kinesin-1 ensemble drives polarized transport of lysosomes into the axon. Proc. Natl. Acad. Sci. U.S.A. *114*, E2955–E2964.

Fecto, F., Yan, J., Vemula, S.P., Liu, E., Yang, Y., Chen, W., Zheng, J.G., Shi, Y., Siddique, N., Arrat, H., et al. (2011). SQSTM1 mutations in familial and sporadic amyotrophic lateral sclerosis. Arch. Neurol. *68*, 1440–1446.

Ferguson, S.M. (2019). Neuronal lysosomes. Neurosci. Lett. *697*, 1–9.

Fifita, J.A., Zhang, K.Y., Galper, J., Williams, K.L., McCann, E.P., Hogan, A.L., Saunders, N., Bauer, D., Tarr, I.S., Pamphlett, R., et al. (2017). Genetic and Pathological Assessment of hnRNPA1, hnRNPA2/B1, and hnRNPA3 in Familial and Sporadic Amyotrophic Lateral Sclerosis. Neurodegener Dis *17*, 304–312.

Fitzgerald, K.A., McWhirter, S.M., Faia, K.L., Rowe, D.C., Latz, E., Golenbock, D.T., Coyle, A.J., Liao, S.-M., and Maniatis, T. (2003). IKKepsilon and TBK1 are essential components of the IRF3 signaling pathway. Nat. Immunol. *4*, 491–496.

Fransson, A., Ruusala, A., and Aspenström, P. (2003). Atypical Rho GTPases have roles in mitochondrial homeostasis and apoptosis. J. Biol. Chem. *278*, 6495–6502.

Fransson, S., Ruusala, A., and Aspenström, P. (2006). The atypical Rho GTPases Miro-1 and Miro-2 have essential roles in mitochondrial trafficking. Biochem. Biophys. Res. Commun. *344*, 500–510.

Frasa, M.A.M., Maximiano, F.C., Smolarczyk, K., Francis, R.E., Betson, M.E., Lozano, E., Goldenring, J., Seabra, M.C., Rak, A., Ahmadian, M.R., et al. (2010). Armus is a Rac1 effector that inactivates Rab7 and regulates E-cadherin degradation. Curr. Biol. *20*, 198–208.

Freibaum, B.D., Lu, Y., Lopez-Gonzalez, R., Kim, N.C., Almeida, S., Lee, K.-H., Badders, N., Valentine, M., Miller, B.L., Wong, P.C., et al. (2015). GGGGCC repeat expansion in C9orf72 compromises nucleocytoplasmic transport. Nature *525*, 129–133.

Freischmidt, A., Wieland, T., Richter, B., Ruf, W., Schaeffer, V., Müller, K., Marroquin, N., Nordin, F., Hübers, A., Weydt, P., et al. (2015). Haploinsufficiency of TBK1 causes familial ALS and fronto-temporal dementia. Nat. Neurosci. *18*, 631–636.

Fu, M.-M., Nirschl, J.J., and Holzbaur, E.L.F. (2014). LC3 binding to the scaffolding protein JIP1 regulates processive dynein-driven transport of autophagosomes. Dev. Cell *29*, 577–590.

Fujita, T., Maturana, A.D., Ikuta, J., Hamada, J., Walchli, S., Suzuki, T., Sawa, H., Wooten, M.W., Okajima, T., Tatematsu, K., et al. (2007). Axonal guidance protein FEZ1 associates with tubulin and kinesin motor protein to transport mitochondria in neurites of NGF-stimulated PC12 cells. Biochem. Biophys. Res. Commun. *361*, 605–610.

Fukuda, M. (2011). TBC proteins: GAPs for mammalian small GTPase Rab? Biosci. Rep. *31*, 159–168.

Gadadhar, S., Bodakuntla, S., Natarajan, K., and Janke, C. (2017). The tubulin code at a glance. J. Cell. Sci. *130*, 1347–1353.

Gal, J., Ström, A.-L., Kwinter, D.M., Kilty, R., Zhang, J., Shi, P., Fu, W., Wooten, M.W., and Zhu, H. (2009). Sequestosome 1/p62 links familial ALS mutant SOD1 to LC3 via an ubiquitin-independent mechanism. J. Neurochem. *111*, 1062–1073.

Gallon, M., and Cullen, P.J. (2015). Retromer and sorting nexins in endosomal sorting. Biochem. Soc. Trans. *43*, 33–47.

Gama, J.B., Pereira, C., Simões, P.A., Celestino, R., Reis, R.M., Barbosa, D.J., Pires, H.R., Carvalho, C., Amorim, J., Carvalho, A.X., et al. (2017). Molecular mechanism of dynein recruitment to kinetochores by the Rod-Zw10-Zwilch complex and Spindly. J. Cell Biol. *216*, 943–960.

Gao, J., Langemeyer, L., Kümmel, D., Reggiori, F., and Ungermann, C. (2018). Molecular mechanism to target the endosomal Mon1-Ccz1 GEF complex to the pre-autophagosomal structure. Elife *7*.

Gatica, D., Lahiri, V., and Klionsky, D.J. (2018). Cargo recognition and degradation by selective autophagy. Nat. Cell Biol. *20*, 233–242.

Gay, N.J., and Keith, F.J. (1991). Drosophila Toll and IL-1 receptor. Nature *351*, 355–356.

Gendron, T.F., Bieniek, K.F., Zhang, Y.-J., Jansen-West, K., Ash, P.E.A., Caulfield, T., Daughrity, L., Dunmore, J.H., Castanedes-Casey, M., Chew, J., et al. (2013). Antisense transcripts of the expanded C9ORF72 hexanucleotide repeat form nuclear RNA foci and undergo repeat-associated non-ATG translation in c9FTD/ALS. Acta Neuropathol. *126*, 829–844.

Gillingham, A.K., Sinka, R., Torres, I.L., Lilley, K.S., and Munro, S. (2014). Toward a comprehensive map of the effectors of rab GTPases. Dev. Cell *31*, 358–373.

Gilmore, T.D., and Wolenski, F.S. (2012). NF-κB: where did it come from and why? Immunol. Rev. *246*, 14–35.

Goethals, S., Ydens, E., Timmerman, V., and Janssens, S. (2010). Toll-like receptor expression in the peripheral nerve. Glia *58*, 1701–1709.

Goldstein, O., Gana-Weisz, M., Nefussy, B., Vainer, B., Nayshool, O., Bar-Shira, A., Traynor, B.J., Drory, V.E., and Orr-Urtreger, A. (2018). High frequency of C9orf72 hexanucleotide repeat expansion in amyotrophic lateral sclerosis patients from two founder populations sharing the same risk haplotype. Neurobiol. Aging *64*, 160.e1-160.e7.

Goncalves, A., Bürckstümmer, T., Dixit, E., Scheicher, R., Górna, M.W., Karayel, E., Sugar, C., Stukalov, A., Berg, T., Kralovics, R., et al. (2011). Functional dissection of the TBK1 molecular network. PLoS ONE *6*, e23971.

Goode, A., Butler, K., Long, J., Cavey, J., Scott, D., Shaw, B., Sollenberger, J., Gell, C., Johansen, T., Oldham, N.J., et al. (2016). Defective recognition of LC3B by mutant SQSTM1/p62 implicates impairment of autophagy as a pathogenic mechanism in ALS-FTLD. Autophagy *12*, 1094–1104.

Gordon, P.H., Cheng, B., Katz, I.B., Pinto, M., Hays, A.P., Mitsumoto, H., and Rowland, L.P. (2006). The natural history of primary lateral sclerosis. Neurology *66*, 647–653.

Gordon, P.H., Cheng, B., Katz, I.B., Mitsumoto, H., and Rowland, L.P. (2009). Clinical features that distinguish PLS, upper motor neuron-dominant ALS, and typical ALS. Neurology *72*, 1948–1952.

Goto-Silva, L., McShane, M.P., Salinas, S., Kalaidzidis, Y., Schiavo, G., and Zerial, M. (2019). Retrograde transport of Akt by a neuronal Rab5-APPL1 endosome. Sci Rep *9*, 2433.

Gowrishankar, S., Wu, Y., and Ferguson, S.M. (2017). Impaired JIP3-dependent axonal lysosome transport promotes amyloid plaque pathology. J. Cell Biol. *216*, 3291–3305.

Grad, L.I., Rouleau, G.A., Ravits, J., and Cashman, N.R. (2017). Clinical Spectrum of Amyotrophic Lateral Sclerosis (ALS). Cold Spring Harb Perspect Med *7*.

Granatiero, V., and Manfredi, G. (2019). Mitochondrial Transport and Turnover in the Pathogenesis of Amyotrophic Lateral Sclerosis. Biology (Basel) *8*.

Greenway, M.J., Andersen, P.M., Russ, C., Ennis, S., Cashman, S., Donaghy, C., Patterson, V., Swingler, R., Kieran, D., Prehn, J., et al. (2006). ANG mutations segregate with familial and "sporadic" amyotrophic lateral sclerosis. Nat. Genet. *38*, 411–413.

Griffis, E.R., Stuurman, N., and Vale, R.D. (2007). Spindly, a novel protein essential for silencing the spindle assembly checkpoint, recruits dynein to the kinetochore. J. Cell Biol. *177*, 1005–1015.

Grigoriev, I., Splinter, D., Keijzer, N., Wulf, P.S., Demmers, J., Ohtsuka, T., Modesti, M., Maly, I.V., Grosveld, F., Hoogenraad, C.C., et al. (2007). Rab6 regulates transport and targeting of exocytotic carriers. Dev. Cell *13*, 305–314.

Grimes, M.L., Zhou, J., Beattie, E.C., Yuen, E.C., Hall, D.E., Valletta, J.S., Topp, K.S., LaVail, J.H., Bunnett, N.W., and Mobley, W.C. (1996). Endocytosis of activated TrkA: evidence that nerve growth factor induces formation of signaling endosomes. J. Neurosci. *16*, 7950–7964.

Grimes, M.L., Beattie, E., and Mobley, W.C. (1997). A signaling organelle containing the nerve growth factor-activated receptor tyrosine kinase, TrkA. Proc. Natl. Acad. Sci. U.S.A. *94*, 9909–9914.

Gromicho, M., Oliveira Santos, M., Pinto, A., Pronto-Laborinho, A., and De Carvalho, M. (2017). Young-onset rapidly progressive ALS associated with heterozygous FUS mutation. Amyotroph Lateral Scler Frontotemporal Degener *18*, 451–453.

Grotjahn, D.A., Chowdhury, S., Xu, Y., McKenney, R.J., Schroer, T.A., and Lander, G.C. (2018). Cryo-electron tomography reveals that dynactin recruits a team of dyneins for processive motility. Nat. Struct. Mol. Biol. *25*, 203–207.

Guardia, C.M., Farías, G.G., Jia, R., Pu, J., and Bonifacino, J.S. (2016). BORC Functions Upstream of Kinesins 1 and 3 to Coordinate Regional Movement of Lysosomes along Different Microtubule Tracks. Cell Rep *17*, 1950–1961.

Guedes-Dias, P., and Holzbaur, E.L.F. (2019). Axonal transport: Driving synaptic function. Science *366*.

Guerra, F., and Bucci, C. (2016). Multiple Roles of the Small GTPase Rab7. Cells *5*.

Gumy, L.F., Katrukha, E.A., Grigoriev, I., Jaarsma, D., Kapitein, L.C., Akhmanova, A., and Hoogenraad, C.C. (2017). MAP2 Defines a Pre-axonal Filtering Zone to Regulate KIF1- versus KIF5-Dependent Cargo Transport in Sensory Neurons. Neuron *94*, 347-362.e7.

Guo, W., Naujock, M., Fumagalli, L., Vandoorne, T., Baatsen, P., Boon, R., Ordovás, L., Patel, A., Welters, M., Vanwelden, T., et al. (2017). HDAC6 inhibition reverses axonal transport defects in motor neurons derived from FUS-ALS patients. Nat Commun *8*, 861.

Guo, X., Macleod, G.T., Wellington, A., Hu, F., Panchumarthi, S., Schoenfield, M., Marin, L., Charlton, M.P., Atwood, H.L., and Zinsmaier, K.E. (2005). The GTPase dMiro is required for axonal transport of mitochondria to Drosophila synapses. Neuron *47*, 379–393.

Guo, X., Farías, G.G., Mattera, R., and Bonifacino, J.S. (2016). Rab5 and its effector FHF contribute to neuronal polarity through dynein-dependent retrieval of somatodendritic proteins from the axon. Proc. Natl. Acad. Sci. U.S.A. *113*, E5318-5327.

Gurney, M.E., Pu, H., Chiu, A.Y., Dal Canto, M.C., Polchow, C.Y., Alexander, D.D., Caliendo, J., Hentati, A., Kwon, Y.W., and Deng, H.X. (1994). Motor neuron degeneration in mice that express a human Cu,Zn superoxide dismutase mutation. Science *264*, 1772–1775.

Hadano, S., Hand, C.K., Osuga, H., Yanagisawa, Y., Otomo, A., Devon, R.S., Miyamoto, N., Showguchi-Miyata, J., Okada, Y., Singaraja, R., et al. (2001). A gene encoding a putative GTPase regulator is mutated in familial amyotrophic lateral sclerosis 2. Nat. Genet. *29*, 166–173.

Hadano, S., Mitsui, S., Pan, L., Otomo, A., Kubo, M., Sato, K., Ono, S., Onodera, W., Abe, K., Chen, X., et al. (2016). Functional links between SQSTM1 and ALS2 in the pathogenesis of ALS: cumulative impact on the protection against mutant SOD1-mediated motor dysfunction in mice. Hum. Mol. Genet. *25*, 3321–3340.

Haidet-Phillips, A.M., Hester, M.E., Miranda, C.J., Meyer, K., Braun, L., Frakes, A., Song, S., Likhite, S., Murtha, M.J., Foust, K.D., et al. (2011). Astrocytes from familial and sporadic ALS patients are toxic to motor neurons. Nat. Biotechnol. *29*, 824–828.

Hamburger, V., and Levi-Montalcini, R. (1949). Proliferation, differentiation and degeneration in the spinal ganglia of the chick embryo under normal and experimental conditions. J. Exp. Zool. *111*, 457–501.

Hanafusa, H., Yagi, T., Ikeda, H., Hisamoto, N., Nishioka, T., Kaibuchi, K., Shirakabe, K., and Matsumoto, K. (2019). LRRK1 phosphorylation of Rab7 at S72 links trafficking of EGFR-containing endosomes to its effector RILP. J. Cell. Sci. *132*.

Hancock, W.O. (2014). Bidirectional cargo transport: moving beyond tug of war. Nat. Rev. Mol. Cell Biol. *15*, 615–628.

Hardiman, O., Al-Chalabi, A., Chio, A., Corr, E.M., Logroscino, G., Robberecht, W., Shaw, P.J., Simmons, Z., and van den Berg, L.H. (2017). Amyotrophic lateral sclerosis. Nat Rev Dis Primers *3*, 17071.

Harper, J.W., Ordureau, A., and Heo, J.-M. (2018). Building and decoding ubiquitin chains for mitophagy. Nat. Rev. Mol. Cell Biol. *19*, 93–108.

Harraz, M.M., Marden, J.J., Zhou, W., Zhang, Y., Williams, A., Sharov, V.S., Nelson, K., Luo, M., Paulson, H., Schöneich, C., et al. (2008). SOD1 mutations disrupt redox-sensitive Rac regulation of NADPH oxidase in a familial ALS model. J. Clin. Invest. *118*, 659–670.

Harrington, A.W., and Ginty, D.D. (2013). Long-distance retrograde neurotrophic factor signalling in neurons. Nat. Rev. Neurosci. *14*, 177–187.

Hasan, M., and Yan, N. (2016). Therapeutic potential of targeting TBK1 in autoimmune diseases and interferonopathies. Pharmacol. Res. *111*, 336–342.

Hayes, L.R., Duan, L., Bowen, K., Kalab, P., and Rothstein, J.D. (2020). C9orf72 arginine-rich dipeptide repeat proteins disrupt karyopherin-mediated nuclear import. Elife *9*.

Heo, J.-M., Ordureau, A., Paulo, J.A., Rinehart, J., and Harper, J.W. (2015). The PINK1-PARKIN Mitochondrial Ubiquitylation Pathway Drives a Program of OPTN/NDP52 Recruitment and TBK1 Activation to Promote Mitophagy. Mol. Cell *60*, 7–20.

Heo, J.-M., Ordureau, A., Swarup, S., Paulo, J.A., Shen, K., Sabatini, D.M., and Harper, J.W. (2018). RAB7A phosphorylation by TBK1 promotes mitophagy via the PINK-PARKIN pathway. Sci Adv *4*, eaav0443.

Hirano, A., Donnenfeld, H., Sasaki, S., and Nakano, I. (1984a). Fine structural observations of neurofilamentous changes in amyotrophic lateral sclerosis. J. Neuropathol. Exp. Neurol. *43*, 461–470.

Hirano, A., Nakano, I., Kurland, L.T., Mulder, D.W., Holley, P.W., and Saccomanno, G. (1984b). Fine structural study of neurofibrillary changes in a family with amyotrophic lateral sclerosis. J. Neuropathol. Exp. Neurol. *43*, 471–480.

Hirano, M., Quinzii, C.M., Mitsumoto, H., Hays, A.P., Roberts, J.K., Richard, P., and Rowland, L.P. (2011). Senataxin mutations and amyotrophic lateral sclerosis. Amyotroph Lateral Scler *12*, 223–227.

Hirokawa, N., and Noda, Y. (2008). Intracellular transport and kinesin superfamily proteins, KIFs: structure, function, and dynamics. Physiol. Rev. *88*, 1089–1118.

Hirokawa, N., and Tanaka, Y. (2015). Kinesin superfamily proteins (KIFs): Various functions and their relevance for important phenomena in life and diseases. Exp. Cell Res. *334*, 16–25.

Hirokawa, N., Noda, Y., Tanaka, Y., and Niwa, S. (2009). Kinesin superfamily motor proteins and intracellular transport. Nat. Rev. Mol. Cell Biol. *10*, 682–696.

Hoelz, A., Glavy, J.S., and Beck, M. (2016). Toward the atomic structure of the nuclear pore complex: when top down meets bottom up. Nat. Struct. Mol. Biol. *23*, 624–630.

Hollenbeck, P.J., and Saxton, W.M. (2005). The axonal transport of mitochondria. J. Cell. Sci. *118*, 5411–5419.

Hoogenraad, C.C., and Akhmanova, A. (2016). Bicaudal D Family of Motor Adaptors: Linking Dynein Motility to Cargo Binding. Trends Cell Biol. *26*, 327–340.

Horgan, C.P., Hanscom, S.R., Jolly, R.S., Futter, C.E., and McCaffrey, M.W. (2010). Rab11-FIP3 links the Rab11 GTPase and cytoplasmic dynein to mediate transport to the endosomal-recycling compartment. J. Cell. Sci. *123*, 181–191.

Horiuchi, H., Lippé, R., McBride, H.M., Rubino, M., Woodman, P., Stenmark, H., Rybin, V., Wilm, M., Ashman, K., Mann, M., et al. (1997). A novel Rab5 GDP/GTP exchange factor complexed to Rabaptin-5 links nucleotide exchange to effector recruitment and function. Cell *90*, 1149–1159.

Howland, D.S., Liu, J., She, Y., Goad, B., Maragakis, N.J., Kim, B., Erickson, J., Kulik, J., DeVito, L., Psaltis, G., et al. (2002). Focal loss of the glutamate transporter EAAT2 in a transgenic rat model of SOD1 mutant-mediated amyotrophic lateral sclerosis (ALS). Proc. Natl. Acad. Sci. U.S.A. *99*, 1604–1609.

Hu, D.J.-K., Baffet, A.D., Nayak, T., Akhmanova, A., Doye, V., and Vallee, R.B. (2013). Dynein recruitment to nuclear pores activates apical nuclear migration and mitotic entry in brain progenitor cells. Cell *154*, 1300–1313.

Hutagalung, A.H., and Novick, P.J. (2011). Role of Rab GTPases in membrane traffic and cell physiology. Physiol. Rev. *91*, 119–149.

Iacoangeli, A., Al Khleifat, A., Jones, A.R., Sproviero, W., Shatunov, A., Opie-Martin, S., Alzheimer's Disease Neuroimaging Initiative, Morrison, K.E., Shaw, P.J., Shaw, C.E., et al. (2019). C9orf72 intermediate expansions of 24-30 repeats are associated with ALS. Acta Neuropathol Commun *7*, 115.

Igoudjil, A., Magrané, J., Fischer, L.R., Kim, H.J., Hervias, I., Dumont, M., Cortez, C., Glass, J.D., Starkov, A.A., and Manfredi, G. (2011). In vivo pathogenic role of mutant SOD1 localized in the mitochondrial intermembrane space. J. Neurosci. *31*, 15826–15837.

Im, Y.J., Raychaudhuri, S., Prinz, W.A., and Hurley, J.H. (2005). Structural mechanism for sterol sensing and transport by OSBP-related proteins. Nature *437*, 154–158.

Ingre, C., Roos, P.M., Piehl, F., Kamel, F., and Fang, F. (2015). Risk factors for amyotrophic lateral sclerosis. Clin Epidemiol *7*, 181–193.

Jaber, N., Mohd-Naim, N., Wang, Z., DeLeon, J.L., Kim, S., Zhong, H., Sheshadri, N., Dou, Z., Edinger, A.L., Du, G., et al. (2016). Vps34 regulates Rab7 and late endocytic trafficking through recruitment of the GTPase-activating protein Armus. J. Cell. Sci. *129*, 4424–4435.

Janke, C., and Montagnac, G. (2017). Causes and Consequences of Microtubule Acetylation. Curr. Biol. *27*, R1287–R1292.

Janssens, K., Goethals, S., Atkinson, D., Ermanoska, B., Fransen, E., Jordanova, A., Auer-Grumbach, M., Asselbergh, B., and Timmerman, V. (2014). Human Rab7 mutation mimics features of Charcot-Marie-Tooth neuropathy type 2B in Drosophila. Neurobiol. Dis. *65*, 211–219.

Jia, D., Zhang, J.-S., Li, F., Wang, J., Deng, Z., White, M.A., Osborne, D.G., Phillips-Krawczak, C., Gomez, T.S., Li, H., et al. (2016). Structural and mechanistic insights into regulation of the retromer coat by TBC1d5. Nat Commun *7*, 13305.

Jia, R., Guardia, C.M., Pu, J., Chen, Y., and Bonifacino, J.S. (2017). BORC coordinates encounter and fusion of lysosomes with autophagosomes. Autophagy *13*, 1648–1663.

Jimenez-Orgaz, A., Kvainickas, A., Nägele, H., Denner, J., Eimer, S., Dengjel, J., and Steinberg, F. (2018). Control of RAB7 activity and localization through the retromer-TBC1D5 complex enables RAB7-dependent mitophagy. EMBO J. *37*, 235–254.

Joensen, P. (2012). Incidence of amyotrophic lateral sclerosis in the Faroe Islands. Acta Neurol. Scand. *126*, 62–66.

Johansson, M., Rocha, N., Zwart, W., Jordens, I., Janssen, L., Kuijl, C., Olkkonen, V.M., and Neefjes, J. (2007). Activation of endosomal dynein motors by stepwise assembly of Rab7-RILP-p150Glued, ORP1L, and the receptor betalll spectrin. J. Cell Biol. *176*, 459–471.

Johnson, J.O., Mandrioli, J., Benatar, M., Abramzon, Y., Van Deerlin, V.M., Trojanowski, J.Q., Gibbs, J.R., Brunetti, M., Gronka, S., Wuu, J., et al. (2010). Exome sequencing reveals VCP mutations as a cause of familial ALS. Neuron *68*, 857–864.

Johnson, J.O., Pioro, E.P., Boehringer, A., Chia, R., Feit, H., Renton, A.E., Pliner, H.A., Abramzon, Y., Marangi, G., Winborn, B.J., et al. (2014). Mutations in the Matrin 3 gene cause familial amyotrophic lateral sclerosis. Nat. Neurosci. *17*, 664–666.

Jordens, I., Fernandez-Borja, M., Marsman, M., Dusseljee, S., Janssen, L., Calafat, J., Janssen, H., Wubbolts, R., and Neefjes, J. (2001). The Rab7 effector protein RILP controls lysosomal transport by inducing the recruitment of dynein-dynactin motors. Curr. Biol. *11*, 1680–1685.

Jovičić, A., Mertens, J., Boeynaems, S., Bogaert, E., Chai, N., Yamada, S.B., Paul, J.W., Sun, S., Herdy, J.R., Bieri, G., et al. (2015). Modifiers of C9orf72 dipeptide repeat toxicity connect nucleocytoplasmic transport defects to FTD/ALS. Nat. Neurosci. *18*, 1226–1229.

Ju, J.-S., Fuentealba, R.A., Miller, S.E., Jackson, E., Piwnica-Worms, D., Baloh, R.H., and Weihl, C.C. (2009). Valosin-containing protein (VCP) is required for autophagy and is disrupted in VCP disease. J. Cell Biol. *187*, 875–888.

Juneja, T., Pericak-Vance, M.A., Laing, N.G., Dave, S., and Siddique, T. (1997). Prognosis in familial amyotrophic lateral sclerosis: progression and survival in patients with glu100gly and ala4val mutations in Cu,Zn superoxide dismutase. Neurology *48*, 55–57.

Kabashi, E., Agar, J.N., Taylor, D.M., Minotti, S., and Durham, H.D. (2004). Focal dysfunction of the proteasome: a pathogenic factor in a mouse model of amyotrophic lateral sclerosis. J. Neurochem. *89*, 1325–1335.

Kabir, J., Lobo, M., and Zachary, I. (2002). Staurosporine induces endothelial cell apoptosis via focal adhesion kinase dephosphorylation and focal adhesion disassembly independent of focal adhesion kinase proteolysis. Biochem. J. *367*, 145–155.

Kalinski, A.L., Kar, A.N., Craver, J., Tosolini, A.P., Sleigh, J.N., Lee, S.J., Hawthorne, A., Brito-Vargas, P., Miller-Randolph, S., Passino, R., et al. (2019). Deacetylation of Miro1 by HDAC6 blocks mitochondrial transport and mediates axon growth inhibition. J. Cell Biol. *218*, 1871–1890.

Kanemitsu-Fujita, A., Morishita, S., Kjaer, S., Fukuda, M., Schiavo, G., and Nakamura, T. (2018). Comparable affinity of RabGDIα to GTP- and GDP-bound forms of Rab7 supports a four-state transition model for Rab7 subcellular localization. BioRxiv 287516.

Kang, J.-S., Tian, J.-H., Pan, P.-Y., Zald, P., Li, C., Deng, C., and Sheng, Z.-H. (2008). Docking of axonal mitochondria by syntaphilin controls their mobility and affects short-term facilitation. Cell *132*, 137–148.

Kang, S.H., Li, Y., Fukaya, M., Lorenzini, I., Cleveland, D.W., Ostrow, L.W., Rothstein, J.D., and Bergles, D.E. (2013). Degeneration and impaired regeneration of gray matter oligodendrocytes in amyotrophic lateral sclerosis. Nat. Neurosci. *16*, 571–579.

Kapeli, K., Pratt, G.A., Vu, A.Q., Hutt, K.R., Martinez, F.J., Sundararaman, B., Batra, R., Freese, P., Lambert, N.J., Huelga, S.C., et al. (2016). Distinct and shared functions of ALS-associated proteins TDP-43, FUS and TAF15 revealed by multisystem analyses. Nat Commun *7*, 12143.

Kato, H., Takeuchi, O., Sato, S., Yoneyama, M., Yamamoto, M., Matsui, K., Uematsu, S., Jung, A., Kawai, T., Ishii, K.J., et al. (2006). Differential roles of MDA5 and RIG-I helicases in the recognition of RNA viruses. Nature *441*, 101–105.

Kellogg, E.H., Hejab, N.M.A., Poepsel, S., Downing, K.H., DiMaio, F., and Nogales, E. (2018). Near-atomic model of microtubule-tau interactions. Science *360*, 1242–1246.

Kieran, D., Hafezparast, M., Bohnert, S., Dick, J.R.T., Martin, J., Schiavo, G., Fisher, E.M.C., and Greensmith, L. (2005). A mutation in dynein rescues axonal transport defects and extends the life span of ALS mice. J. Cell Biol. *169*, 561–567.

Kiernan, M.C., Vucic, S., Cheah, B.C., Turner, M.R., Eisen, A., Hardiman, O., Burrell, J.R., and Zoing, M.C. (2011). Amyotrophic lateral sclerosis. Lancet *377*, 942–955.

Kim, H.J., and Taylor, J.P. (2017). Lost in Transportation: Nucleocytoplasmic Transport Defects in ALS and Other Neurodegenerative Diseases. Neuron *96*, 285–297.

Kim, H.J., Kim, N.C., Wang, Y.-D., Scarborough, E.A., Moore, J., Diaz, Z., MacLea, K.S., Freibaum, B., Li, S., Molliex, A., et al. (2013). Mutations in prion-like domains in hnRNPA2B1 and hnRNPA1 cause multisystem proteinopathy and ALS. Nature *495*, 467–473.

Kino, Y., Washizu, C., Kurosawa, M., Yamada, M., Miyazaki, H., Akagi, T., Hashikawa, T., Doi, H., Takumi, T., Hicks, G.G., et al. (2015). FUS/TLS deficiency causes behavioral and pathological abnormalities distinct from amyotrophic lateral sclerosis. Acta Neuropathol Commun *3*, 24.

Klöpper, T.H., Kienle, N., Fasshauer, D., and Munro, S. (2012). Untangling the evolution of Rab G proteins: implications of a comprehensive genomic analysis. BMC Biol. *10*, 71.

Kocaturk, N.M., and Gozuacik, D. (2018). Crosstalk Between Mammalian Autophagy and the Ubiquitin-Proteasome System. Front Cell Dev Biol *6*, 128.

Kondo, T., Funayama, M., Tsukita, K., Hotta, A., Yasuda, A., Nori, S., Kaneko, S., Nakamura, M., Takahashi, R., Okano, H., et al. (2014). Focal transplantation of human iPSC-derived glial-rich neural progenitors improves lifespan of ALS mice. Stem Cell Reports *3*, 242–249.

Kononenko, N.L., Claßen, G.A., Kuijpers, M., Puchkov, D., Maritzen, T., Tempes, A., Malik, A.R., Skalecka, A., Bera, S., Jaworski, J., et al. (2017). Retrograde transport of TrkB-containing autophagosomes via the adaptor AP-2 mediates neuronal complexity and prevents neurodegeneration. Nat Commun *8*, 14819.

Koppers, M., Blokhuis, A.M., Westeneng, H.-J., Terpstra, M.L., Zundel, C.A.C., Vieira de Sá, R., Schellevis, R.D., Waite, A.J., Blake, D.J., Veldink, J.H., et al. (2015). C9orf72 ablation in mice does not cause motor neuron degeneration or motor deficits. Ann. Neurol. *78*, 426–438.

Kraemer, B.C., Schuck, T., Wheeler, J.M., Robinson, L.C., Trojanowski, J.Q., Lee, V.M.Y., and Schellenberg, G.D. (2010). Loss of murine TDP-43 disrupts motor function and plays an essential role in embryogenesis. Acta Neuropathol. *119*, 409–419.

Krasniak, C.S., and Ahmad, S.T. (2016). The role of CHMP2BIntron5 in autophagy and frontotemporal dementia. Brain Res. *1649*, 151–157.

Kulkarni, A., Dong, A., Kulkarni, V.V., Chen, J., Laxton, O., Anand, A., and Maday, S. (2019). Differential regulation of autophagy during metabolic stress in astrocytes and neurons. Autophagy 1–17.

Kumar, S., Gu, Y., Abudu, Y.P., Bruun, J.-A., Jain, A., Farzam, F., Mudd, M., Anonsen, J.H., Rusten, T.E., Kasof, G., et al. (2019). Phosphorylation of Syntaxin 17 by TBK1 Controls Autophagy Initiation. Dev. Cell *49*, 130-144.e6.

Kwiatkowski, T.J., Bosco, D.A., Leclerc, A.L., Tamrazian, E., Vanderburg, C.R., Russ, C., Davis, A., Gilchrist, J., Kasarskis, E.J., Munsat, T., et al. (2009). Mutations in the FUS/TLS gene on chromosome 16 cause familial amyotrophic lateral sclerosis. Science *323*, 1205–1208.

Lai, C., Xie, C., McCormack, S.G., Chiang, H.-C., Michalak, M.K., Lin, X., Chandran, J., Shim, H., Shimoji, M., Cookson, M.R., et al. (2006). Amyotrophic lateral sclerosis 2-deficiency leads to neuronal degeneration in amyotrophic lateral sclerosis through altered AMPA receptor trafficking. J. Neurosci. *26*, 11798–11806.

Lai, C., Xie, C., Shim, H., Chandran, J., Howell, B.W., and Cai, H. (2009). Regulation of endosomal motility and degradation by amyotrophic lateral sclerosis 2/alsin. Mol Brain *2*, 23.

Laird, F.M., Farah, M.H., Ackerley, S., Hoke, A., Maragakis, N., Rothstein, J.D., Griffin, J., Price, D.L., Martin, L.J., and Wong, P.C. (2008). Motor neuron disease occurring in a mutant dynactin mouse model is characterized by defects in vesicular trafficking. J. Neurosci. *28*, 1997–2005.

Lalli, G., and Schiavo, G. (2002). Analysis of retrograde transport in motor neurons reveals common endocytic carriers for tetanus toxin and neurotrophin receptor p75NTR. J. Cell Biol. *156*, 233–239.

Lamb, C.A., Yoshimori, T., and Tooze, S.A. (2013). The autophagosome: origins unknown, biogenesis complex. Nat. Rev. Mol. Cell Biol. *14*, 759–774.

Larabi, A., Devos, J.M., Ng, S.-L., Nanao, M.H., Round, A., Maniatis, T., and Panne, D. (2013). Crystal structure and mechanism of activation of TANK-binding kinase 1. Cell Rep *3*, 734–746.

Lazarou, M., Sliter, D.A., Kane, L.A., Sarraf, S.A., Wang, C., Burman, J.L., Sideris, D.P., Fogel, A.I., and Youle, R.J. (2015). The ubiquitin kinase PINK1 recruits autophagy receptors to induce mitophagy. Nature *524*, 309–314.

Lee, I.-G., Olenick, M.A., Boczkowska, M., Franzini-Armstrong, C., Holzbaur, E.L.F., and Dominguez, R. (2018). A conserved interaction of the dynein light intermediate chain with dynein-dynactin effectors necessary for processivity. Nat Commun *9*, 986.

Lee, J.Y., Lee, J.D., Phipps, S., Noakes, P.G., and Woodruff, T.M. (2015). Absence of toll-like receptor 4 (TLR4) extends survival in the hSOD1 G93A mouse model of amyotrophic lateral sclerosis. J Neuroinflammation *12*, 90.

Lee, Y., Morrison, B.M., Li, Y., Lengacher, S., Farah, M.H., Hoffman, P.N., Liu, Y., Tsingalia, A., Jin, L., Zhang, P.-W., et al. (2012). Oligodendroglia metabolically support axons and contribute to neurodegeneration. Nature *487*, 443–448.

Li, S., Wang, L., Berman, M., Kong, Y.-Y., and Dorf, M.E. (2011). Mapping a dynamic innate immunity protein interaction network regulating type I interferon production. Immunity *35*, 426–440.

Li, X., Rydzewski, N., Hider, A., Zhang, X., Yang, J., Wang, W., Gao, Q., Cheng, X., and Xu, H. (2016). A molecular mechanism to regulate lysosome motility for lysosome positioning and tubulation. Nat. Cell Biol. *18*, 404–417.

Li, Y.R., King, O.D., Shorter, J., and Gitler, A.D. (2013). Stress granules as crucibles of ALS pathogenesis. J. Cell Biol. *201*, 361–372.

Liao, B., Zhao, W., Beers, D.R., Henkel, J.S., and Appel, S.H. (2012). Transformation from a neuroprotective to a neurotoxic microglial phenotype in a mouse model of ALS. Exp. Neurol. *237*, 147–152.

Liao, Y.-C., Fernandopulle, M.S., Wang, G., Choi, H., Hao, L., Drerup, C.M., Patel, R., Qamar, S., Nixon-Abell, J., Shen, Y., et al. (2019). RNA Granules Hitchhike on Lysosomes for Long-Distance Transport, Using Annexin A11 as a Molecular Tether. Cell *179*, 147-164.e20.

Liewluck, T., and Saperstein, D.S. (2015). Progressive Muscular Atrophy. Neurol Clin *33*, 761–773.

Ligon, L.A., LaMonte, B.H., Wallace, K.E., Weber, N., Kalb, R.G., and Holzbaur, E.L.F. (2005). Mutant superoxide dismutase disrupts cytoplasmic dynein in motor neurons. Neuroreport *16*, 533–536.

Lillo, P., and Hodges, J.R. (2009). Frontotemporal dementia and motor neurone disease: overlapping clinic-pathological disorders. J Clin Neurosci *16*, 1131–1135.

Lin, X., Zhang, J., Chen, L., Chen, Y., Xu, X., Hong, W., and Wang, T. (2017). Tyrosine phosphorylation of Rab7 by Src kinase. Cell. Signal. *35*, 84–94.

Lipka, J., Kapitein, L.C., Jaworski, J., and Hoogenraad, C.C. (2016). Microtubule-binding protein doublecortin-like kinase 1 (DCLK1) guides kinesin-3-mediated cargo transport to dendrites. EMBO J. *35*, 302–318.

Lippé, R., Miaczynska, M., Rybin, V., Runge, A., and Zerial, M. (2001). Functional synergy between Rab5 effector Rabaptin-5 and exchange factor Rabex-5 when physically associated in a complex. Mol. Biol. Cell *12*, 2219–2228.

Liu-Yesucevitz, L., Bilgutay, A., Zhang, Y.-J., Vanderweyde, T., Vanderwyde, T., Citro, A., Mehta, T., Zaarur, N., McKee, A., Bowser, R., et al. (2010). Tar DNA binding protein-43 (TDP-43) associates with stress granules: analysis of cultured cells and pathological brain tissue. PLoS ONE *5*, e13250.

Logroscino, G., Traynor, B.J., Hardiman, O., Chiò, A., Mitchell, D., Swingler, R.J., Millul, A., Benn, E., Beghi, E., and EURALS (2010). Incidence of amyotrophic lateral sclerosis in Europe. J. Neurol. Neurosurg. Psychiatry *81*, 385–390.

Lomen-Hoerth, C., Anderson, T., and Miller, B. (2002). The overlap of amyotrophic lateral sclerosis and frontotemporal dementia. Neurology *59*, 1077–1079.

López-Doménech, G., Covill-Cooke, C., Ivankovic, D., Halff, E.F., Sheehan, D.F., Norkett, R., Birsa, N., and Kittler, J.T. (2018). Miro proteins coordinate microtubule- and actin-dependent mitochondrial transport and distribution. EMBO J. *37*, 321–336.

Lork, M., Kreike, M., Staal, J., and Beyaert, R. (2018). Importance of Validating Antibodies and Small Compound Inhibitors Using Genetic Knockout Studies-T Cell Receptor-Induced CYLD Phosphorylation by IKKε/TBK1 as a Case Study. Front Cell Dev Biol *6*, 40.

Lu, Y.-C., Yeh, W.-C., and Ohashi, P.S. (2008). LPS/TLR4 signal transduction pathway. Cytokine *42*, 145–151.

Ma, X., Helgason, E., Phung, Q.T., Quan, C.L., Iyer, R.S., Lee, M.W., Bowman, K.K., Starovasnik, M.A., and Dueber, E.C. (2012). Molecular basis of Tank-binding kinase 1 activation by transautophosphorylation. Proc. Natl. Acad. Sci. U.S.A. *109*, 9378–9383.

Ma, X., Liu, K., Li, J., Li, H., Li, J., Liu, Y., Yang, C., and Liang, H. (2018). A non-canonical GTPase interaction enables ORP1L-Rab7-RILP complex formation and late endosome positioning. J. Biol. Chem. *293*, 14155–14164.

Macaskill, A.F., Rinholm, J.E., Twelvetrees, A.E., Arancibia-Carcamo, I.L., Muir, J., Fransson, A., Aspenstrom, P., Attwell, D., and Kittler, J.T. (2009). Miro1 is a calcium sensor for glutamate receptor-dependent localization of mitochondria at synapses. Neuron *61*, 541–555.

Mackenzie, I.R.A., Bigio, E.H., Ince, P.G., Geser, F., Neumann, M., Cairns, N.J., Kwong, L.K., Forman, M.S., Ravits, J., Stewart, H., et al. (2007). Pathological TDP-43 distinguishes sporadic amyotrophic lateral sclerosis from amyotrophic lateral sclerosis with SOD1 mutations. Ann. Neurol. *61*, 427–434.

Maday, S., and Holzbaur, E.L.F. (2014). Autophagosome biogenesis in primary neurons follows an ordered and spatially regulated pathway. Dev. Cell *30*, 71–85.

Maday, S., and Holzbaur, E.L.F. (2016). Compartment-Specific Regulation of Autophagy in Primary Neurons. J. Neurosci. *36*, 5933–5945.

Maday, S., Wallace, K.E., and Holzbaur, E.L.F. (2012). Autophagosomes initiate distally and mature during transport toward the cell soma in primary neurons. J. Cell Biol. *196*, 407–417.

Maday, S., Twelvetrees, A.E., Moughamian, A.J., and Holzbaur, E.L.F. (2014). Axonal transport: cargo-specific mechanisms of motility and regulation. Neuron *84*, 292–309.

Magiera, M.M., Singh, P., and Janke, C. (2018a). SnapShot: Functions of Tubulin Posttranslational Modifications. Cell *173*, 1552-1552.e1.

Magiera, M.M., Bodakuntla, S., Žiak, J., Lacomme, S., Marques Sousa, P., Leboucher, S., Hausrat, T.J., Bosc, C., Andrieux, A., Kneussel, M., et al. (2018b). Excessive tubulin polyglutamylation causes neurodegeneration and perturbs neuronal transport. EMBO J. *37*.

Magrané, J., Sahawneh, M.A., Przedborski, S., Estévez, Á.G., and Manfredi, G. (2012). Mitochondrial dynamics and bioenergetic dysfunction is associated with synaptic alterations in mutant SOD1 motor neurons. J. Neurosci. *32*, 229–242.

Magrané, J., Cortez, C., Gan, W.-B., and Manfredi, G. (2014). Abnormal mitochondrial transport and morphology are common pathological denominators in SOD1 and TDP43 ALS mouse models. Hum. Mol. Genet. *23*, 1413–1424.

de Majo, M., Topp, S.D., Smith, B.N., Nishimura, A.L., Chen, H.-J., Gkazi, A.S., Miller, J., Wong, C.H., Vance, C., Baas, F., et al. (2018). ALS-associated missense and nonsense TBK1 mutations can both cause loss of kinase function. Neurobiol. Aging *71*, 266.e1-266.e10.

Majounie, E., Renton, A.E., Mok, K., Dopper, E.G.P., Waite, A., Rollinson, S., Chiò, A., Restagno, G., Nicolaou, N., Simon-Sanchez, J., et al. (2012). Frequency of the C9orf72 hexanucleotide repeat expansion in patients with amyotrophic lateral sclerosis and frontotemporal dementia: a cross-sectional study. Lancet Neurol *11*, 323–330.

Mandal, A., and Drerup, C.M. (2019). Axonal Transport and Mitochondrial Function in Neurons. Front Cell Neurosci *13*, 373.

Marat, A.L., Dokainish, H., and McPherson, P.S. (2011). DENN domain proteins: regulators of Rab GTPases. J. Biol. Chem. *286*, 13791–13800.

Marchetto, M.C.N., Muotri, A.R., Mu, Y., Smith, A.M., Cezar, G.G., and Gage, F.H. (2008). Non-cell-autonomous effect of human SOD1 G37R astrocytes on motor neurons derived from human embryonic stem cells. Cell Stem Cell *3*, 649–657.

Markovinovic, A., Cimbro, R., Ljutic, T., Kriz, J., Rogelj, B., and Munitic, I. (2017). Optineurin in amyotrophic lateral sclerosis: Multifunctional adaptor protein at the crossroads of different neuroprotective mechanisms. Prog. Neurobiol. *154*, 1–20.

Maruyama, H., Morino, H., Ito, H., Izumi, Y., Kato, H., Watanabe, Y., Kinoshita, Y., Kamada, M., Nodera, H., Suzuki, H., et al. (2010). Mutations of optineurin in amyotrophic lateral sclerosis. Nature *465*, 223–226.

Matanis, T., Akhmanova, A., Wulf, P., Del Nery, E., Weide, T., Stepanova, T., Galjart, N., Grosveld, F., Goud, B., De Zeeuw, C.I., et al. (2002). Bicaudal-D regulates COPI-independent Golgi-ER transport by recruiting the dynein-dynactin motor complex. Nat. Cell Biol. *4*, 986–992.

Matsumoto, G., Shimogori, T., Hattori, N., and Nukina, N. (2015). TBK1 controls autophagosomal engulfment of polyubiquitinated mitochondria through p62/SQSTM1 phosphorylation. Hum. Mol. Genet. *24*, 4429–4442.

McCord, J.M., and Fridovich, I. (1969). Superoxide dismutase. An enzymic function for erythrocuprein (hemocuprein). J. Biol. Chem. *244*, 6049–6055.

McCray, B.A., Skordalakes, E., and Taylor, J.P. (2010). Disease mutations in Rab7 result in unregulated nucleotide exchange and inappropriate activation. Hum. Mol. Genet. *19*, 1033–1047.

McKenney, R.J., Huynh, W., Vale, R.D., and Sirajuddin, M. (2016). Tyrosination of α-tubulin controls the initiation of processive dynein-dynactin motility. EMBO J. *35*, 1175–1185.

McLaughlin, R.L., Phukan, J., McCormack, W., Lynch, D.S., Greenway, M., Cronin, S., Saunders, J., Slowik, A., Tomik, B., Andersen, P.M., et al. (2010). Angiogenin levels and ANG genotypes: dysregulation in amyotrophic lateral sclerosis. PLoS ONE *5*, e15402.

Mejzini, R., Flynn, L.L., Pitout, I.L., Fletcher, S., Wilton, S.D., and Akkari, P.A. (2019). ALS Genetics, Mechanisms, and Therapeutics: Where Are We Now? Front Neurosci *13*, 1310.

Melamed, Z., López-Erauskin, J., Baughn, M.W., Zhang, O., Drenner, K., Sun, Y., Freyermuth, F., McMahon, M.A., Beccari, M.S., Artates, J.W., et al. (2019). Premature polyadenylation-mediated loss of stathmin-2 is a hallmark of TDP-43-dependent neurodegeneration. Nat. Neurosci. *22*, 180–190.

Mimori-Kiyosue, Y., Shiina, N., and Tsukita, S. (2000). The dynamic behavior of the APC-binding protein EB1 on the distal ends of microtubules. Curr. Biol. *10*, 865–868.

Minowa-Nozawa, A., Nozawa, T., Okamoto-Furuta, K., Kohda, H., and Nakagawa, I. (2017). Rab35 GTPase recruits NDP52 to autophagy targets. EMBO J. *36*, 2790–2807.

Misgeld, T., Kerschensteiner, M., Bareyre, F.M., Burgess, R.W., and Lichtman, J.W. (2007). Imaging axonal transport of mitochondria in vivo. Nat. Methods *4*, 559–561.

Mitchell, J.C., McGoldrick, P., Vance, C., Hortobagyi, T., Sreedharan, J., Rogelj, B., Tudor, E.L., Smith, B.N., Klasen, C., Miller, C.C.J., et al. (2013). Overexpression of human wild-type FUS causes progressive motor neuron degeneration in an age- and dose-dependent fashion. Acta Neuropathol. *125*, 273–288.

Mitchell, J.C., Constable, R., So, E., Vance, C., Scotter, E., Glover, L., Hortobagyi, T., Arnold, E.S., Ling, S.-C., McAlonis, M., et al. (2015). Wild type human TDP-43 potentiates ALS-linked mutant TDP-43 driven progressive motor and cortical neuron degeneration with pathological features of ALS. Acta Neuropathol Commun *3*, 36.

Mitchison, T., and Kirschner, M. (1984). Dynamic instability of microtubule growth. Nature *312*, 237–242.

Mizielinska, S., Grönke, S., Niccoli, T., Ridler, C.E., Clayton, E.L., Devoy, A., Moens, T., Norona, F.E., Woollacott, I.O.C., Pietrzyk, J., et al. (2014). C9orf72 repeat expansions cause neurodegeneration in Drosophila through arginine-rich proteins. Science *345*, 1192–1194.

Mizuno-Yamasaki, E., Rivera-Molina, F., and Novick, P. (2012). GTPase networks in membrane traffic. Annu. Rev. Biochem. *81*, 637–659.

Mizushima, N., and Komatsu, M. (2011). Autophagy: renovation of cells and tissues. Cell *147*, 728–741.

Mizushima, N., Yamamoto, A., Matsui, M., Yoshimori, T., and Ohsumi, Y. (2004). In vivo analysis of autophagy in response to nutrient starvation using transgenic mice expressing a fluorescent autophagosome marker. Mol. Biol. Cell *15*, 1101–1111.

Mizushima, N., Yoshimori, T., and Ohsumi, Y. (2011). The role of Atg proteins in autophagosome formation. Annu. Rev. Cell Dev. Biol. *27*, 107–132.

Modica, G., and Lefrancois, S. (2017). Post-translational modifications: How to modulate Rab7 functions. Small GTPases 1–7.

Modica, G., Skorobogata, O., Sauvageau, E., Vissa, A., Yip, C.M., Kim, P.K., Wurtele, H., and Lefrancois, S. (2017). Rab7 palmitoylation is required for efficient endosome-to-TGN trafficking. J. Cell. Sci. *130*, 2579–2590.

Mohler, J., and Wieschaus, E.F. (1986). Dominant maternal-effect mutations of Drosophila melanogaster causing the production of double-abdomen embryos. Genetics *112*, 803–822.

Molliex, A., Temirov, J., Lee, J., Coughlin, M., Kanagaraj, A.P., Kim, H.J., Mittag, T., and Taylor, J.P. (2015). Phase separation by low complexity domains promotes stress granule assembly and drives pathological fibrillization. Cell *163*, 123–133.

Monroy, B.Y., Sawyer, D.L., Ackermann, B.E., Borden, M.M., Tan, T.C., and Ori-McKenney, K.M. (2018). Competition between microtubule-associated proteins directs motor transport. Nat Commun *9*, 1487.

Monroy, B.Y., Tan, T.C., Oclaman, J.M., Han, J.S., Simó, S., Niwa, S., Nowakowski, D.W., McKenney, R.J., and Ori-McKenney, K.M. (2020). A Combinatorial MAP Code Dictates Polarized Microtubule Transport. Dev. Cell.

Montagnac, G., Sibarita, J.-B., Loubéry, S., Daviet, L., Romao, M., Raposo, G., and Chavrier, P. (2009). ARF6 Interacts with JIP4 to control a motor switch mechanism regulating endosome traffic in cytokinesis. Curr. Biol. *19*, 184–195.

Montecchiani, C., Pedace, L., Lo Giudice, T., Casella, A., Mearini, M., Gaudiello, F., Pedroso, J.L., Terracciano, C., Caltagirone, C., Massa, R., et al. (2016). ALS5/SPG11/KIAA1840 mutations cause autosomal recessive axonal Charcot-Marie-Tooth disease. Brain *139*, 73–85.

Moore, A.S., and Holzbaur, E.L.F. (2016). Dynamic recruitment and activation of ALS-associated TBK1 with its target optineurin are required for efficient mitophagy. Proc. Natl. Acad. Sci. U.S.A. *113*, E3349-3358.

Morfini, G.A., Bosco, D.A., Brown, H., Gatto, R., Kaminska, A., Song, Y., Molla, L., Baker, L., Marangoni, M.N., Berth, S., et al. (2013). Inhibition of fast axonal transport by pathogenic SOD1 involves activation of p38 MAP kinase. PLoS ONE *8*, e65235.

Morgan, S., Shatunov, A., Sproviero, W., Jones, A.R., Shoai, M., Hughes, D., Al Khleifat, A., Malaspina, A., Morrison, K.E., Shaw, P.J., et al. (2017). A comprehensive analysis of rare genetic variation in amyotrophic lateral sclerosis in the UK. Brain *140*, 1611–1618.

Mori, K., Arzberger, T., Grässer, F.A., Gijselinck, I., May, S., Rentzsch, K., Weng, S.-M., Schludi, M.H., van der Zee, J., Cruts, M., et al. (2013). Bidirectional transcripts of the expanded C9orf72 hexanucleotide repeat are translated into aggregating dipeptide repeat proteins. Acta Neuropathol. *126*, 881–893.

Moughamian, A.J., and Holzbaur, E.L.F. (2012). Dynactin is required for transport initiation from the distal axon. Neuron *74*, 331–343.

Mukherjee, S., Liu, X., Arasaki, K., McDonough, J., Galán, J.E., and Roy, C.R. (2011). Modulation of Rab GTPase function by a protein phosphocholine transferase. Nature *477*, 103–106.

Müller, M.P., and Goody, R.S. (2018). Molecular control of Rab activity by GEFs, GAPs and GDI. Small GTPases *9*, 5–21.

Müller, M.P., Peters, H., Blümer, J., Blankenfeldt, W., Goody, R.S., and Itzen, A. (2010). The Legionella effector protein DrrA AMPylates the membrane traffic regulator Rab1b. Science *329*, 946–949.

Münch, C., Rosenbohm, A., Sperfeld, A.-D., Uttner, I., Reske, S., Krause, B.J., Sedlmeier, R., Meyer, T., Hanemann, C.O., Stumm, G., et al. (2005). Heterozygous R1101K mutation of the DCTN1 gene in a family with ALS and FTD. Ann. Neurol. *58*, 777–780.

Muresan, V., and Ladescu Muresan, Z. (2016). Shared Molecular Mechanisms in Alzheimer's Disease and Amyotrophic Lateral Sclerosis: Neurofilament-Dependent Transport of sAPP, FUS, TDP-43 and SOD1, with Endoplasmic Reticulum-Like Tubules. Neurodegener Dis *16*, 55–61.

Murphy, N.A., Arthur, K.C., Tienari, P.J., Houlden, H., Chiò, A., and Traynor, B.J. (2017). Age-related penetrance of the C9orf72 repeat expansion. Sci Rep *7*, 2116.

Nagai, M., Re, D.B., Nagata, T., Chalazonitis, A., Jessell, T.M., Wichterle, H., and Przedborski, S. (2007). Astrocytes expressing ALS-linked mutated SOD1 release factors selectively toxic to motor neurons. Nat. Neurosci. *10*, 615–622.

Nehlig, A., Molina, A., Rodrigues-Ferreira, S., Honoré, S., and Nahmias, C. (2017). Regulation of end-binding protein EB1 in the control of microtubule dynamics. Cell. Mol. Life Sci. *74*, 2381–2393.

Neumann, M., Sampathu, D.M., Kwong, L.K., Truax, A.C., Micsenyi, M.C., Chou, T.T., Bruce, J., Schuck, T., Grossman, M., Clark, C.M., et al. (2006). Ubiquitinated TDP-43 in frontotemporal lobar degeneration and amyotrophic lateral sclerosis. Science *314*, 130–133.

Neumann, S., Chassefeyre, R., Campbell, G.E., and Encalada, S.E. (2017). KymoAnalyzer: a software tool for the quantitative analysis of intracellular transport in neurons. Traffic *18*, 71–88.

Nguyen, D.K.H., Thombre, R., and Wang, J. (2019). Autophagy as a common pathway in amyotrophic lateral sclerosis. Neurosci. Lett. *697*, 34–48.

Nicolas, A., Kenna, K.P., Renton, A.E., Ticozzi, N., Faghri, F., Chia, R., Dominov, J.A., Kenna, B.J., Nalls, M.A., Keagle, P., et al. (2018). Genome-wide Analyses Identify KIF5A as a Novel ALS Gene. Neuron *97*, 1268-1283.e6.

Nie, L., Cai, S.-Y., Shao, J.-Z., and Chen, J. (2018). Toll-Like Receptors, Associated Biological Roles, and Signaling Networks in Non-Mammals. Front Immunol *9*, 1523.

Nishitoh, H., Kadowaki, H., Nagai, A., Maruyama, T., Yokota, T., Fukutomi, H., Noguchi, T., Matsuzawa, A., Takeda, K., and Ichijo, H. (2008). ALS-linked mutant SOD1 induces ER stress- and ASK1-dependent motor neuron death by targeting Derlin-1. Genes Dev. *22*, 1451–1464.

Niwa, S., Tao, L., Lu, S.Y., Liew, G.M., Feng, W., Nachury, M.V., and Shen, K. (2017). BORC Regulates the Axonal Transport of Synaptic Vesicle Precursors by Activating ARL-8. Curr. Biol. *27*, 2569-2578.e4.

Nordmann, M., Cabrera, M., Perz, A., Bröcker, C., Ostrowicz, C., Engelbrecht-Vandré, S., and Ungermann, C. (2010). The Mon1-Ccz1 complex is the GEF of the late endosomal Rab7 homolog Ypt7. Curr. Biol. *20*, 1654–1659.

Oakes, J.A., Davies, M.C., and Collins, M.O. (2017). TBK1: a new player in ALS linking autophagy and neuroinflammation. Mol Brain *10*, 5.

Odorizzi, G. (2015). Membrane manipulations by the ESCRT machinery. F1000Res *4*, 516.

Oesterlin, L.K., Goody, R.S., and Itzen, A. (2012). Posttranslational modifications of Rab proteins cause effective displacement of GDP dissociation inhibitor. Proc. Natl. Acad. Sci. U.S.A. *109*, 5621–5626.

Olenick, M.A., and Holzbaur, E.L.F. (2019). Dynein activators and adaptors at a glance. J. Cell. Sci. *132*.

Olenick, M.A., Tokito, M., Boczkowska, M., Dominguez, R., and Holzbaur, E.L.F. (2016). Hook Adaptors Induce Unidirectional Processive Motility by Enhancing the Dynein-Dynactin Interaction. J. Biol. Chem. *291*, 18239–18251.

Olenick, M.A., Dominguez, R., and Holzbaur, E.L.F. (2019). Dynein activator Hook1 is required for trafficking of BDNF-signaling endosomes in neurons. J. Cell Biol. *218*, 220–233.

Onoue, K., Jofuku, A., Ban-Ishihara, R., Ishihara, T., Maeda, M., Koshiba, T., Itoh, T., Fukuda, M., Otera, H., Oka, T., et al. (2013). Fis1 acts as a mitochondrial recruitment factor for TBC1D15 that is involved in regulation of mitochondrial morphology. J. Cell. Sci. *126*, 176–185.

Orlacchio, A., Babalini, C., Borreca, A., Patrono, C., Massa, R., Basaran, S., Munhoz, R.P., Rogaeva, E.A., St George-Hyslop, P.H., Bernardi, G., et al. (2010). SPATACSIN mutations cause autosomal recessive juvenile amyotrophic lateral sclerosis. Brain *133*, 591–598.

O'Rourke, J.G., Bogdanik, L., Yáñez, A., Lall, D., Wolf, A.J., Muhammad, A.K.M.G., Ho, R., Carmona, S., Vit, J.P., Zarrow, J., et al. (2016). C9orf72 is required for proper macrophage and microglial function in mice. Science *351*, 1324–1329.

Pankiv, S., Alemu, E.A., Brech, A., Bruun, J.-A., Lamark, T., Overvatn, A., Bjørkøy, G., and Johansen, T. (2010). FYCO1 is a Rab7 effector that binds to LC3 and PI3P to mediate microtubule plus end-directed vesicle transport. J. Cell Biol. *188*, 253–269.

Pansarasa, O., Bordoni, M., Diamanti, L., Sproviero, D., Gagliardi, S., and Cereda, C. (2018). SOD1 in Amyotrophic Lateral Sclerosis: "Ambivalent" Behavior Connected to the Disease. Int J Mol Sci *19*.

Pantelidou, M., Zographos, S.E., Lederer, C.W., Kyriakides, T., Pfaffl, M.W., and Santama, N. (2007). Differential expression of molecular motors in the motor cortex of sporadic ALS. Neurobiol. Dis. *26*, 577–589.

Papadeas, S.T., Kraig, S.E., O'Banion, C., Lepore, A.C., and Maragakis, N.J. (2011). Astrocytes carrying the superoxide dismutase 1 (SOD1G93A) mutation induce wild-type motor neuron degeneration in vivo. Proc. Natl. Acad. Sci. U.S.A. *108*, 17803–17808.

Park, J.H., and Roll-Mecak, A. (2018). The tubulin code in neuronal polarity. Curr. Opin. Neurobiol. *51*, 95–102.

Parkinson, N., Ince, P.G., Smith, M.O., Highley, R., Skibinski, G., Andersen, P.M., Morrison, K.E., Pall, H.S., Hardiman, O., Collinge, J., et al. (2006). ALS phenotypes with mutations in CHMP2B (charged multivesicular body protein 2B). Neurology *67*, 1074–1077.

Patil, H., Cho, K., Lee, J., Yang, Y., Orry, A., and Ferreira, P.A. (2013). Kinesin-1 and mitochondrial motility control by discrimination of structurally equivalent but distinct subdomains in Ran-GTP-binding domains of Ran-binding protein 2. Open Biol *3*, 120183.

Pereira-Leal, J.B., and Seabra, M.C. (2000). The mammalian Rab family of small GTPases: definition of family and subfamily sequence motifs suggests a mechanism for functional specificity in the Ras superfamily. J. Mol. Biol. *301*, 1077–1087.

Pérez-Brangulí, F., Mishra, H.K., Prots, I., Havlicek, S., Kohl, Z., Saul, D., Rummel, C., Dorca-Arevalo, J., Regensburger, M., Graef, D., et al. (2014). Dysfunction of spatacsin leads to axonal pathology in SPG11-linked hereditary spastic paraplegia. Hum. Mol. Genet. *23*, 4859–4874.

Peris, L., Thery, M., Fauré, J., Saoudi, Y., Lafanechère, L., Chilton, J.K., Gordon-Weeks, P., Galjart, N., Bornens, M., Wordeman, L., et al. (2006). Tubulin tyrosination is a major factor affecting the recruitment of CAP-Gly proteins at microtubule plus ends. J. Cell Biol. *174*, 839–849.

Peris, L., Wagenbach, M., Lafanechère, L., Brocard, J., Moore, A.T., Kozielski, F., Job, D., Wordeman, L., and Andrieux, A. (2009). Motor-dependent microtubule disassembly driven by tubulin tyrosination. J. Cell Biol. *185*, 1159–1166.

Pfeffer, S.R. (2005). Structural clues to Rab GTPase functional diversity. J. Biol. Chem. *280*, 15485–15488.

Pfeffer, S.R. (2017). Rab GTPases: master regulators that establish the secretory and endocytic pathways. Mol. Biol. Cell *28*, 712–715.

Phukan, J., Elamin, M., Bede, P., Jordan, N., Gallagher, L., Byrne, S., Lynch, C., Pender, N., and Hardiman, O. (2012). The syndrome of cognitive impairment in amyotrophic lateral sclerosis: a population-based study. J. Neurol. Neurosurg. Psychiatry *83*, 102–108.

Pilli, M., Arko-Mensah, J., Ponpuak, M., Roberts, E., Master, S., Mandell, M.A., Dupont, N., Ornatowski, W., Jiang, S., Bradfute, S.B., et al. (2012). TBK-1 promotes autophagy-mediated antimicrobial defense by controlling autophagosome maturation. Immunity *37*, 223–234.

Pilling, A.D., Horiuchi, D., Lively, C.M., and Saxton, W.M. (2006). Kinesin-1 and Dynein are the primary motors for fast transport of mitochondria in Drosophila motor axons. Mol. Biol. Cell *17*, 2057–2068.

Plank, C., Zelphati, O., and Mykhaylyk, O. (2011). Magnetically enhanced nucleic acid delivery. Ten years of magnetofection-progress and prospects. Adv. Drug Deliv. Rev. *63*, 1300–1331.

Pomerantz, J.L., and Baltimore, D. (1999). NF-kappaB activation by a signaling complex containing TRAF2, TANK and TBK1, a novel IKK-related kinase. EMBO J. *18*, 6694–6704.

Ponomareva, O.Y., Eliceiri, K.W., and Halloran, M.C. (2016). Charcot-Marie-Tooth 2b associated Rab7 mutations cause axon growth and guidance defects during vertebrate sensory neuron development. Neural Dev *11*, 2.

Popovic, D., Akutsu, M., Novak, I., Harper, J.W., Behrends, C., and Dikic, I. (2012). Rab GTPase-activating proteins in autophagy: regulation of endocytic and autophagy pathways by direct binding to human ATG8 modifiers. Mol. Cell. Biol. *32*, 1733–1744.

Poteryaev, D., Datta, S., Ackema, K., Zerial, M., and Spang, A. (2010). Identification of the switch in early-to-late endosome transition. Cell *141*, 497–508.

Pottier, C., Bieniek, K.F., Finch, N., van de Vorst, M., Baker, M., Perkersen, R., Brown, P., Ravenscroft, T., van Blitterswijk, M., Nicholson, A.M., et al. (2015). Whole-genome sequencing reveals important role for TBK1 and OPTN mutations in frontotemporal lobar degeneration without motor neuron disease. Acta Neuropathol. *130*, 77–92.

Pourcelot, M., Zemirli, N., Silva Da Costa, L., Loyant, R., Garcin, D., Vitour, D., Munitic, I., Vazquez, A., and Arnoult, D. (2016). The Golgi apparatus acts as a platform for TBK1 activation after viral RNA sensing. BMC Biol. *14*, 69.

Progida, C., Nielsen, M.S., Koster, G., Bucci, C., and Bakke, O. (2012). Dynamics of Rab7b-dependent transport of sorting receptors. Traffic *13*, 1273–1285.

Protter, D.S.W., and Parker, R. (2016). Principles and Properties of Stress Granules. Trends Cell Biol. *26*, 668–679.

Pu, J., Schindler, C., Jia, R., Jarnik, M., Backlund, P., and Bonifacino, J.S. (2015). BORC, a multisubunit complex that regulates lysosome positioning. Dev. Cell *33*, 176–188.

Puls, I., Jonnakuty, C., LaMonte, B.H., Holzbaur, E.L.F., Tokito, M., Mann, E., Floeter, M.K., Bidus, K., Drayna, D., Oh, S.J., et al. (2003). Mutant dynactin in motor neuron disease. Nat. Genet. *33*, 455–456.

Qi, D., Hu, L., Jiao, T., Zhang, T., Tong, X., and Ye, X. (2018). Phosphatase Cdc25A Negatively Regulates the Antiviral Immune Response by Inhibiting TBK1 Activity. J. Virol. *92*.

Qian, K., Huang, H., Peterson, A., Hu, B., Maragakis, N.J., Ming, G.-L., Chen, H., and Zhang, S.-C. (2017). Sporadic ALS Astrocytes Induce Neuronal Degeneration In Vivo. Stem Cell Reports *8*, 843–855.

Rabinovici, G.D., and Miller, B.L. (2010). Frontotemporal lobar degeneration: epidemiology, pathophysiology, diagnosis and management. CNS Drugs *24*, 375–398.

Raiborg, C., Wenzel, E.M., Pedersen, N.M., Olsvik, H., Schink, K.O., Schultz, S.W., Vietri, M., Nisi, V., Bucci, C., Brech, A., et al. (2015). Repeated ER-endosome contacts promote endosome translocation and neurite outgrowth. Nature *520*, 234–238.

Rambold, A.S., Kostelecky, B., Elia, N., and Lippincott-Schwartz, J. (2011). Tubular network formation protects mitochondria from autophagosomal degradation during nutrient starvation. Proc. Natl. Acad. Sci. U.S.A. *108*, 10190–10195.

Ravits, J.M., and La Spada, A.R. (2009). ALS motor phenotype heterogeneity, focality, and spread: deconstructing motor neuron degeneration. Neurology *73*, 805–811.

Reaume, A.G., Elliott, J.L., Hoffman, E.K., Kowall, N.W., Ferrante, R.J., Siwek, D.F., Wilcox, H.M., Flood, D.G., Beal, M.F., Brown, R.H., et al. (1996). Motor neurons in Cu/Zn superoxide dismutase-deficient mice develop normally but exhibit enhanced cell death after axonal injury. Nat. Genet. *13*, 43–47.

Reck-Peterson, S.L., Redwine, W.B., Vale, R.D., and Carter, A.P. (2018). The cytoplasmic dynein transport machinery and its many cargoes. Nat. Rev. Mol. Cell Biol. *19*, 382–398.

Redwine, W.B., DeSantis, M.E., Hollyer, I., Htet, Z.M., Tran, P.T., Swanson, S.K., Florens, L., Washburn, M.P., and Reck-Peterson, S.L. (2017). The human cytoplasmic dynein interactome reveals novel activators of motility. Elife *6*.

Reed, N.A., Cai, D., Blasius, T.L., Jih, G.T., Meyhofer, E., Gaertig, J., and Verhey, K.J. (2006). Microtubule acetylation promotes kinesin-1 binding and transport. Curr. Biol. *16*, 2166–2172.

Reichardt, L.F. (2006). Neurotrophin-regulated signalling pathways. Philos. Trans. R. Soc. Lond., B, Biol. Sci. *361*, 1545–1564.

Renton, A.E., Majounie, E., Waite, A., Simón-Sánchez, J., Rollinson, S., Gibbs, J.R., Schymick, J.C., Laaksovirta, H., van Swieten, J.C., Myllykangas, L., et al. (2011). A hexanucleotide repeat expansion in C9ORF72 is the cause of chromosome 9p21-linked ALS-FTD. Neuron *72*, 257–268.

Renton, A.E., Chiò, A., and Traynor, B.J. (2014). State of play in amyotrophic lateral sclerosis genetics. Nat. Neurosci. *17*, 17–23.

Richter, B., Sliter, D.A., Herhaus, L., Stolz, A., Wang, C., Beli, P., Zaffagnini, G., Wild, P., Martens, S., Wagner, S.A., et al. (2016). Phosphorylation of OPTN by TBK1 enhances its binding to Ub chains and promotes selective autophagy of damaged mitochondria. Proc. Natl. Acad. Sci. U.S.A. *113*, 4039–4044.

Rink, J., Ghigo, E., Kalaidzidis, Y., and Zerial, M. (2005). Rab conversion as a mechanism of progression from early to late endosomes. Cell *122*, 735–749.

Ritter, J.L., Zhu, Z., Thai, T.C., Mahadevan, N.R., Mertins, P., Knelson, E.H., Piel, B.P., Han, S., Jaffe, J.D., Carr, S.A., et al. (2020). Phosphorylation of RAB7 by TBK1/IKKε Regulates Innate Immune Signaling in Triple-Negative Breast Cancer. Cancer Res. *80*, 44–56.

Rocha, N., Kuijl, C., van der Kant, R., Janssen, L., Houben, D., Janssen, H., Zwart, W., and Neefjes, J. (2009). Cholesterol sensor ORP1L contacts the ER protein VAP to control Rab7-RILP-p150 Glued and late endosome positioning. J. Cell Biol. *185*, 1209–1225.

Rojas, R., van Vlijmen, T., Mardones, G.A., Prabhu, Y., Rojas, A.L., Mohammed, S., Heck, A.J.R., Raposo, G., van der Sluijs, P., and Bonifacino, J.S. (2008). Regulation of retromer recruitment to endosomes by sequential action of Rab5 and Rab7. J. Cell Biol. *183*, 513–526.

Rosa-Ferreira, C., and Munro, S. (2011). Arl8 and SKIP act together to link lysosomes to kinesin-1. Dev. Cell *21*, 1171–1178.

Rosen, D.R., Siddique, T., Patterson, D., Figlewicz, D.A., Sapp, P., Hentati, A., Donaldson, D., Goto, J., O'Regan, J.P., and Deng, H.X. (1993). Mutations in Cu/Zn superoxide dismutase gene are associated with familial amyotrophic lateral sclerosis. Nature *362*, 59–62.

Rossor, A.M., Polke, J.M., Houlden, H., and Reilly, M.M. (2013). Clinical implications of genetic advances in Charcot-Marie-Tooth disease. Nat Rev Neurol *9*, 562–571.

Rothstein, J.D., Van Kammen, M., Levey, A.I., Martin, L.J., and Kuncl, R.W. (1995). Selective loss of glial glutamate transporter GLT-1 in amyotrophic lateral sclerosis. Ann. Neurol. *38*, 73–84.

Rozas, P., Bargsted, L., Martínez, F., Hetz, C., and Medinas, D.B. (2017). The ER proteostasis network in ALS: Determining the differential motoneuron vulnerability. Neurosci. Lett. *636*, 9–15.

Rubino, E., Rainero, I., Chiò, A., Rogaeva, E., Galimberti, D., Fenoglio, P., Grinberg, Y., Isaia, G., Calvo, A., Gentile, S., et al. (2012). SQSTM1 mutations in frontotemporal lobar degeneration and amyotrophic lateral sclerosis. Neurology *79*, 1556–1562.

Rudnick, N.D., Griffey, C.J., Guarnieri, P., Gerbino, V., Wang, X., Piersaint, J.A., Tapia, J.C., Rich, M.M., and Maniatis, T. (2017). Distinct roles for motor neuron autophagy early and late in the SOD1G93A mouse model of ALS. Proc. Natl. Acad. Sci. U.S.A. *114*, E8294–E8303.

Ryan, T.A., and Tumbarello, D.A. (2018). Optineurin: A Coordinator of Membrane-Associated Cargo Trafficking and Autophagy. Front Immunol *9*, 1024.

Sapmaz, A., Berlin, I., Bos, E., Wijdeven, R.H., Janssen, H., Konietzny, R., Akkermans, J.J., Erson-Bensan, A.E., Koning, R.I., Kessler, B.M., et al. (2019). USP32 regulates late endosomal transport and recycling through deubiquitylation of Rab7. Nat Commun *10*, 1454.

Sasayama, H., Shimamura, M., Tokuda, T., Azuma, Y., Yoshida, T., Mizuno, T., Nakagawa, M., Fujikake, N., Nagai, Y., and Yamaguchi, M. (2012). Knockdown of the Drosophila fused in sarcoma (FUS) homologue causes deficient locomotive behavior and shortening of motoneuron terminal branches. PLoS ONE *7*, e39483.

Satpathy, S., Wagner, S.A., Beli, P., Gupta, R., Kristiansen, T.A., Malinova, D., Francavilla, C., Tolar, P., Bishop, G.A., Hostager, B.S., et al. (2015). Systems-wide analysis of BCR signalosomes and downstream phosphorylation and ubiquitylation. Mol. Syst. Biol. *11*, 810.

Saxena, S., Bucci, C., Weis, J., and Kruttgen, A. (2005). The small GTPase Rab7 controls the endosomal trafficking and neuritogenic signaling of the nerve growth factor receptor TrkA. J. Neurosci. *25*, 10930–10940.

Saxena, S., Cabuy, E., and Caroni, P. (2009). A role for motoneuron subtype-selective ER stress in disease manifestations of FALS mice. Nat. Neurosci. *12*, 627–636.

Saxton, W.M., and Hollenbeck, P.J. (2012). The axonal transport of mitochondria. J. Cell. Sci. *125*, 2095–2104.

Scaduto, R.C., and Grotyohann, L.W. (1999). Measurement of mitochondrial membrane potential using fluorescent rhodamine derivatives. Biophys. J. *76*, 469–477.

Scherer, J., Yi, J., and Vallee, R.B. (2014). PKA-dependent dynein switching from lysosomes to adenovirus: a novel form of host-virus competition. J. Cell Biol. *205*, 163–177.

Schlager, M.A., Kapitein, L.C., Grigoriev, I., Burzynski, G.M., Wulf, P.S., Keijzer, N., de Graaff, E., Fukuda, M., Shepherd, I.T., Akhmanova, A., et al. (2010). Pericentrosomal targeting of Rab6 secretory vesicles by Bicaudal-D-related protein 1 (BICDR-1) regulates neuritogenesis. EMBO J. *29*, 1637–1651.

Schroeder, C.M., and Vale, R.D. (2016). Assembly and activation of dynein-dynactin by the cargo adaptor protein Hook3. J. Cell Biol. *214*, 309–318.

Schroer, T.A. (2004). Dynactin. Annu. Rev. Cell Dev. Biol. *20*, 759–779.

Seaman, M.N.J. (2012). The retromer complex - endosomal protein recycling and beyond. J. Cell. Sci. *125*, 4693–4702.

Seaman, M.N.J., Harbour, M.E., Tattersall, D., Read, E., and Bright, N. (2009). Membrane recruitment of the cargo-selective retromer subcomplex is catalysed by the small GTPase Rab7 and inhibited by the Rab-GAP TBC1D5. J. Cell. Sci. *122*, 2371–2382.

Segal, R.A. (2003). Selectivity in neurotrophin signaling: theme and variations. Annu. Rev. Neurosci. *26*, 299–330.

Sekine, S., and Youle, R.J. (2018). PINK1 import regulation; a fine system to convey mitochondrial stress to the cytosol. BMC Biol. *16*, 2.

Sellier, C., Campanari, M.-L., Julie Corbier, C., Gaucherot, A., Kolb-Cheynel, I., Oulad-Abdelghani, M., Ruffenach, F., Page, A., Ciura, S., Kabashi, E., et al. (2016). Loss of C9ORF72 impairs autophagy and synergizes with polyQ Ataxin-2 to induce motor neuron dysfunction and cell death. EMBO J. *35*, 1276–1297.

Shapiro, R.S., and Anderson, K.V. (2006). Drosophila Ik2, a member of the I kappa B kinase family, is required for mRNA localization during oogenesis. Development *133*, 1467–1475.

Shelkovnikova, T.A., Peters, O.M., Deykin, A.V., Connor-Robson, N., Robinson, H., Ustyugov, A.A., Bachurin, S.O., Ermolkevich, T.G., Goldman, I.L., Sadchikova, E.R., et al. (2013). Fused in sarcoma (FUS) protein lacking nuclear localization signal (NLS) and major RNA binding motifs triggers proteinopathy and severe motor phenotype in transgenic mice. J. Biol. Chem. *288*, 25266–25274.

Shi, K.Y., Mori, E., Nizami, Z.F., Lin, Y., Kato, M., Xiang, S., Wu, L.C., Ding, M., Yu, Y., Gall, J.G., et al. (2017). Toxic PRn poly-dipeptides encoded by the C9orf72 repeat expansion block nuclear import and export. Proc. Natl. Acad. Sci. U.S.A. *114*, E1111–E1117.

Shinde, S.R., and Maddika, S. (2016). PTEN modulates EGFR late endocytic trafficking and degradation by dephosphorylating Rab7. Nat Commun *7*, 10689.

Shirane, M., and Nakayama, K.I. (2006). Protrudin induces neurite formation by directional membrane trafficking. Science *314*, 818–821.

Shoesmith, C.L., Findlater, K., Rowe, A., and Strong, M.J. (2007). Prognosis of amyotrophic lateral sclerosis with respiratory onset. J. Neurol. Neurosurg. Psychiatry *78*, 629–631.

Sleigh, J.N., Rossor, A.M., Fellows, A.D., Tosolini, A.P., and Schiavo, G. (2019). Axonal transport and neurological disease. Nat Rev Neurol *15*, 691–703.

Sloboda, R.D., Dentler, W.L., and Rosenbaum, J.L. (1976). Microtubule-associated proteins and the stimulation of tubulin assembly in vitro. Biochemistry *15*, 4497–4505.

van der Sluijs, P., Hull, M., Huber, L.A., Mâle, P., Goud, B., and Mellman, I. (1992). Reversible phosphorylation--dephosphorylation determines the localization of rab4 during the cell cycle. EMBO J. *11*, 4379–4389.

Smith, B.N., Ticozzi, N., Fallini, C., Gkazi, A.S., Topp, S., Kenna, K.P., Scotter, E.L., Kost, J., Keagle, P., Miller, J.W., et al. (2014). Exome-wide rare variant analysis identifies TUBA4A mutations associated with familial ALS. Neuron *84*, 324–331.

Smith, B.N., Topp, S.D., Fallini, C., Shibata, H., Chen, H.-J., Troakes, C., King, A., Ticozzi, N., Kenna, K.P., Soragia-Gkazi, A., et al. (2017). Mutations in the vesicular trafficking protein annexin A11 are associated with amyotrophic lateral sclerosis. Sci Transl Med *9*.

Song, G., Liu, B., Li, Z., Wu, H., Wang, P., Zhao, K., Jiang, G., Zhang, L., and Gao, C. (2016a). E3 ubiquitin ligase RNF128 promotes innate antiviral immunity through K63-linked ubiquitination of TBK1. Nat. Immunol. *17*, 1342–1351.

Song, P., Trajkovic, K., Tsunemi, T., and Krainc, D. (2016b). Parkin Modulates Endosomal Organization and Function of the Endo-Lysosomal Pathway. J. Neurosci. *36*, 2425–2437.

Soppina, V., Rai, A.K., Ramaiya, A.J., Barak, P., and Mallik, R. (2009). Tug-of-war between dissimilar teams of microtubule motors regulates transport and fission of endosomes. Proc. Natl. Acad. Sci. U.S.A. *106*, 19381–19386.

Souquere, S., Mollet, S., Kress, M., Dautry, F., Pierron, G., and Weil, D. (2009). Unravelling the ultrastructure of stress granules and associated P-bodies in human cells. J. Cell. Sci. *122*, 3619–3626.

Spector, D.L. (2006). SnapShot: Cellular bodies. Cell *127*, 1071.

Spinosa, M.R., Progida, C., De Luca, A., Colucci, A.M.R., Alifano, P., and Bucci, C. (2008). Functional characterization of Rab7 mutant proteins associated with Charcot-Marie-Tooth type 2B disease. J. Neurosci. *28*, 1640–1648.

van Spronsen, M., Mikhaylova, M., Lipka, J., Schlager, M.A., van den Heuvel, D.J., Kuijpers, M., Wulf, P.S., Keijzer, N., Demmers, J., Kapitein, L.C., et al. (2013). TRAK/Milton motor-adaptor proteins steer mitochondrial trafficking to axons and dendrites. Neuron *77*, 485–502.

Sreedharan, J., Blair, I.P., Tripathi, V.B., Hu, X., Vance, C., Rogelj, B., Ackerley, S., Durnall, J.C., Williams, K.L., Buratti, E., et al. (2008). TDP-43 mutations in familial and sporadic amyotrophic lateral sclerosis. Science *319*, 1668–1672.

Steger, M., Tonelli, F., Ito, G., Davies, P., Trost, M., Vetter, M., Wachter, S., Lorentzen, E., Duddy, G., Wilson, S., et al. (2016). Phosphoproteomics reveals that Parkinson's disease kinase LRRK2 regulates a subset of Rab GTPases. Elife *5*.

Stein, M.-P., Feng, Y., Cooper, K.L., Welford, A.M., and Wandinger-Ness, A. (2003). Human VPS34 and p150 are Rab7 interacting partners. Traffic *4*, 754–771.

Stenmark, H. (2009). Rab GTPases as coordinators of vesicle traffic. Nat. Rev. Mol. Cell Biol. *10*, 513–525.

Stolz, A., Ernst, A., and Dikic, I. (2014). Cargo recognition and trafficking in selective autophagy. Nat. Cell Biol. *16*, 495–501.

Stowers, R.S., Megeath, L.J., Górska-Andrzejak, J., Meinertzhagen, I.A., and Schwarz, T.L. (2002). Axonal transport of mitochondria to synapses depends on milton, a novel Drosophila protein. Neuron *36*, 1063–1077.

Striz, A.C., and Tuma, P.L. (2016). The GTP-bound and Sumoylated Form of the rab17 Small Molecular Weight GTPase Selectively Binds Syntaxin 2 in Polarized Hepatic WIF-B Cells. J. Biol. Chem. *291*, 9721–9732.

Strong, M.J., Grace, G.M., Freedman, M., Lomen-Hoerth, C., Woolley, S., Goldstein, L.H., Murphy, J., Shoesmith, C., Rosenfeld, J., Leigh, P.N., et al. (2009). Consensus criteria for the diagnosis of frontotemporal cognitive and behavioural syndromes in amyotrophic lateral sclerosis. Amyotroph Lateral Scler *10*, 131–146.

Sun, F., Zhu, C., Dixit, R., and Cavalli, V. (2011). Sunday Driver/JIP3 binds kinesin heavy chain directly and enhances its motility. EMBO J. *30*, 3416–3429.

Sung, H., Tandarich, L.C., Nguyen, K., and Hollenbeck, P.J. (2016). Compartmentalized Regulation of Parkin-Mediated Mitochondrial Quality Control in the Drosophila Nervous System In Vivo. J. Neurosci. *36*, 7375–7391.

Svitkina, T. (2018). The Actin Cytoskeleton and Actin-Based Motility. Cold Spring Harb Perspect Biol *10*.

Sweeney, H.L., and Holzbaur, E.L.F. (2018). Motor Proteins. Cold Spring Harb Perspect Biol *10*.

Swinnen, B., and Robberecht, W. (2014). The phenotypic variability of amyotrophic lateral sclerosis. Nat Rev Neurol *10*, 661–670.

Talbot, K. (2009). Motor neuron disease: the bare essentials. Pract Neurol *9*, 303–309.

Tartaglia, M.C., Rowe, A., Findlater, K., Orange, J.B., Grace, G., and Strong, M.J. (2007). Differentiation between primary lateral sclerosis and amyotrophic lateral sclerosis: examination of symptoms and signs at disease onset and during follow-up. Arch. Neurol. *64*, 232–236.

Tas, R.P., Chazeau, A., Cloin, B.M.C., Lambers, M.L.A., Hoogenraad, C.C., and Kapitein, L.C. (2017). Differentiation between Oppositely Oriented Microtubules Controls Polarized Neuronal Transport. Neuron *96*, 1264-1271.e5.

Taylor, J.P., Brown, R.H., and Cleveland, D.W. (2016). Decoding ALS: from genes to mechanism. Nature *539*, 197–206.

Thurston, T.L.M., Ryzhakov, G., Bloor, S., von Muhlinen, N., and Randow, F. (2009). The TBK1 adaptor and autophagy receptor NDP52 restricts the proliferation of ubiquitin-coated bacteria. Nat. Immunol. *10*, 1215–1221.

Ticozzi, N., Vance, C., Leclerc, A.L., Keagle, P., Glass, J.D., McKenna-Yasek, D., Sapp, P.C., Silani, V., Bosco, D.A., Shaw, C.E., et al. (2011). Mutational analysis reveals the FUS homolog TAF15 as a candidate gene for familial amyotrophic lateral sclerosis. Am. J. Med. Genet. B Neuropsychiatr. Genet. *156B*, 285–290.

Tinevez, J.-Y., Perry, N., Schindelin, J., Hoopes, G.M., Reynolds, G.D., Laplantine, E., Bednarek, S.Y., Shorte, S.L., and Eliceiri, K.W. (2017). TrackMate: An open and extensible platform for single-particle tracking. Methods *115*, 80–90.

Todd, T.W., and Petrucelli, L. (2016). Insights into the pathogenic mechanisms of Chromosome 9 open reading frame 72 (C9orf72) repeat expansions. J. Neurochem. *138 Suppl 1*, 145–162.

Toyofuku, T., Morimoto, K., Sasawatari, S., and Kumanogoh, A. (2015). Leucine-Rich Repeat Kinase 1 Regulates Autophagy through Turning On TBC1D2-Dependent Rab7 Inactivation. Mol. Cell. Biol. *35*, 3044–3058.

Toyoshima, I., Sugawara, M., Kato, K., Wada, C., Hirota, K., Hasegawa, K., Kowa, H., Sheetz, M.P., and Masamune, O. (1998). Kinesin and cytoplasmic dynein in spinal spheroids with motor neuron disease. J. Neurol. Sci. *159*, 38–44.

Tu, D., Zhu, Z., Zhou, A.Y., Yun, C., Lee, K.-E., Toms, A.V., Li, Y., Dunn, G.P., Chan, E., Thai, T., et al. (2013). Structure and ubiquitination-dependent activation of TANK-binding kinase 1. Cell Rep *3*, 747–758.

Turner, M.R., Scaber, J., Goodfellow, J.A., Lord, M.E., Marsden, R., and Talbot, K. (2010). The diagnostic pathway and prognosis in bulbar-onset amyotrophic lateral sclerosis. J. Neurol. Sci. *294*, 81–85.

Twelvetrees, A.E., Pernigo, S., Sanger, A., Guedes-Dias, P., Schiavo, G., Steiner, R.A., Dodding, M.P., and Holzbaur, E.L.F. (2016). The Dynamic Localization of Cytoplasmic Dynein in Neurons Is Driven by Kinesin-1. Neuron *90*, 1000–1015.

Tyzack, G.E., Luisier, R., Taha, D.M., Neeves, J., Modic, M., Mitchell, J.S., Meyer, I., Greensmith, L., Newcombe, J., Ule, J., et al. (2019). Widespread FUS mislocalization is a molecular hallmark of amyotrophic lateral sclerosis. Brain *142*, 2572–2580.

Urnavicius, L., Lau, C.K., Elshenawy, M.M., Morales-Rios, E., Motz, C., Yildiz, A., and Carter, A.P. (2018). Cryo-EM shows how dynactin recruits two dyneins for faster movement. Nature *554*, 202–206.

Urushitani, M., Kurisu, J., Tsukita, K., and Takahashi, R. (2002). Proteasomal inhibition by misfolded mutant superoxide dismutase 1 induces selective motor neuron death in familial amyotrophic lateral sclerosis. J. Neurochem. *83*, 1030–1042.

Vallee, R.B., McKenney, R.J., and Ori-McKenney, K.M. (2012). Multiple modes of cytoplasmic dynein regulation. Nat. Cell Biol. *14*, 224–230.

Van Damme, P., Bogaert, E., Dewil, M., Hersmus, N., Kiraly, D., Scheveneels, W., Bockx, I., Braeken, D., Verpoorten, N., Verhoeven, K., et al. (2007). Astrocytes regulate GluR2 expression in motor neurons and their vulnerability to excitotoxicity. Proc. Natl. Acad. Sci. U.S.A. *104*, 14825–14830.

van den Boom, J., and Meyer, H. (2018). VCP/p97-Mediated Unfolding as a Principle in Protein Homeostasis and Signaling. Mol. Cell *69*, 182–194.

Vance, C., Rogelj, B., Hortobágyi, T., De Vos, K.J., Nishimura, A.L., Sreedharan, J., Hu, X., Smith, B., Ruddy, D., Wright, P., et al. (2009). Mutations in FUS, an RNA processing protein, cause familial amyotrophic lateral sclerosis type 6. Science *323*, 1208–1211.

Vance, C., Scotter, E.L., Nishimura, A.L., Troakes, C., Mitchell, J.C., Kathe, C., Urwin, H., Manser, C., Miller, C.C., Hortobágyi, T., et al. (2013). ALS mutant FUS disrupts nuclear localization and sequesters wild-type FUS within cytoplasmic stress granules. Hum. Mol. Genet. *22*, 2676–2688.

Vande Velde, C., McDonald, K.K., Boukhedimi, Y., McAlonis-Downes, M., Lobsiger, C.S., Bel Hadj, S., Zandona, A., Julien, J.-P., Shah, S.B., and Cleveland, D.W. (2011). Misfolded SOD1 associated with motor neuron mitochondria alters mitochondrial shape and distribution prior to clinical onset. PLoS ONE *6*, e22031.

Vargas, J.N.S., Wang, C., Bunker, E., Hao, L., Maric, D., Schiavo, G., Randow, F., and Youle, R.J. (2019). Spatiotemporal Control of ULK1 Activation by NDP52 and TBK1 during Selective Autophagy. Mol. Cell *74*, 347-362.e6.

Vergarajauregui, S., Martina, J.A., and Puertollano, R. (2009). Identification of the penta-EF-hand protein ALG-2 as a Ca2+-dependent interactor of mucolipin-1. J. Biol. Chem. *284*, 36357–36366.

Verhey, K.J., Meyer, D., Deehan, R., Blenis, J., Schnapp, B.J., Rapoport, T.A., and Margolis, B. (2001). Cargo of kinesin identified as JIP scaffolding proteins and associated signaling molecules. J. Cell Biol. *152*, 959–970.

Vicencio, E., Beltrán, S., Labrador, L., Manque, P., Nassif, M., and Woehlbier, U. (2020). Implications of Selective Autophagy Dysfunction for ALS Pathology. Cells *9*.

Villarroel-Campos, D., Schiavo, G., and Lazo, O.M. (2018). The many disguises of the signalling endosome. FEBS Lett. *592*, 3615–3632.

Walenta, J.H., Didier, A.J., Liu, X., and Krämer, H. (2001). The Golgi-associated hook3 protein is a member of a novel family of microtubule-binding proteins. J. Cell Biol. *152*, 923–934.

Wallace, M (2014). Regulation of Rab7 activity by phosphorylation at Serine 72. Thesis (PhD) University College London.

Wallet, S.M., Puri, V., and Gibson, F.C. (2018). Linkage of Infection to Adverse Systemic Complications: Periodontal Disease, Toll-Like Receptors, and Other Pattern Recognition Systems. Vaccines (Basel) *6*.

Wang, X., and Schwarz, T.L. (2009). The mechanism of Ca2+ -dependent regulation of kinesin-mediated mitochondrial motility. Cell *136*, 163–174.

Wang, Y., and Mandelkow, E. (2016). Tau in physiology and pathology. Nat. Rev. Neurosci. *17*, 5–21.

Wang, C., Chen, T., Zhang, J., Yang, M., Li, N., Xu, X., and Cao, X. (2009). The E3 ubiquitin ligase Nrdp1 “preferentially” promotes TLR-mediated production of type I interferon. Nat. Immunol. *10*, 744–752.

Wang, T., Block, M.A., Cowen, S., Davies, A.M., Devereaux, E., Gingipalli, L., Johannes, J., Larsen, N.A., Su, Q., Tucker, J.A., et al. (2012). Discovery of azabenzimidazole derivatives as potent, selective inhibitors of TBK1/IKKε kinases. Bioorg. Med. Chem. Lett. *22*, 2063–2069.

Wang, W., Li, L., Lin, W.-L., Dickson, D.W., Petrucelli, L., Zhang, T., and Wang, X. (2013). The ALS disease-associated mutant TDP-43 impairs mitochondrial dynamics and function in motor neurons. Hum. Mol. Genet. *22*, 4706–4719.

Warita, H., Itoyama, Y., and Abe, K. (1999). Selective impairment of fast anterograde axonal transport in the peripheral nerves of asymptomatic transgenic mice with a G93A mutant SOD1 gene. Brain Res. *819*, 120–131.

Waterman-Storer, C.M., Karki, S., and Holzbaur, E.L. (1995). The p150Glued component of the dynactin complex binds to both microtubules and the actin-related protein centractin (Arp-1). Proc. Natl. Acad. Sci. U.S.A. *92*, 1634–1638.

Webster, C.P., Smith, E.F., Bauer, C.S., Moller, A., Hautbergue, G.M., Ferraiuolo, L., Myszczynska, M.A., Higginbottom, A., Walsh, M.J., Whitworth, A.J., et al. (2016). The C9orf72 protein interacts with Rab1a and the ULK1 complex to regulate initiation of autophagy. EMBO J. *35*, 1656–1676.

Westeneng, H.-J., Debray, T.P.A., Visser, A.E., van Eijk, R.P.A., Rooney, J.P.K., Calvo, A., Martin, S., McDermott, C.J., Thompson, A.G., Pinto, S., et al. (2018). Prognosis for patients with amyotrophic lateral sclerosis: development and validation of a personalised prediction model. Lancet Neurol *17*, 423–433.

Wijdeven, R.H., Janssen, H., Nahidiazar, L., Janssen, L., Jalink, K., Berlin, I., and Neefjes, J. (2016). Cholesterol and ORP1L-mediated ER contact sites control autophagosome transport and fusion with the endocytic pathway. Nat Commun *7*, 11808.

Wild, P., Farhan, H., McEwan, D.G., Wagner, S., Rogov, V.V., Brady, N.R., Richter, B., Korac, J., Waidmann, O., Choudhary, C., et al. (2011). Phosphorylation of the autophagy receptor optineurin restricts Salmonella growth. Science *333*, 228–233.

Wilke, C., Baets, J., De Bleecker, J.L., Deconinck, T., Biskup, S., Hayer, S.N., Züchner, S., Schüle, R., De Jonghe, P., and Synofzik, M. (2018). Beyond ALS and FTD: the phenotypic spectrum of TBK1 mutations includes PSP-like and cerebellar phenotypes. Neurobiol. Aging *62*, 244.e9-244.e13.

Willett, R., Martina, J.A., Zewe, J.P., Wills, R., Hammond, G.R.V., and Puertollano, R. (2017). TFEB regulates lysosomal positioning by modulating TMEM55B expression and JIP4 recruitment to lysosomes. Nat Commun *8*, 1580.

Williams, K.L., Warraich, S.T., Yang, S., Solski, J.A., Fernando, R., Rouleau, G.A., Nicholson, G.A., and Blair, I.P. (2012). UBQLN2/ubiquilin 2 mutation and pathology in familial amyotrophic lateral sclerosis. Neurobiol. Aging *33*, 2527.e3-10.

Williamson, T.L., and Cleveland, D.W. (1999). Slowing of axonal transport is a very early event in the toxicity of ALS-linked SOD1 mutants to motor neurons. Nat. Neurosci. *2*, 50–56.

Witte, H., Neukirchen, D., and Bradke, F. (2008). Microtubule stabilization specifies initial neuronal polarization. J. Cell Biol. *180*, 619–632.

Wong, Y.C., and Holzbaur, E.L.F. (2014). Optineurin is an autophagy receptor for damaged mitochondria in parkin-mediated mitophagy that is disrupted by an ALS-linked mutation. Proc. Natl. Acad. Sci. U.S.A. *111*, E4439-4448.

Wong, Y.C., Ysselstein, D., and Krainc, D. (2018). Mitochondria-lysosome contacts regulate mitochondrial fission via RAB7 GTP hydrolysis. Nature *554*, 382–386.

Wong, Y.C., Peng, W., and Krainc, D. (2019). Lysosomal Regulation of Inter-mitochondrial Contact Fate and Motility in Charcot-Marie-Tooth Type 2. Dev. Cell *50*, 339-354.e4.

Wozniak, M.J., Melzer, M., Dorner, C., Haring, H.-U., and Lammers, R. (2005). The novel protein KBP regulates mitochondria localization by interaction with a kinesin-like protein. BMC Cell Biol. *6*, 35.

Wu, C.-H., Fallini, C., Ticozzi, N., Keagle, P.J., Sapp, P.C., Piotrowska, K., Lowe, P., Koppers, M., McKenna-Yasek, D., Baron, D.M., et al. (2012). Mutations in the profilin 1 gene cause familial amyotrophic lateral sclerosis. Nature *488*, 499–503.

Wu, M., Wang, T., Loh, E., Hong, W., and Song, H. (2005). Structural basis for recruitment of RILP by small GTPase Rab7. EMBO J. *24*, 1491–1501.

Wurmser, A.E., Sato, T.K., and Emr, S.D. (2000). New component of the vacuolar class C-Vps complex couples nucleotide exchange on the Ypt7 GTPase to SNARE-dependent docking and fusion. J. Cell Biol. *151*, 551–562.

Xiao, Q., Zhao, W., Beers, D.R., Yen, A.A., Xie, W., Henkel, J.S., and Appel, S.H. (2007). Mutant SOD1(G93A) microglia are more neurotoxic relative to wild-type microglia. J. Neurochem. *102*, 2008–2019.

Xu, D., Jin, T., Zhu, H., Chen, H., Ofengeim, D., Zou, C., Mifflin, L., Pan, L., Amin, P., Li, W., et al. (2018). TBK1 Suppresses RIPK1-Driven Apoptosis and Inflammation during Development and in Aging. Cell *174*, 1477-1491.e19.

Xu, Z., Schaedel, L., Portran, D., Aguilar, A., Gaillard, J., Marinkovich, M.P., Théry, M., and Nachury, M.V. (2017). Microtubules acquire resistance from mechanical breakage through intralumenal acetylation. Science *356*, 328–332.

Yamaguchi, A., and Takanashi, K. (2016). FUS interacts with nuclear matrix-associated protein SAFB1 as well as Matrin3 to regulate splicing and ligand-mediated transcription. Sci Rep *6*, 35195.

Yamanaka, K., and Komine, O. (2018). The multi-dimensional roles of astrocytes in ALS. Neurosci. Res. *126*, 31–38.

Yamanaka, K., Boillee, S., Roberts, E.A., Garcia, M.L., McAlonis-Downes, M., Mikse, O.R., Cleveland, D.W., and Goldstein, L.S.B. (2008a). Mutant SOD1 in cell types other than motor neurons and oligodendrocytes accelerates onset of disease in ALS mice. Proc. Natl. Acad. Sci. U.S.A. *105*, 7594–7599.

Yamanaka, K., Chun, S.J., Boillee, S., Fujimori-Tonou, N., Yamashita, H., Gutmann, D.H., Takahashi, R., Misawa, H., and Cleveland, D.W. (2008b). Astrocytes as determinants of disease progression in inherited amyotrophic lateral sclerosis. Nat. Neurosci. *11*, 251–253.

Yamano, K., Fogel, A.I., Wang, C., van der Bliek, A.M., and Youle, R.J. (2014). Mitochondrial Rab GAPs govern autophagosome biogenesis during mitophagy. Elife *3*, e01612.

Yang, M., Liang, C., Swaminathan, K., Herrlinger, S., Lai, F., Shiekhattar, R., and Chen, J.-F. (2016). A C9ORF72/SMCR8-containing complex regulates ULK1 and plays a dual role in autophagy. Sci Adv *2*, e1601167.

Yang, Y., Hentati, A., Deng, H.X., Dabbagh, O., Sasaki, T., Hirano, M., Hung, W.Y., Ouahchi, K., Yan, J., Azim, A.C., et al. (2001). The gene encoding alsin, a protein with three guanine-nucleotide exchange factor domains, is mutated in a form of recessive amyotrophic lateral sclerosis. Nat. Genet. *29*, 160–165.

Yasuda, S., Morishita, S., Fujita, A., Nanao, T., Wada, N., Waguri, S., Schiavo, G., Fukuda, M., and Nakamura, T. (2016). Mon1-Ccz1 activates Rab7 only on late endosomes and dissociates from the lysosome in mammalian cells. J. Cell. Sci. *129*, 329–340.

Ye, J., Cheung, J., Gerbino, V., Ahlsén, G., Zimanyi, C., Hirsh, D., and Maniatis, T. (2019). Effects of ALS-associated TANK binding kinase 1 mutations on protein–protein interactions and kinase activity. PNAS.

Ye, M., Lehigh, K.M., and Ginty, D.D. (2018). Multivesicular bodies mediate long-range retrograde NGF-TrkA signaling. Elife *7*.

Yoneyama, M., Kikuchi, M., Natsukawa, T., Shinobu, N., Imaizumi, T., Miyagishi, M., Taira, K., Akira, S., and Fujita, T. (2004). The RNA helicase RIG-I has an essential function in double-stranded RNA-induced innate antiviral responses. Nat. Immunol. *5*, 730–737.

Yuan, A., Kumar, A., Peterhoff, C., Duff, K., and Nixon, R.A. (2008). Axonal transport rates in vivo are unaffected by tau deletion or overexpression in mice. J. Neurosci. *28*, 1682–1687.

Zerial, M., and McBride, H. (2001). Rab proteins as membrane organizers. Nat. Rev. Mol. Cell Biol. *2*, 107–117.

Zhang, C., Shang, G., Gui, X., Zhang, X., Bai, X.-C., and Chen, Z.J. (2019). Structural basis of STING binding with and phosphorylation by TBK1. Nature *567*, 394–398.

Zhang, F., Ström, A.-L., Fukada, K., Lee, S., Hayward, L.J., and Zhu, H. (2007a). Interaction between familial amyotrophic lateral sclerosis (ALS)-linked SOD1 mutants and the dynein complex. J. Biol. Chem. *282*, 16691–16699.

Zhang, J., Schulze, K.L., Hiesinger, P.R., Suyama, K., Wang, S., Fish, M., Acar, M., Hoskins, R.A., Bellen, H.J., and Scott, M.P. (2007b). Thirty-one flavors of Drosophila rab proteins. Genetics *176*, 1307–1322.

Zhang, K., Fishel Ben Kenan, R., Osakada, Y., Xu, W., Sinit, R.S., Chen, L., Zhao, X., Chen, J.-Y., Cui, B., and Wu, C. (2013). Defective axonal transport of Rab7 GTPase results in dysregulated trophic signaling. J. Neurosci. *33*, 7451–7462.

Zhang, K., Foster, H.E., Rondelet, A., Lacey, S.E., Bahi-Buisson, N., Bird, A.W., and Carter, A.P. (2017). Cryo-EM Reveals How Human Cytoplasmic Dynein Is Auto-inhibited and Activated. Cell *169*, 1303-1314.e18.

Zhang, K.Y., Yang, S., Warraich, S.T., and Blair, I.P. (2014). Ubiquilin 2: a component of the ubiquitin-proteasome system with an emerging role in neurodegeneration. Int. J. Biochem. Cell Biol. *50*, 123–126.

Zhang, X.D., Gillespie, S.K., and Hersey, P. (2004). Staurosporine induces apoptosis of melanoma by both caspase-dependent and -independent apoptotic pathways. Mol. Cancer Ther. *3*, 187–197.

Zhang, Y., Moheban, D.B., Conway, B.R., Bhattacharyya, A., and Segal, R.A. (2000). Cell surface Trk receptors mediate NGF-induced survival while internalized receptors regulate NGF-induced differentiation. J. Neurosci. *20*, 5671–5678.

Zhen, Y., and Stenmark, H. (2015). Cellular functions of Rab GTPases at a glance. J. Cell. Sci. *128*, 3171–3176.

Zhou, B., Cai, Q., Xie, Y., and Sheng, Z.-H. (2012). Snapin recruits dynein to BDNF-TrkB signaling endosomes for retrograde axonal transport and is essential for dendrite growth of cortical neurons. Cell Rep *2*, 42–51.

Zhou, Y., Guo, M., Wang, X., Li, J., Wang, Y., Ye, L., Dai, M., Zhou, L., Persidsky, Y., and Ho, W. (2013). TLR3 activation efficiency by high or low molecular mass poly I:C. Innate Immun *19*, 184–192.

Zou, Z.-Y., Zhou, Z.-R., Che, C.-H., Liu, C.-Y., He, R.-L., and Huang, H.-P. (2017). Genetic epidemiology of amyotrophic lateral sclerosis: a systematic review and meta-analysis. J. Neurol. Neurosurg. Psychiatry *88*, 540–549.

Zweifel, L.S., Kuruvilla, R., and Ginty, D.D. (2005). Functions and mechanisms of retrograde neurotrophin signalling. Nat. Rev. Neurosci. *6*, 615–625.

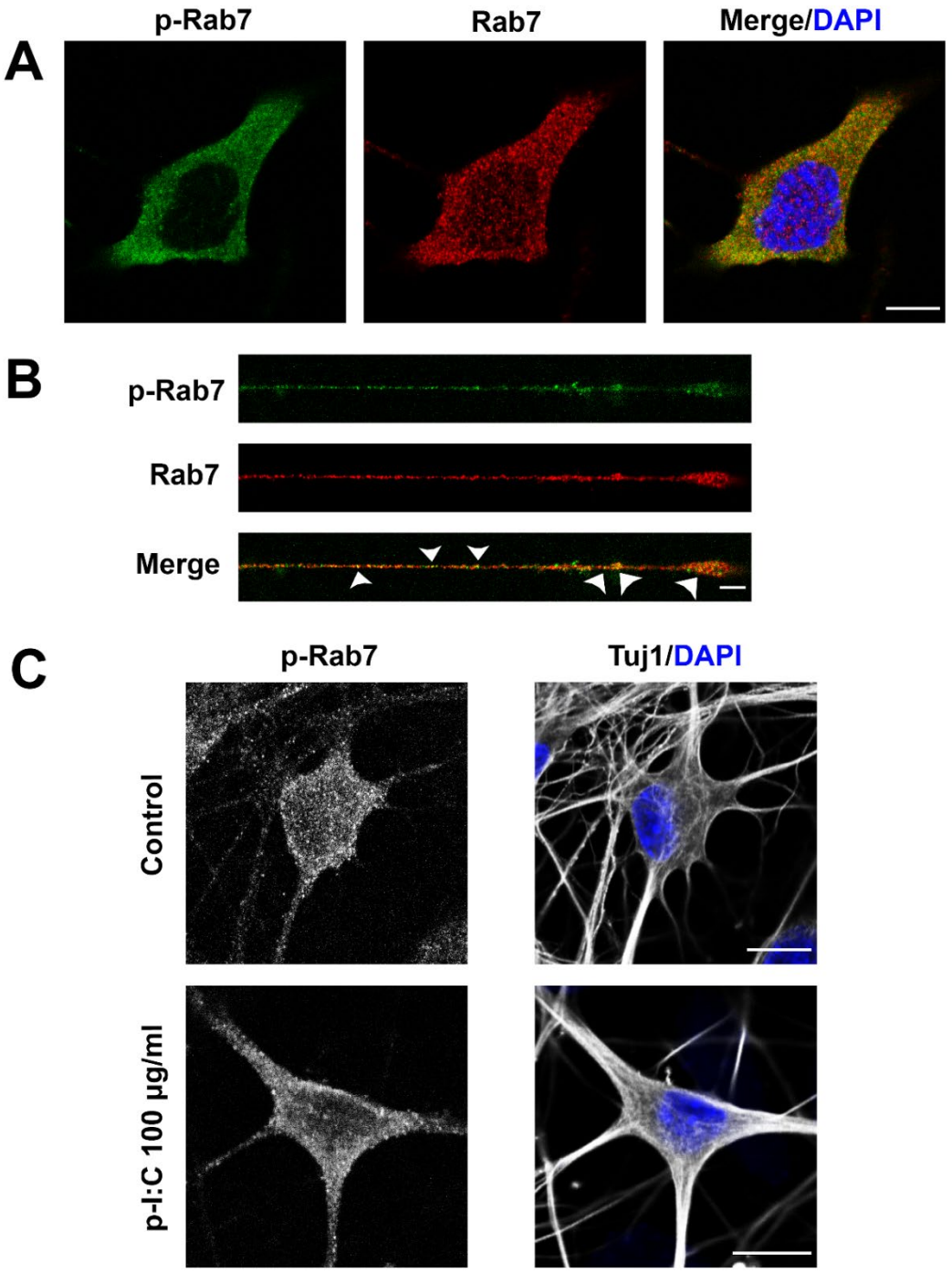

Supplementary figure S4.1. The intensity of phosphorylated Rab7-S72 is not modified by poly I:C treatment. (A) Differentiated NSC-34 cells were fixed and stained for phosphorylated and total Rab7. p-Rab7 exhibits a mixed punctuate and cytosolic patter along the cell body. Scale bar, 10 µm. **(B)** The punctuate pattern is also visible on neurites. Arrowheads indicate puncta double positive for p-Rab7 and Rab7. Scale bar, 5 µm. (C) 6 DIV primary MN in culture were treated with poly I:C 100 µg/ml for 2 h, fixed and stained as indicated. p-Rab7 distribution is not affected by poly I:C treatment. Scale bar, 10 µm.